In-sequence tectonic evolution of Ediacaran nappes in the southeastern branch of the Brasília Orogen (SE Brazil): Constraints from metamorphic iterative thermodynamic modeling and monazite petrochronology

Published version:

DOI:10.1016/j.lithos.2023.107459

LITHOS

In-sequence tectonic evolution of Ediacaran nappes in the southeastern branch of the Brasília Orogen (SE Brazil): constraints from metamorphic iterative thermodynamic modeling and monazite petrochronology

--Manuscript Draft--

Manuscript Number:	LITHOS11675R1
Article Type:	Regular Article
Keywords:	Monazite petrochronology, iterative thermodynamic modeling, Brasília Orogen metamorphism, P-T-t-D paths
Corresponding Author:	Beatriz Benetti, Ph.D. University of Turin Turin, BRAZIL
First Author:	Beatriz Benetti, Ph.D.
Order of Authors:	Beatriz Benetti, Ph.D.
	Mário da Costa Campos Neto, PhD
	Rodolfo Carosi, PhD
	George Luvizotto, PhD
	Salvatore Iaccarino, PhD
	Chiara Montomoli, PhD
Abstract:	The metamorphic and kinematic evolution of medium-high grade rocks of the Andrelândia Nappe System (ANS), the orogenic wedge of the Southern Brasilia Orogen (SBO), was investigated in this work. Field and microstructural observations were combined with metamorphic petrology (i.e., iterative thermodynamic modeling) and monazite petrochronology to reconstruct the tectono-metamorphic history of the ANS rocks. The Liberdade Nappe experienced prograde metamorphism at ca. 610 Ma, achieving peak metamorphic conditions of ca. 650°C and 9.5-10 kbar. This stage was followed by isothermal decompression linked to tectonic transport toward SE, at ca. 570 Ma. On the contrary, the Andrelândia Nappe experienced prograde metamorphism later, at ca. 580 Ma, reaching peak metamorphic conditions of ca. 680°C and 11-12 kbar. The obtained results indicate that each nappe of the Andrelândia System records a single metamorphic cycle of burial and decompression, although it took place at different ages over a period of ca. 60 myr, from 630 to 570 Ma. The nappes experienced prograde and retrograde metamorphism whose ages progressively decreased toward the bottom of the nappe stack. We attribute this pattern to propagation of older buried material from the orogenic wedge (i.e., Liberdade Nappe), via thrust-and-fold, upon recently accreted rocks (i.e., Andrelândia Nappe), conducting a younger metamorphism event on the footwall of the ductile thrusted nappes. This mechanism is consistent with the ANS in-sequence fold-and-thrust architecture.
Suggested Reviewers:	Alice Westin, PhD University of São Paulo alice.teixeira@usp.br Dr. Westin has worked in the Southern Brasilia Belt, with several papers published in the area.
	Gregory Dumond, PhD Dumond, PhD gdumond@uark.edu Dr. Dumond research is focused on collisional belt evolution, applying as methodology macro- and microstructural studies, thermodynamic modeling, and monazite geochronology.
	Regiane Fumes, PhD regiane.fumes@unesp.br Dra. Fumes has developed her work using monazite petrochonology and metamorphic modeling techiniques in the Southern Brasília Belt.

	Glaucia Queiroga, PhD Queiroga, PhD glauciaqueiroga@ufop.edu.br Dra. Queiroga has an expertise in metamorphic petrology and monazite petrochronology. She has developed her research in the Neoproterozoic fold-thrust belts from Brazil.
Opposed Reviewers:	

Title page

In-sequence tectonic evolution of Ediacaran nappes in the southeastern branch of the Brasília Orogen (SE Brazil): constraints from metamorphic iterative thermodynamic modeling and monazite petrochronology

Beatriz Benetti[a,b*], Mario da Costa Campos Neto[b], Rodolfo Carosi[a], George Luvizotto[c], Salvatore Iaccarino[a], Chiara Montomoli[a,d]

Beatriz Benetti[a,b*] - e-mail: beatrizyuri.benettisilva@unito.it

Mario da Costa Campos Neto[b] – e-mail: camposnt@usp.br

Rodolfo Carosi[a] – e-mail: rodolfo.carosi@unito.it

George Luvizotto[c] – e-mail: george.luvizotto@unesp.br

Salvatore Iaccarino[a] – e-mail: salvatore.iaccarino@unito.it

Chiara Montomoli[a,d] – e-mail: chiara.montomoli@unito.it

Corresponding author:

*Beatriz Benetti – beatrizyuri.benettisilva@unito.it - ORCID: 0000-0001-5698-3075

Present address: Geological Survey of Brazil – SGB/CPRM, Av Pasteur 404, Rio de Janeiro - RJ, Brazil

Affiliations:

a Dipartimento di Scienze della Terra, Università degli Studi di Torino, Turin, Italy

b Instituto de Geociências, Universidade de São Paulo, São Paulo, Brazil

c Departamento de Geologia, Universidade do Estado de São Paulo

d Istituto di Geoscienze e Georisorse, IGG-CNR, Pisa, Italy

August 18th, 2023

Dear Editor,

I am pleased to submit an original research manuscript entitled "Tectonic evolution of Ediacaran nappes in the southeastern branch of the Brasília Orogen (SE Brazil): constraints from metamorphic iterative thermodynamic modeling and monazite petrochronology" written by Benetti, B., Campos Neto, M.C., Carosi, R., Luvizotto, G., Iaccarino, S., and Montomoli C.to be examined for publication on LITHOS.

The paper presents new data and interpretations about the tectonic, metamorphic, and time evolution of the Andrelândia Nappe System, the orogenic wedge hinterland of the Southern Brasilia Orogen. The manuscript contains field and microstructural observations combined with the leading-edge techniques in metamorphic petrology (i.e., thermodynamic iterative modeling) and geochronology (i.e., monazite petrochronology). The obtained data carry precious information and implications concerning the tectono-metamorphic events experienced by the Andrelândia Nappe System rocks. The combination of our new data with literature information suggest that the Andrelândia Nappe System spread of ages is related to different periods when the different nappes of the system experienced prograde and retrograde metamorphism during the Southern Brasilia Belt protracted and progressive continental collision development.

I confirm that the manuscript has not been published and is not under consideration for publication elsewhere, and look forward to hearing from you in due course.

Yours sincerely,
Corresponding author:
Beatriz Benetti, PhD (on behalf of all authors)
Dipartimento Scienze della Terra, Università degli Studi di Torino
Email: beatrizyuri.benettisilva@unito.it

Yours sincerely,
Corresponding author:
Beatriz Benetti, PhD (on behalf of all authors)
Dipartimento Scienze della Terra, Università degli Studi di Torino
Email: beatrizyuri.benettisilva@unito.it

Dear Editor,

We sincerely appreciated the reviewers comments and editorial work aimed to improve our manuscript. We have considered the comments and suggestions of the two reviewers, improving the manuscript accordingly.

We have attached a revised version of the manuscript where new parts are highlighted with red text and the deleted ones are strikethrough. In addition, we also provide updated figures. In the following parts, we reply to the reviewers comments specifying in detail how we have addressed the raised points. Original comments are in black text, whereas our replies are in blue text. We indicate with "Line" the corresponding lines, in the revised version of the manuscript with changes marked. In the cases, where we do not share the same point of view of the reviewers, we explain our reasons.

In addition, taking into account reviewers comments to emphasize the subject of the present work we decided to modify the title to "In-sequence tectonic evolution of Ediacaran nappes in the southeastern branch of the Brasília Orogen (SE Brazil): constraints from metamorphic iterative thermodynamic modeling and monazite petrochronology".

Reviewer #1: Relevance of the manuscript to the Lithos audience: This manuscript by Benetti et al. represents a multi-disciplinary attempt to constrain the Neoproterozoic tectono-metamorphic evolution of two nappes within the Brasília orogen in southeast Brazil. The most intriguing result of this study is documentation of differences in age and timing of deep crustal metamorphism that are consistent with thrust loading and subsequent decompression in an evolving orogenic wedge. This manuscript is well aligned with the journal's aim and scope and would be an excellent contribution.

General Comments to the Authors and Editor: I think this manuscript makes an importat contribution to our understanding of the metamorphism and tectonism recorded in the Brasília orogen, and it is very well written. It is certainly suitable for Lithos, and I have only modest comments and suggestions mentioned below. It is an excellent integration of petrology and monazite geochronology. As I am not an expert on the geology of the Brasilia orogen, I have reserved my comments to general ones throughout the text.
We thank the reviewer#1 for his detailed review of our manuscript and your positive comments. We have addressed the raised points, as detailed explained below.
Comments and Suggestions by line for the Authors:

Lines 30-35 I would clarify these sentences by re-writing them as: "The nappes experienced prograde and retrograde metamorphism that progressively decreased toward the bottom of the nappe stack. We attribute this to propagation of older material from inner parts of the orogenic wedge during thrusting of nappes over recently accreted rocks, leading to younger metamorphism in the external parts of the wedge. This mechanism is consistent with the in-sequence fold-and-thrust belt architecture to the ANS."
Done (see Line 31-40).
However, it is not clear to me what you mean by "external parts of the wedge". In the paper, you seem to conclude that the deepest levels of the wedge experienced the youngest metamorphism. Wouldn't it be better to say "deeper" instead of "external"? I may not understand this correctly, but please word it differently so that your audience does understand. You use some of this same text in Lines 606-606. Be sure to clarify this in those lines, too.
When we refer to external parts, we mean the "footwall of the ductile thrust". The text was modified in both suggested parts to make it clear (see Line 38 and 652).
Lines 54-55 I would re-write as "… changes during the development of an orogen as recorded

by its kinematic history and internal structure."
Done (see Line 65-66)
Line 59 "… hinterland of an orogenic wedge."
Done (see Line 73).
Line 60 "… intense debate during the past several decades."
Done (see Line 74).
Lines 61-62 "… that the ANS evolution was due to polymetamorphism related to two separate tectonic events during different orogenic cycles. The first event was…"
Done (see Line 75-78).
Lines 67-68 "… isograds during NW-SE contraction at 600-560 Ma. The tectonic event is attributed to the…"
Done (see Line 83-85).
Lines 69-70 "The second model proposes that the ANS evolution was due to a single orogenic cycle."
Done (see Line 87-88).
Line 70 You cite the authors who prefer the second model at the end of this sentence. It's not necessary to say "According to them…"
Done (see Line 88-89)
Line 78 What you have done is much more than "elementary". I would replace this word with "fundamental".
Done (see Line 97)
Line 79 "internal" should be "internally".
Done (see Line 99).
Line 80 These techniques can be used to make "pseudosections", but more generally, we refer to this as "… databases to create phase equilibria models that can be used to constrain…"
Done (see Line 99-100).
Line 82 Change "to set up" to "to link"
We prefer not to repeat the word "link" in a phrase.
Line 85 "… or titanite can provide ages for specific metamorphic reactions and deformation events…"
Done (see Line 104-105).
Lines 86-88 "This approach is one of the most effective ways to understand the complex frameworks of collisional belts."
Done (see Line 107-108).
Lines 89-92 These two sentences can simply and more effectively occur at the end of the previous paragraph. There's no need to have them as a separate paragraph.
Done (see Line 96-114).
Line 318 H20 should be H2O.
Done (see Line 345).
Line 416 What do you mean by "punctual"? Perhaps you could say "… 84 EMPA spot analyses were…" You could also use this phrase for the beginning of Line 436.
Done (see Line 443 and 463).
Line 446 Th is rarely a trace element in monazite. It often occurs at the wt.% level.
Done (472).
Line 455 It is important to clarify that monazite's microstructural position and its internal chemical zonation both help provide this information.
Done (see Line 481-482).
Line 462-463 I would rephrase this as "If monazite grows at these conditions prior to growth of garnet, the monazite will display… "
Done (see Line 489-490).
Line 464 If garnet is growing and incorporating Y, it is doing so as the product of a reaction

and not as a reactant. I would re-write this as "When monazite grows in equilibrium with garnet, the monazite tends to be depleted in Y since this element partitions strongly in garnet."
Done (see Line 492-493).
Line 484 "The monazite grains…"
Done (see Line 515).
Lines 496-497 "…presented here help elucidate the complex…"
Done (see Line 529).
Lines 516-520 This is what is called a run-on sentence. It would be clearer if you break this long sentence up into two or more sentences.
Done (see Line 552-556).
Line 527 In this line and in Line 83, you use the term "blastesis-deformation" relationships and refer to Passchier and Trouw (2005). "Blastesis" does not occur anywhere in this book. The more common phrase (and also used by these authors) is "porphyroblast-matrix" relationships.
The reference of Passchier and Trouw (2005) used for referring to the "blastesis-deformation" relationships was deleted (see Line 103).
Line 549 Change "time constraints" to "timing constraints".
Done (see Line 590).
Line 593 It is not usually appropriate to cite a reference unless it is either accepted or in press. You should ask the editor if this is okay or not for (Westin et al., submitted).
This reference was deleted (see Line 627 and -639).
Lines 603-606 See my first comment for Lines 30-35.
Done (see Line 652).

Well done!

Thanks again to Rev#1 for the very constructive comments to improve this manuscript.

Gregory Dumond
University of Arkansas

Reviewer #2: B. Benetti and co-authors investigate the tectono-metamorphic evolution of the Andrelândia Nappe System (ANS) in Southern Brasilia Orogen (SBO) using thermodynamic iterative modeling and monazite petrochronology. The main results were determining the maximum P-T conditions and the ages of prograde metamorphism, and part of the retrograde metamorphism, of the Liberdade and the Andrelândia nappes. These results are interpreted in the context of the SBO evolution and collision between the Paranapanema and São Francisco cratons. This work presents a lot of new geochemical and geochronologic data that certainly contribute to the understanding of the regional geology, however, it lacks a clear problematic, and the work is missing a discussion regarding the implications of your work for Tectonic/Petrologic studies worldwide, and/or the evolution of Neoproterozoic fold-and-thrust belts, to deserve publications in a journal like LITHOS. Also the interpretations regarding thrust stacking, decompression and exhumation of the studied complexes are conceptually poor. Authors must go deeper in the bibliography of the formation of FTBs and the tectonics problems behinds it, specially regarding new studies. I have regards in the way you present your geochronological data, once your ages have decrease progressively, using the mean age is meaningless and your must use the ranges of the maximum and minimum age of your samples, it changes your main conclusions. I also suggest estimating depths for the metamorphic events you constrain your P-T-t, using a geothermal gradient for collisional orogens. The beginning of your study is confusing, whereas part of the discussion is clearer, and so you may rebuild part of your introduction and discussion before publication.

We would like to thank Rev#2 for the very detailed and constructive review done. We made significant changes in the abstract and introduction following his suggestion to leave the work problem clear and improve the bibliography. Regarding the geochronological data the EMPA monazite dating, different from other isotopic methodologies, requires that few punctual data be accumulated until achieve an acceptable level of precision (see Williams et al.,2006, Chemical Geology, vol. 225). We explained better this topic below. Finally, the estimative of depths and geothermal gradients were added in the text and new Figs.14 and 15.

Point-by-point Reviews:

Abstract.16-20: useless first and second sentences, I suggest saying directly that you found medium-high P-T rocks in the Andrelandia Nappe System and that you aim to decipher the metamorphic and kinematic evolution of this fold-and-thrust belt. Also, just saying it's a topic of debate is not enough. What is the debate about?
Done (see Line 16-21). Regarding the "topic of debate", how this phrase was deleted, the nature of this discussion is explained after in the introduction (see Line 72-95).
l.23. Prograde metamorphism is a process, so the Nappe does not "attain" it, change by "experienced", and "attained" for your measured P-T.
Done (see Line 24).
l.27 be consistent when using ~ or ca. for temperature.
Done (see Line 25).
l. 29-30. myr instead of Ma if you are referring to an interval of time.
Done (see Line 31).
l.30-31. "prograde and retrograde metamorphism".
Done (see Line 32).
Decrease of what? Depth, T, P ?
The phrase was modified to make clear that the decrease cited is related to the ages (see Line 31-33).
l. 32-35. Here it becomes confusing. The thrusting occur during tectonic burial? What is the older material? The Liberdade Nappe units? Above which younger material? The Andrelandia Nappe units?
The phrase was modified to make it clear that the thrust took place after tectonic burial and the older and younger accreted material cited is correlated to, respectively, the Liberdade and Andrelândia Nappe (see Line 34-38).
If you are interpreting both prograde and retrograde metamorphism occuring during thrust stacking, what changes in you tectonic evolution to trigger retrograde metamorphism?
Several mechanisms could trigger the onset of the thrust stacking, and consequently the retrograde metamorphism in the hanging-wall and prograde in the footwall, such as a change in the critical wedge angle or an insertion of a stiff material under the wedge. However, this is not discussed in this manuscript, being beyond the topic. We mostly focused on the diachronic equilibration (both of prograde and retrograde metamorphisms) within the nappe stack, in the discussion and consequently in the abstract.
First you say that your ages and P-T-t paths record "a single metamorphic cycle of burial and decompression" and after you say that folding and thrusting conduct "a younger metamorphism event on external parts of the wedge". Thus, it's one or multiple metamorphic events? I seems that you still didn't decide if your retrograde metamorphism occur during tectonic burial or exhumation. Same observations for the highlights, please decide if you interpret one single of multiple metamorphic events.
What we were trying to say is that each one of the nappes of the Andrelândia System records only one metamorphic loop (prograde followed for decompression and retrograde metamorphism). This achievement is especially important because, as explained in the

introduction, some research considers that the ANS underwent two metamorphic loops, one of high-pressure and another of high temperature. If so, all the nappes of the system would record two metamorphic loops, which is not the case. Then, we modified the text and emphasized that each one of the nappes underwent one tectonic cycle of burial and decompression in different ages, not the system as a whole as previously written (see Line 28-31).

40-42. Crustal accretion occurs by tectonic processes as well, such as by thrust stacking and this is a process you are focusing on your study, so it's crucial to cite it here.

Done (see Line 46).

Consider reading and citing the works of Davis and Dahlen that explain the growth of fold-and-thrust belts and accretionary wedges, as well as Ruddiman et al., 1997, Willett, 1999, Beaumont et al., 2001; Egholm et al., 2009; Whipple, 2009 for the tectonic vs. erosion role on mountain building.

We added the following references Beaumont et al., 2001, Davies et al., 1983, Whipple, 2009 and, Willett, 1999 (see Line 48-49).

"Tectonic and post-orogenic thinning" by tectonic erosion? Extension? Delamination? Please be more precise.

The phrase was modified to be more precise about the mechanism of crust removal during orogenesis as suggested by rev#2 (see Line 47).

42-45. External and internal "factors" are very broad, and "structure" means nothing in this context, you mean tectonic. I suggest excluding this phrase to avoid mistakes, it's the same as the first one, and does not connect with the next one. Also, surface processes are not discussed on your paper, so I don't see the point on using the first lines of your manuscript to talk about surface-deep Earth interactions.

Done (49-51).

47-49. "the balance of the orogen active forces leads to exhumation" this is a very vague phrase to talk about exhumation. Exhumation actually occurs due to erosion or extension, but it can be forced by tectonic shortening or any geodynamic process forcing rock uplift if your erosion rate is strong enough to indeed "exhume" rocks. Please revise bibliography... (England and Molnar, 1990 and Molnar and England, 1990; works of T. Ehler, B. Carrapa, S. Willett…).

We modified this sentence to highlight the mechanism of exhumation (e.g., erosion, normal faulting, and ductile flow; see Line 54-56). In addition, the references of England & Molnar, 1990; Ring et al., 1999 were added (see Line 56-57).

49-50. How? Thrust stacking increases the geothermal gradient?

Link this quite random phrases to the processes you are studying.

To link the introduction with one of our main conclusions, that is the metamorphism as a consequence of loading of an overlying nappe, a phrase explaining the hot iron model was added. This model admits that the overthrust of hot rocks over colder ones can serve as a heat source for the footwall rocks metamorphism (see Line 62-64). The references of England & Molnar, 1993, and Le Fort, 1975 were added (see line 63-64).

52-57. It's true but quite obvious, any rock record a P-T. Change the goal saying that the P-T recorded in deeply buried rocks is valuable to understand the deep-Earth dynamics of accretionary wedges. Cite also what is still not fully understood amongst the processes that form fold-and-thrust belts (and why P-T-t studies are useful).

Done (see Line 64-68).

60. Exclude "Indeed", it's for when you are arguing about something previously said.

Deleted (see Line 74).

65. Reference, especially when you use ages.

The following references were added Coelho et al., 2017, Li et al., 2021, Reno et al., 2012 and, Trouw et al., 2013 (see Line 81-82).

68. Reference, please.

The following references were added Coelho et al., 2017, Fontainha et al., 2020, Heilbron et al., 2017, Trouw et al., 2013 and, Zuquim et al., 2011 (see Line 84-85).
75. What are the available ages?
We added to the text the published metamorphic ages, which are from 630 to 580 Ma (see Line 93-94).
90. Change "modern techniques in metamorphic petrology and geochronology" for the methods you used, such as pseudosection thermodynamic modeling and in-situ monazite petrocrhonology.
The suggested part was deleted and modified accordingly (see Line 110).
I still think that the aim of your work is too vague, please specify something like "to unravel the depth and timing of tectonic processes forcing the build of the ANS fold-and-thrust belt, such as tectonic burial and exhumation".
We modified the last paragraph of the introduction to be more specific as suggested (See Line 112-113).
111. "bodies" change for "plutons".
Done (see Line 133).
146-154. What are the main lithotypes of the Andrelandia Nappe? At least the ones you cite the ages and P-T conditions.
The Andrelândia Nappe main lithotypes were added (see Line 170-171).
155. This section is already your data? It should be called "Results" and then subdivided in sections such as "Field obsersarvations" or "Structures and stratigraphy". You also should write clearly that these are new data from field work performed in this study.
Done (see line 179-180)
156-159. If you want to keep these phrases, they should come in the Geological setting. "Basement cores" instead of basement nucleus. "Allochtonous units"
We decided to keep this phrase in the field observations section, once it is a brief introduction of the study area, which will be linked with the other paragraphs of the section. The suggested modifications for "basement cores" and "Allochthonous Units" were done (see Lines 183-184).
162. Which minerals are kinematic indicators? Write even if you have a figure.
In this part of the text, we are presenting the field-based observations, then we preferred just adding information about macro-scale kinematic indicators (see Line 187).
173. Same as before, please specify the kinematic indicator.
Same as above, we prefer to give information, in this section, related to field observations. In section 3.2.1, where is described microstructural aspects of the Liberdade Nappe, we added information about which minerals are the kinematic indicators (see Line 233-234).
190. Make it a subsection of your Results section.
Done (see Line 215)
269. It's okay to use mineral abbreviations, but then you should be consistent and use it from the beginning, and including the meaning of abbreviations in you supplementary material.
To be consistent in the whole section, we deleted the mineral abbreviations. In the other sections, they are used and follow Whitney and Evans (2010) as indicated in the Line 228.
272. Use metamorphic paths to when you show the P-T-t paths with the pseudosections. Here, use "metamorphic phase" or "metamorphic assemblage".
Done (see Line 298).
292. Another subsection of "Results".
Done (see Line 319).
334-344. If you have EPMA geochemical composition of your metamorphic minerals, why don't you model the isopleths to show more accurate metamorphic conditions?
In the present work, we adopted as a thermobarometric strategy the iterative thermodynamic modeling (ITM, Lanari & Duesterhoeft 2019; Duesterhoeft & Lanari 2020; Lanari & Hermann 2021), which combines the advantages of both forward (e.g., pseudosection crossed with

mineral isopleths) and inverse thermodynamic models (e.g., multi-equilibrium thermobarometry). ITM builds a forward thermodynamic model and further, performs an iterative optimization through statistical routines that compare model outcomes (e.g., pseudosections and isopleths) and observations (e.g., mineral composition extracted from the compositional maps). The mineral compositions obtained through the EPMA were used to calibrate quantitative compositional maps (see Fig. 7 and 9). The compositions used in iterative optimization are indicated in red circles in the compositional maps (see Fig. 7, 9, and sup. Fig. file A2 e A3). These chosen mineral compositions were used for calculating the quality factor of mineral composition (Q_{cmp}; see sup. Fig. file A4, A5, and A6). The Q_{cmp} will evaluate where in the *P-T* diagram the chosen mineral composition will best match with the model. In other words, the ITM will show results of the modeled isopleths in a different graphical interface. Instead of displaying the mineral composition isolines and the user checks the match between them and the observed mineral composition, the ITM calculates the isopleths and then checks itself the probability of specific mineral composition being stable (Q_{cmp}=100%) in the P-T diagram (see sup. Fig. file A4, A5, and A6). In a certain way, quality factors (for modes and mineral compositions), represented in quality factors maps, give an idea of the fit (and/or misfit) between modelled modes and mineral compositions (i.e., the isopleths) against the observed ones in the samples. In addition, we would like to point out that there is no work in the literature saying that the methodology applied in this work is less accurate than isopleth thermobarometry. On the contrary, we regard this methodology as a leading-edge method to extract as much as possible information on P-T-X sample's evolution and statistically check/visualizing the results with higher accuracy (see e.g. Lanari & Hermann 2021).

345-357. You cite intersections between mineral chemistry, but you don't show them in the figure. Please show the isopleths if you calculate them.
See the comment above regarding the compositional isopleths calculation (but please note how this is expressed in the quality factors maps). The areas where the thermodynamic model reproduces the plagioclase core and rim, muscovite, and garnet (Q_{cmp}=100%) compositions are delimited in Fig. 7b and 9b. In the supplementary figure A4, A5, and A6 are displayed the *P-T* maps of the mineral chemistry composition quality factor (Q_{cmp}).
390. Another subsection of "Results".
Done (see Line 417).
472. "two episodes of monazite growth"
Done (see Line 502).
475. After garnet crystallization.
Done (see Line 505).
477. Early prograde metamorphism. Exclude "path"
Done (see Line 507).
476-478. This phrase relates with the first metamorphic episode or with the second one?
I was added in text that the Th-rich are related to the M_{LN1} stage (see Line 508).
474-480. Please interpret your ages based on their range of dates, the mean age here is poor in significance once you have a clear gradual decrease of your ages. For minimum ages, use your younger date.
In our manuscript, we followed the recommendations of Williams et al. (2006) for reporting microprobe monazite ages, which require a different treatment compared to some isotopic techniques. For EMPA monazites geochronology is recommended that individual analysis be referred to as “measurements” or “analyses”, but not as dates, or ages (which carries a geological meaning). According to Williams et al. (2006, Chemical Geology, vol. 225) pag. 5: “the essence of the method (EMPA monazite dating) is that numerous data points (analysis) are collected from each monazite compositional domain in order to produce a single date with an associated error”. Therefore, the EMPA monazite geochronology approach requires that the

individual measurements are accumulated until an acceptable level of precision has been achieved (weighted mean age) (see e.g., Fig. 5 and 6 in Williams et al. (2006).
Additionally, the mean age 608 +/- 4 Ma appears here but not in the results, is it correct?
Sorry for the mistake, it was an oversight, the right age is 609±4 Ma (see Line 506).
Can you associate your older age with the S1 foliation?
Yes, we can. This information was added to the text (see Line 508).
484-491. Same about the minimum age, use your younger date in this context.
Add "Ma" to the age.
As explained above, it is necessary in EMPA monazite dating that the analyses of each compositional domain are combined using a weighted mean or other statistical procedure to place constraints on geological features (see Williams et al. 2006).
Also, time of deformation is very generic if you have several deformational episodes, repeat it's linked with S2 foliation, if it's your interpretation.
Done (see Line 511).
Also, if S2 formation in the Andrelandia Nappe forms during prograde metamorphism, I think it's inconsistent relating your S2 with the "decompression". I think conceptual discussion regarding tectonic processes generating foliations and metamorphic assemblages is lacking.
We related the LN S_2 foliation with decompression, and in opposite the AN S_2 fabric with prograde metamorphism. These temporal contrasts observed between the prograde and retrograde metamorphism between the nappes were further explained in section 4.3 by the mechanism of thrust load and decompression (see Line 612-617).
Can you estimate a geothermal gradient? You could then estimate the depth of metamorphic events using your P-T estimates, and this would enrich your discussion and Fig. 15.
We added the data of depth and the apparent geothermal gradient of both nappes (see Line 534-536 and 543-544), and Fig 14 and 15 were modified adding information of depth in the P-T diagrams.
502-505. Same observation regarding the minimum age, and this would change your abstract and other parts of your text in which you use the mean age. After this, clarify if the minimum age of your dated crystal is linked with MLN2 or MLN3 line 505.
See the comment above regarding the strategies to present the EMPA monazite ages.
509. Same observation as before about the minimum age.
See the comment above regarding the strategies to present the EMPA monazite ages.
515-539. These paragraphs are useful only if you discuss your data along with, that is the purpose of this chapter. Please give considerations showing why your data are important to disentangle, at least partially, the different interpretations previously given.
Our interpretation that the monazite populations are linked with the episodic growth during a single metamorphic loop of prograde and retrograde metamorphism differs from those that interpret them as related to two metamorphic events, one of high pressure and another of high temperature as a consequence of two different tectonic events (e.g., Brasilia and Ribeira collisions). To highlight this, we included a phrase explaining that the petrochronology study performed provided means for linking the monazite ages with episodic growth of monazites in a single metamorphic loop of burial and decompression in each of the nappes of the system, in the opposite of interpreting the spread of ages with multiple metamorphic loops (see Line 576-579).
Also, some of these phrases are conceptually wrong, such as "heating during exhumation", if you want to bring these kinds of phrases, you should discuss the significance of them.
This expression was modified to “heating during decompression” (see Line 562) to make it conceptually right.
I suggest excluding the section "Tectonic implications", once it's basically the same as "Tectonometamorphic evolution of the Andrelandia Nappe System (ANS)" and exclude phrases
We prefer to leave the sections “Tectono-metamorphic evolution of the Andrelandia Nappe System (ANS)” and “Tectonic implications” as previously done. We do not think that both

sections are the same. In the tectono-metamorphic evolution of the ANS we present P-T-t-D paths of both studied nappes and compare our achievements with those from the literature. While the tectonic implications, we explained the geodynamic mechanism responsible for the P-T-t-D paths of the nappes.
541-543. For the next sentences, please bring them along with the discussion with previous data.
See the justificative given above to let these sections separated.
567. Specify "decrease". Depth? Metamorphic P-T?
The phrase was modified to highlight that the decrease written is related to the metamorphic ages (see Line 606-610).
569-576. Cite Fig. 15 here. I suggest merging this paragraph and the next one, once they say the same thing, but the second with ages and contextualization within the regional geology.
Done (see 610-612).
577-593. This paragraph and the previous one, coupled with Fig. 15 are quite clear. So I suggest adjusting your abstract and rebuild part of your introduction based on the structural and metamorphic processes playing in the formation of accretionary wedges, more than with the general phrases that you bring in the introduction that are not really related with your work. Your focus is deep-seated processes forming fold-and-thrust belts, thus focus on that.
The suggested modifications of the abstract and introduction were done. We included in the introduction an explanation of two important mechanisms linked to the main topic of our work, the in-sequence flow of deep-seated rocks (see line 57-59) and the hot iron model (see line 62-64).
Also, it lacks some sentences saying what's the relevance of your work in a global context, or why your study is important for the general knowledge of fold-and-thrust belts etc. Otherwise the relevance of your work keeps too regional.
Two sentences were added to give a more global context for our work (see Lines 618-622). We tried to emphasize that the in-sequence thrust-and-fold architecture of the ANS is also described in several orogenic belts worldwide, suggesting that the mechanism of thrust-and-fold nappes propagation over recent accreted material can induce younger metamorphism and could be used to explain the structural and metamorphic record of collisional wedges.
584-606. Your conclusions are clearer than your abstract. Also in the discussion and conclusions you don't discuss single metamorphic event of multiple, as you does in the abstract in a confusing way. I suggest changing the focus in the abstract in a way to avoid misinterpretations.
We agree that we did not make clear in the text what we meant about the single metamorphic event. The way we wrote previously seemed that the whole ANS underwent a single metamorphic loop. We explained better this in the text (see Lines 576-579 and 586-589) and modified the abstract (see Line 28-31) to make clear that we are saying that each one of the nappes underwent one single metamorphic loop of burial and decompression, rather two loops (one of high pressure and a second of high temperature), as interpreted for some authors.

ABSTRACT

The metamorphic and kinematic evolution of medium-high grade rocks of the Andrelândia Nappe System (ANS), the orogenic wedge of the Southern Brasilia Orogen (SBO), was investigated in this work. Field and microstructural observations were combined with metamorphic petrology (i.e., iterative thermodynamic modeling) and monazite petrochronology to reconstruct the tectono-metamorphic history of the ANS rocks. The Liberdade Nappe experienced prograde metamorphism at *ca.* 610 Ma, achieving peak metamorphic conditions of *ca.* 650°C and 9.5-10 kbar. This stage was followed by isothermal decompression linked to tectonic transport toward SE, at *ca.* 570 Ma. On the contrary, the Andrelândia Nappe experienced prograde metamorphism later, at *ca.* 580 Ma, reaching peak metamorphic conditions of *ca.* 680°C and 11-12 kbar. The obtained results indicate that each nappe of the Andrelândia System records a single metamorphic cycle of burial and decompression, although it took place at different ages over a period of *ca.* 60 myr, from 630 to 570 Ma. The nappes experienced prograde and retrograde metamorphism whose ages progressively decreased toward the bottom of the nappe stack. We attribute this pattern to propagation of older buried material from the orogenic wedge (i.e., Liberdade Nappe), via thrust-and-fold, upon recently accreted rocks (i.e., Andrelândia Nappe), conducting a younger metamorphism event on the footwall of the ductile thrusted nappes. This mechanism is consistent with the ANS in-sequence fold-and-thrust architecture.

KEYWORDS:

Monazite petrochronology, iterative thermodynamic modeling, Brasília Orogen metamorphism, P-T-t-D paths

HIGHLIGHTS

- Tectono-thermal history of Andrelândia Nappe System (ANS) was investigated.
- Each nappe of ANS records a single, diachronous, cycle of burial and decompression.
- Decompression in the hanging wall was coeval with burial in footwall rocks.
- In-sequence propagation of thrust-and-fold nappes drives younger metamorphic events.

In-sequence tectonic evolution of Ediacaran nappes in the southeastern branch of the Brasília Orogen (SE Brazil): constraints from metamorphic iterative thermodynamic modeling and monazite petrochronology

Beatriz Benetti[a,b*], Mario da Costa Campos Neto[b], Rodolfo Carosi[a], George Luvizotto[c], Salvatore Iaccarino[a], Chiara Montomoli[a,d]

Corresponding author:

*Beatriz Benetti – beatrizyuri.benettisilva@unito.it - ORCID: 0000-0001-5698-3075

Present address: Geological Survey of Brazil – SGB/CPRM, Av Pasteur 404, Rio de Janeiro - RJ, Brazil

Affiliations:

a Dipartimento di Scienze della Terra, Università degli Studi di Torino, Turin, Italy

b Instituto de Geociências, Universidade de São Paulo, São Paulo, Brazil

c Departamento de Geologia, Universidade do Estado de São Paulo

d Istituto di Geoscienze e Georisorse, IGG-CNR, Pisa, Italy

ABSTRACT

The metamorphic and kinematic evolution of medium-high grade rocks of the Andrelândia Nappe System (ANS), the orogenic wedge of the Southern Brasilia Orogen (SBO), was investigated in this work. Field and microstructural observations were combined with metamorphic petrology (i.e., iterative thermodynamic modeling) and monazite petrochronology to reconstruct the tectono-metamorphic history of the ANS rocks. The Liberdade Nappe experienced prograde metamorphism at *ca.* 610 Ma, achieving peak metamorphic conditions of *ca.* 650°C and 9.5-10 kbar. This stage was followed by isothermal decompression linked to tectonic transport toward SE, at *ca.* 570 Ma. On the contrary, the Andrelândia Nappe experienced prograde metamorphism later, at *ca.* 580 Ma, reaching peak metamorphic conditions of *ca.* 680°C and 11-12 kbar. The obtained results indicate that each nappe of the Andrelândia System records a single metamorphic cycle of burial and decompression, although it took place at different ages over a period of *ca.* 60 myr, from 630 to 570 Ma. The nappes experienced prograde and retrograde metamorphism whose ages progressively decreased toward the bottom of the nappe stack. We attribute this pattern to propagation of older buried material from the orogenic wedge (i.e., Liberdade Nappe), via thrust-and-fold, upon recently accreted rocks (i.e., Andrelândia Nappe), conducting a younger metamorphism event on the footwall of the ductile thrusted nappes. This mechanism is consistent with the ANS in-sequence fold-and-thrust architecture.

KEYWORDS:

Monazite petrochronology, iterative thermodynamic modeling, Brasília Orogen metamorphism, P-T-t-D paths

1. INTRODUCTION

The growth of a mountain belt is controlled by the balance among accretion of crustal material, such as sediments and magma addition as well as thrust stacking, and removal by erosion, delamination, and post-orogenic extension (Beaumont et al., 2001; Davies et al., 1983; Jamieson and Beaumont, 2013; Vanderhaeghe, 2012; Whipple, 2009; Willett, 1999). An orogenic wedge is constituted by crustal material mainly detached from the subducted lithosphere, accreted, and stored within the orogenic system (Vanderhaeghe, 2012; Vanderhaeghe et al., 2003). During orogenesis, erosion, normal faulting, and ductile flow can lead to exhumation of the deep-seated rocks at the front of the crustal wedge (DeCelles and Mitra, 1995; England & Molnar, 1990; Ring et al., 1999; Vanderhaeghe et al., 2003). Deformation and ductile flow can follow an in-sequence pattern when they present progressive age decreases in the same direction of the tectonic transport (Weller et al., 2021). The accumulation of crustal material within an orogen enriched in radioactive heat-production elements, such as U, Th, and K, modifies its crustal geothermal gradient (England and Thompson, 1984; Rudnick and Fountain, 1995). Moreover, thrust stacking of hot rocks upon colder ones can also be a heat source for metamorphism in the footwall ("the hot iron model"; England & Molnar, 1993; Le Fort, 1975). Therefore, the deep-seated crustal rocks are able to record pressure (*P*) and temperature (*T*) changes during the development of an orogen as recorded by its kinematic and internal structure, providing valuable information to understand the deep dynamics of collisional wedges.

The Andrelândia Nappe System (ANS) is regarded as the Southern Brasilia Orogen (SBO) hinterland of an orogenic wedge. Its tectono-metamorphic evolution has been a target of intense debate during the past several decades. Some researchers (Coelho et al., 2017; Fontainha et al., 2020; Li et., 2021; Trouw et al., 2013) argue that the ANS evolution was due to polymetamorphism related to two separate tectonic events during different orogenic cycles. The first event was related to high-P metamorphic conditions testified by the HP-granulites and E/NE nappe stacking, owing to the Paranapanema and São Francisco Cratons collision in the period from *ca.* 630 to 600 Ma (Coelho et al., 2017; Li et al., 2021; Reno et al., 2012; Trouw et al., 2013). It was followed by a second orogenic event, characterized by medium pressure, greenschist- to amphibolite-facies conditions in the staurolite and sillimanite zones, during NW-SE contraction at 600-560 Ma (Coelho et al., 2017; Fontainha et al., 2020; Heilbron et al., 2017; Trouw et al., 2013; Zuquim et al., 2011). This tectonic event is attributed to the Central Ribeira Orogeny (Fig. 1b). The second model proposes that the ANS evolution was due to a single orogenic cycle. The ANS tectono-metamorphic evolution is linked to the Paranapanema block collision against the São Francisco Craton (Campos Neto et al., 2011; Frugis et al., 2018; Westin et al., 2021). In this hypothesis, the sillimanite and staurolite presence documented by the ANS rocks would result from the decompression/exhumation of the nappe pile rather than testify a second tectono-thermal event. The available metamorphic ages, from 630 to 580 Ma, indicate a thrust propagation from WSW to ENE toward the São Francisco Craton southern edge (Westin et al., 2021 and references therein).

The reconstruction of Pressure-Temperature-time-Deformation (*P-T-t-D*) paths provide fundamental information to understand the tectonic and metamorphic events experienced by rocks accreted to the orogenic wedge. Primarily, the application of internally consistent databases to create phase equilibria models that can be used to constrain metamorphic conditions (Powell and Holland, 2008; Waters, 2019). This data can be linked with microstructural observations to set up the rock fabric relationships with the metamorphic mineral assemblage, i.e., the so-called blastesis-deformation relationships. In addition, the in-situ dating of accessory minerals, such as monazite, zircon, or titanite can provide ages for specific metamorphic reactions and deformation events (e.g., Bosse and Villa, 2019; Kohn et al., 2017; Williams and Jercinovic, 2012). This approach is one of the most effective ways to understand the complex frameworks of collisional belts (Carosi et al., 2018; Waters, 2019). In this contribution, we combine field and microstructural observations with iterative metamorphic thermodynamic modeling and *in-situ* monazite geochronology. This integrative approach provides information about the timing of tectonic processes that drove the build of the ANS fold-and-thrust belt, such as tectonic burial and exhumation, and allowed the reconstruction of the tectono-metamorphic history of the ANS rocks.

2. GEOLOGICAL SETTING

The Brazilian-Pan African event is the name given to a series of diachronic collisions in the São Francisco-Congo Craton side of the West Gondwana paleocontinent (Cordani et al., 2003; Ganade De Araujo et al., 2014; Fig. 1). The Southern Brasilia Orogen (SBO) is one of the orogenic belts built during this tectonic event (Cordani et al., 2003; Fig. 1 and 2). The SBO evolved from the lateral collision between the Paranapanema paleocontinent, the active margin, against the São Francisco paleocontinent, representing the SBO passive margin (Campos Neto, 2000; Campos Neto et al., 2011; Trouw et al., 2013, 2000).

The SBO final architecture resulted in an almost flat-lying fold-nappe pile, with top-to-the-east/northeast tectonic transport (Fig. 3). Three tectonic domains are recognized within the SBO (Campos Neto, 2000; Campos Neto et al., 2011, 2021; Trouw et al., 2013, 2000; Fig. 2 and 3): (1) the active margin of the Paranapanema paleocontinent, constituted by the granulites and migmatites of the Socorro-Guaxupé Nappe, (2) the orogenic wedge hinterland, a pile of metasedimentary nappes of the Andrelândia Nappe System, (3) the passive margin related to the São Francisco paleocontinent, made by the psamo-pelitic sequences of the Carrancas and Lima Duarte Nappes. These tectonics domains are intruded by leucogranites (Fig. 3) and A-type granitic rocks (i.e., Itu Granite Province, Pedra Branca, and Capituva Plutons; Fig. 2) interpreted as post-orogenic plutons.

The SBO is split into two segments by a tectonic window (Fig. 2) exposing the Archean-Paleoproterozoic migmatitic orthogneiss from the basement complexes (Cioffi et al., 2019, 2016; Westin et al., 2016). The Andrelândia Nappe System (ANS) is sandwiched among the UHT-HT metamorphic rocks of the Socorro-Guaxupé Nappe (Campos Neto and Caby, 1999; Motta et al., 2021; Rocha et al., 2017a; Tedeschi et al., 2018; Fig. 3) at the top and, by the low- to medium temperature metasedimentary rocks of the passive margin covers (Fig. 2 and Fig. 3), at the bottom. Internally, the ANS is divided from its uppermost structural level to the bottom by the Três Pontas-Varginha and Carmo da Cachoeira Nappes in the northern sector. In the southern sector, the ANS is segmented into the Pouso Alto (or Aiuruoca, Carvalhos, and Serra da Natureza Klippes equivalent), Liberdade, and Andrelândia Nappes (Fig. 3). Two characteristics are remarkable in the ANS: i) its inverted metamorphic pattern, in which rocks in the high-P granulite metamorphic facies structurally overlap those in amphibolite facies conditions (Campos Neto and Caby, 2000, 1999; Garcia and Campos Neto, 2003; Motta and Moraes, 2017; Trouw et al., 2000, 1998); ii) the decrease of metamorphic ages eastward, which is the same sense of the non-coaxial ductile flow (Campos Neto et al., 2011; Westin et al., 2021).

The Três Pontas-Varginha, Pouso Alto Nappe, and the Auiruoca, Carvalhos, and Serra da Natureza Klippes, lay on the top of the ANS stack. They are made of K-feldspar+garnet+kyanite+rutile-bearing gneiss. These rocks attained metamorphic conditions of *ca*. 830°-900°C and 12-16 kbar in the high-pressure granulite facies conditions (Campos Neto et al., 2010; Campos Neto and Caby, 2000; Cioffi et al., 2012; Fumes et al., 2021; Garcia and Campos Neto, 2003; Li et al., 2021; Reno et al., 2009).

The Liberdade Nappe (LN), the intermediate unit of the ANS, is composed of garnet+kyanite+ilmenite(±sillimanite±rutile)-bearing micaschist and paragneiss with subordinate quartzite, metabasite, and calc-silicate lenses. Metamorphic conditions, in metapelites, are constrained in the *P*-*T* range of 642-715°C and 6-10 kbar (Coelho et al., 2017; Motta and Moraes, 2017; Rodrigues et al., 2019; Santos et al., 2004). Zircon and monazite U-Pb dating retrieved ages around 620-615 Ma (Coelho et al., 2017; Motta and Moraes, 2017; Westin et al., 2021). Moreover, the metamafic rocks, interpreted as retroeclogites (Campos Neto and Caby, 1999; Coelho et al., 2017; Reno et al., 2009; Trouw et al., 2013), experienced *P*-*T* conditions around 700°-800°C and 12-16 kbar (Coelho et al., 2017; Reno et al., 2009; Tedeschi et al., 2017). The metamafic rocks present two clusters of metamorphic ages, the first around 680-660 Ma (Campos Neto et al., 2011; Reno et al., 2009), and the other around 630-625 Ma (Coelho et al., 2017; Tedeschi et al., 2017).

The Andrelândia (AN) and Carmo da Cachoeira Nappes are at the bottom of the ANS stack. They are internally constituted by, from the top to the base, micaschists intercalated with metapsamites, metawackes, and micaschists. The AN displays an inverted metamorphic gradient in which "peak" mineral assemblages vary from garnet+biotite+staurolite at its bottom to the kyanite+garnet+melt at the top. The Andrelândia and Carmo da Cachoeira Nappes attained peak conditions around 650-670°C and 9-10 kbar in *ca.* 600 Ma, followed by almost isothermal decompression in the time span of 600-575 Ma (Frugis et al., 2018; Marimon et al., 2022; Motta and Moraes, 2017; Reno et al., 2012; Santos et al., 2004; Westin et al., 2021).

3. RESULTS

3.1 Field observations

The study area is located in southeast Brazil, in the Minas Gerais state around Pouso Alto County. It comprises a geological section from SW to NE in the Andrelândia Nappe System southern sector (Figs. 2 and 4), highlighting all of its allochthonous units along with the basement cores of the nappe system.

The Pouso Alto Nappe has a spoon-shaped cylindrical SW-oriented synform, with W-SW plunging of the mineral and stretched lineations, and a general transport toward NE evidenced by asymmetric mafic boudin and *S*-*C* fabric kinematic indicators (Fig. 4a and b). The main lithotype described is a medium- to coarse-grained K-feldspar+garnet+kyanite+rutile(±ilmenite±biotite)-bearing gneiss.

The Liberdade Nappe is represented by fine- to medium-grained garnet+ilmenite (±sillimanite ±rutile±kyanite±staurolite)-bearing micaschist interlayered with quartzite. Micaschist displays a main spaced disjunctive schistosity, defined by biotite, white mica, and aluminum silicates shape preferred orientation (SPO). Intrafolial stretched isoclinal passive folds are observed. The ensemble of the foliation describes a large cylindrical synform with an SW-oriented B-axis in a type-3 superposition pattern (Ramsay, 1962) over recumbent isoclinal folding between the basement nucleus and the metasedimentary sequence (Fig. 3). The mineral (sillimanite/fibrolite and micas) lineations are mainly oriented to SE, which, coupled with some kinematics indicators (*S*-*C* fabric and asymmetrical strain shadow structures), point to an eastward transport of the nappe. The Pouso Alegre Complex is made by orthogneisses of a tonalite-granite series related to the Paleoproterozoic basement (Cioffi et al., 2016). A leucogranite body intrudes micaschist of the Liberdade Nappe, the Alagoa migmatite, and the Pouso Alegre Complex (Fig. 3, 4a, and b).

The Andrelândia Nappe crops out in the north of the study area (Fig. 4a and b). It is made of grayish metawackes, and at its lithostratigraphic boundaries metapelites associations prevail. The main lithology described is a garnet+kyanite(±staurolite)-bearing gneiss. The main foliation is a spaced disjunctive schistosity identified by SPO on white mica, biotite, and kyanite. The schistosity strikes ENE-WNW with dips varying from low to high angles, between 20°-80° toward the north. White mica, biotite, quartz, and kyanite are responsible for outlining the mineral and stretching lineation, which trends between N90°-N120° and plunges 10°-50° to E/SE. A kinematic change between the Pouso Alto Nappe, and the Liberdade and Andrelândia is noticed in the area. Whereas the upper nappe points to northeastward tectonic transport, the middle and lower suggest an east-southeastward direction.

3.2 ***Petrography, microstructural relationships, and mineral chemistry***

In order to constrain the relationships between mineral growth and deformation (Fig. 5), several samples from Liberdade and Andrelândia Nappes were petrographically studied. One representative sample of each nappe was selected for performing full thin-sections maps acquired using the Scanning Electron Microscopy and Mineral Liberation Analyzer (SEM-MLA; supplementary figures A1). The location of samples is given in Fig. 4a. An area of each thin-section mapped containing the inferred peak mineral assemblage, avoiding retrometamorphic textures where possible, was investigated using X-ray maps acquired by an electron probe micro-analyzer (EMPA). The analytical procedure employed for EMPA analysis is described in Appendix A. The X-ray maps were converted into oxide weight percentage maps applying internal standards (Andrade et al., 2006) in the software XMapTools 3.4 (Lanari et al., 2014, 2019). Such areas were the basis for estimating the Local Bulk Composition (LBC) needed for petrological modeling (see section 5). The mineral abbreviations follow Whitney and Evans (2010).

3.2.1 Liberdade Nappe (LN)

The Liberdade Nappe micaschist is made up of quartz+plagioclase+white mica+biotite+garnet+ilmenite(±sillimanite±rutile+kyanite±staurolite). The LN displays a spaced disjunctive schistosity (S_2, Fig. 6a), and in some portions presents microstructures of tectonic transport such as a *S*-*C* fabric and isoclinal folds, made up mainly of white mica and sillimanite, denoting top-to-the-SE motion. Quartz has slightly lobate contacts (Fig. 6a), and plagioclase has undulose extinction. The quartz features reveal that this mineral was recrystallized due to the grain boundary migration (GBM) regime and underwent the grain boundary area reduction (GBAR; Passchier and Trouw, 2005). Garnet porphyroblast has in several circumstances a skeletal microstructure (Fig. 6b). It also shows S-shaped inclusions made of quartz (Fig. 6c), defining an internal foliation that is not continuous with the external one. Then, garnet is regarded as a pre- to early-syn-tectonic mineral with respect to the S_2 schistosity. Sillimanite is present as fibrolite, it replaces partial to completely garnet porphyroblasts, forming pseudomorphs (Fig. 6d), and also occurs along intrafolial isoclinal folds (Fig. 6e). Subidiomorphic relic of kyanite wrapped by white mica is observed (Fig. 6f). Staurolite, in a very low modal amount, is fine-grained and often related to garnet rims. Rutile is enclosed in garnet and in the matrix is usually rimmed by ilmenite.

The relationships among minerals suggest three metamorphic stages, here referred as M_{LN1}, M_{LN2}, and M_{LN3}, for the Liberdade Nappe micaschist (Fig. 5). The M_{LN1} stage is pre-S_2, related to prograde/peak metamorphism and it is characterized by quartz+plagioclase+white mica+biotite+garnet+rutile+kyanite(?) as the equilibrium assemblage in the rock. The M_{LN2} stage, in which quartz+plagioclase+white mica+biotite+garnet+kyanite(?)+ilmenite is inferred to be stable, represents a post-peak mineral assemblage. Finally, sillimanite and staurolite are regarded as phases that grew during the late stages of the metamorphic path (M_{LN3} and Syn-S_2).

Sample NESG-388 (Fig. 4a, supplementary figure A1) was selected for the LN mineral chemistry investigation and petrological modeling. The NESG-388 is a white mica+biotite+garnet+ilmenite-bearing mylonitic schist with minor sillimanite, rutile, and staurolite (Fig. 7a). Plagioclase is compositionally zoned, and its anorthite content increases from core to rim (XAn –0.20-0.32) (Fig. 7b). Garnet end-members vary slightly from core to rim: almandine (XAlm)=0.81-0.79, pyrope (XPrp)=0.11-0.07, spessartine (XSps) =0.05-0.06 and grossular (XGrs)=0.05-0.06 (Fig. 7c-f). The Ti (a.p.f.u) in biotite decreases toward the rim, ranging from 0.14 to 0.09, whereas the #Mg (Mg/Fe^{+2}+Mg) ratio displays an inverse correlation, increasing toward the rims, varying from 0.37 to 0.43 (supplementary figures A2a and b). The Si^{4+} (a.p.f.u) of white mica varies from 3.04 to 3.12 (supplementary figure A2d).

3.2.2 *Andrelândia Nappe*

The Andrelândia Nappe is constituted by the major phases: quartz+plagioclase+biotite+white mica+garnet+kyanite+ilmenite(±sillimanite±staurolite) and tourmaline+apatite+monazite+zircon+rutile as accessories. The AN has a S_2 foliation characterized by discontinuous millimetric compositional layers of granoblastic, made by quartz and plagioclase, and lepidoblastic, constituted by white mica and biotite with subordinate garnet and kyanite (Fig. 8a). The AN close to the contact with the Liberdade Nappe is affected by shearing and displays a mylonitic fabric (post-S_2). The kinematic indicators described in the sheared gneisses are S-C fabric and white mica-fish, which point to a top-to-the-E/ESE tectonic transport. Quartz is a medium- to coarse-grained mineral with irregular and lobate boundaries, typical of the GBM recrystallization mechanism (Law, 2014).

Garnet is present as porphyroblast (≤2 cm in size) (Fig. 8b). Discontinuous inclusion trails of opaque minerals within garnet, with respect to the S_2 fabric, testify to the inter-tectonic nature of this mineral (Fig. 8b and d). Thin graphite crystals, ilmenite, and rutile are the typical inclusions in garnet, and staurolite, quartz, plagioclase, biotite, and white mica are subordinate. Kyanite is a coarse-grained subidiomorphic crystal with a long axis aligned along the S_2 foliation (Fig. 8b). Twinning in kyanite is observed. Late fibrolite growth (post-S_2) along shear bands and replacing biotite crystals are observed (Fig. 8c and d). Two generations of staurolite were observed, the first is characterized by tiny crystals enclosed in garnet, whereas the second one is in the matrix, often around garnet rims. A staurolite with biotite and sillimanite inclusions aligned with the external foliation, made by sillimanite, quartz, and biotite, denotes a syn-tectonic origin regarding the post-S_2 fabric (Fig. 8d). The contact between staurolite and garnet, as well as the abrupt change of the internal foliation of both minerals, suggest a pattern of porphyroblasts amalgamated (Fig. 8d, e.g., Passchier and Trouw, 2005).

Based on the above description, three main stages of mineral equilibration were recognized (Fig. 5). The early prograde assemblage (M_{AN1}), preserved in garnet core, is constituted by garnet(core)+quartz+plagioclase+biotite+white mica+staurolite+rutile. The peak assemblage (M_{AN2}) is coeval with the S_2 foliation and is marked by the appearance of kyanite and ilmenite and the consumption of staurolite and rutile. The M_{AN3} assemblage corresponds to retrograde metamorphic assemblage, characterized by a second growth of staurolite around garnet rims together with the late fibrolite appearance, and structures related to the tectonic transport (post-S_2 foliation).

Sample NESG-401 was chosen for a detailed chemical investigation (Fig. 4a, supplementary figure A1). The gneiss is composed of quartz+plagioclase+biotite+white mica+garnet+ilmenite and minor apatite (Fig. 9a). This sample is white mica-poor, which is restricted to the garnet strain shadow zones (supplementary figure A1 and Fig. 9a). The plagioclase is zoned, displaying Ca-poor cores (XAn -0.22) and Ca-rich rims (XAn -0.32). The highest Ca-content (XAn -0.34) occurs in crystals that bound garnet (Fig. 9b). There are two garnet crystals in the X-ray mapped area. The large garnet porphyroblast displays a bell shape profile, whereas the smaller one presents an almost flat profile (Fig. 9c, d, e, and f). The garnet porphyroblast shows an increase in almandine and pyrope toward the rim, whereas spessartine and grossular display the inverse pattern (Core- XAlm-0.6, XPrp-0.06, XSps -0.1, XGrs-0.22; Rim- XAlm-0.72, XPrp-0.13, XSps-0.03, XGrs-0.08) (Fig. 9c, d, e, and f). Spessartine displays a sharp increase in the outermost rim (XSps-0.09/0.1) in both garnet crystals. The biotite composition varies according to its structural position. Crystals close to garnet have higher #Mg and lower Ti (a.p.f.u) compared to grains far from garnet (Bt near garnet XMg- 0.54-0.52 and Ti(a.p.f.u)- 0.8-0.10; Bt in matrix XMg-0.5-0.51 and

Ti(a.p.f.u)- 0.11-0.12) (supplementary figure A3a and b). The Si^{4+} content in white mica is close to the muscovite end-member, between 3.00-3.08 a.p.f.u. (supplementary figure A3d).

3.3 Iterative Thermodynamic Modeling (ITM) and P-T path

The iterative thermodynamic modeling (ITM) integrated with quantitative compositional mapping was applied as the strategy for setting up the metamorphic history of the Andrelândia and Liberdade Nappes using the software Bingo-Antidote a XMapTools add-on (Duesterhoeft and Lanari, 2020; Lanari and Hermann, 2021). This approach provides a means of investigating rocks that were not fully re-equilibrated during their metamorphic paths. Through the quantitative compositional maps, areas\phases within a sample that best represents the reactive phases can be selected for the local bulk composition (LBC) calculation. Furthermore, the Bingo-Antidote software provides series of statistics routines that compare the model results with the observed mineral assemblage, modes, and phase compositions for the LBC studied. The bingo routines calculate the model quality, assessing as much as it matches with the LBC mineral assemblage (Q_{asm}), mineral modes (Q_{mode}), and mineral compositions (Q_{cmp}). The quality factors Q_{asm}, Q_{mode}, and Q_{cmp} vary from 0%, which means there is no match between the model and LBC observations, and 100%, meaning that the model perfectly reproduces the LBC features. In addition, the antidote provides routines, for instance the recipe 14, to evaluate how the quality factors change within the model P-T(-X). The Andrelândia and Liberdade Nappes thin-section areas investigated for obtaining LBCs and mineral compositions (Q_{cmp}) quality factors are displayed in Fig. 7a, 9a, supplementary figures A1, A2, and A3. The maps of quality factors from both samples are shown in supplementary figures A4, A5, and A6.

The isochemical diagrams were calculated for the local bulk composition (LBC) obtained by the Bingo-Antidote using the Theriak-Domino software (de Capitani and Petrakakis, 2010; de Capitani and Brown, 1987) to illustrate the stability of mineral fields. The calculations were performed in the chemical system MnO-Na_2O-CaO-K_2O-FeO-MgO-Al_2O_3-TiO_2-SiO_2-H_2O. The water amount was chosen using recipe 14 of the antidote, a statistical routine that asses how the quality factors (Q_{asm}, Q_{mode}, and Q_{cmp}), the mineral chemistry, and mode would vary along a given range of H_2O, at fixed *P-T* conditions. The diagrams were calculated for the *P-T* range of 4-12 kbar and 550-725 °C. The database tc55 (Holland and Powell, 1998), provided and employed in the Bingo-Antidote software, was used for the isochemical diagrams calculations. The respective solution models were utilized: feldspar (Baldwin et al., 2005), garnet (White et al., 2005), biotite (White et al., 2005), staurolite (Holland and Powell, 1998), cordierite (Holland and Powell, 1998), white mica (Coggon and Holland, 2002), ilmenite (White et al., 2007) and melt (White et al., 2007).

3.3.1 Sample NESG-388 - Liberdade Nappe

The calculated isochemical diagram for the Liberdade Nappe LBC is presented in Fig. 10a. The observed peak mineral assemblage, quartz+plagioclase+white mica+biotite+ilmenite, is stable in the penta-variant field constrained in the *P-T* range of 6.5-12 kbar and 600-670°C. Assuming the mineral phase equilibrium, the optimal *P-T* condition is expected to be achieved at 628°C and 7.5 kbar. At this condition, the quality factors for the mode (Q_{mode}) is 92%, and the system mineral chemistry (Q_{cmp}) is 86% (Fig. 10b).

The mineral *P-T* chemistry composition maps are presented in supplementary figure A4. They display a more complex story used to trace the *P-T* path (Fig. 10b). The An-poor plagioclase core compositions (Q_{cmp}=100%) are stable in higher pressure, 8.5 kbar up to 11.5 kbar, and in large temperature conditions, from 500°C to 700°C. On the contrary, plagioclase rim composition records a lower pressure condition, down to 8 kbar, and temperatures from 590°C to 660°C. Although the optimal *P-T* conditions obtained by the antidote, peak conditions are better constrained by plagioclase rim composition (Q_{cmp} =100%), around 650°C and 9.5-10 kbar. The Na-Ca diffusion in plagioclase is considered slower than garnet Ca-Fe-Mg-Mn in temperatures above 600°C (Caddick et al., 2010; Lanari and Hermann, 2021). These described diffusional behaviors are the likely causes of plagioclase core records better the prograde conditions rather than garnet.

Plagioclase rim (Q_{cmp} =100%), and garnet (Q_{cmp} =90-100%) mineral chemistry compositions in addition with the mineral modes (Q_{mode} =100%) intersect at the hexa-variant field in which Qz+Pl+Bt+Grt+Ms+Ky+Ilm are the stable phases. The intersection is around 650°C and 7-7.5 kbar, suggesting an almost isothermal decompression path. Relics of kyanite are described in the LN (Fig. 6f), supporting that this mineral was stable at some moment of the LN *P-T* path. Lastly, the *P-T* path later stage is recorded by the compositional match between the plagioclase rim and muscovite (Pl-Q_{cmp} =100%; Ms-Q_{cmp} =95%) in the hexa-variant field where Qz+Pl+Grt+Bt+Ms+Ilm+Sil+H_2O are stable. A *P-T* path (Fig. 10b) is suggested based on the above mineral chemistry and mode optimal quality factors fields, and the M_{LN1}, M_{LN2}, and M_{LN3} metamorphic stages described in section 4.1. The quantitative map of the Ti-in-biotite thermometer (Henry et al., 2005) was applied (supplementary figure A2c). It displays values from 650 to 580°C consistent with the findings obtained by the ITM approach.

3.3.2 Sample NESG-401 – Andrelândia Nappe

Fig. 11a displays the isochemical diagram built for the Andrelândia Nappe LBC that better represents the peak-to post-peak conditions. Bulk compositions that consider phases that are not fully equilibrated in the system, such as minerals relics or displaying compositional zoning, can affect the thermodynamic models quality (Lanari and Engi, 2017). Once one garnet of the LBC is strongly zoned and likely its core was unreactive at peak condition, for avoiding the question described above, the garnet core area was subtracted and is not considered in the bulk composition. Although, the isochemical diagram taking into account the garnet core composition and the *P-T* stability field map for garnet core composition (garnet core Q_{cmp}) are provided in the supplementary figure A5. Therefore, the M_{AN1} stage, which corresponds to a mineral assemblage preserved in the garnet core, does not appear in the suggested *P-T* path.

The peak mineral assemblage, Qz+Pl+Bt+Grt+Ky+Ms+Ilm+H_2O, was constrained in the quadri-variant field delimitated in the *P-T* range of 620°C-675°C and 7-10 kbar. The optimal *P-T* condition obtained is 676°C and 8.1 kbar with Q_{cmp}= 92% and Q_{mode}=95% (Fig. 11b). The mineral phases chemical composition of sample NESG-401 preserves three stages of the metamorphic path, the prograde, decompression, and cooling (Fig. 11b), which were traced using *P-T* stability field maps (supplementary figure A6). The prograde path was traced taking into account the compositions of garnet mantle (Q_{cmp} =100%), which records early stages of amphibolite facies around 550-570°C and 8-9 kbar, plagioclase core (Q_{cmp} =100%), and white mica (Q_{cmp} =85-80%). Indeed, the antidote optimal conditions calculations seem to underestimate the peak condition. The plagioclase core and white mica chemical composition provide a better constrain, crossing at *ca.* 660°C-670°C and 11.5-12 kbar, at these conditions, Qz+Pl+Bt+Grt+Ky+Ms+Ilm are the stable phases (M_{AN2} stage). An almost isothermal decompression is suggested based on the mineral modes (Q_{mode}= 95-100%) field of stability, which is at lower pressure of 6-8 kbar but at almost the same temperature range, from 625 to 680 °C. At last, garnet rim chemical composition (Q_{cmp} =80%) provided information about the AN cooling stage. It is equilibrated at 550°C and 4.5 kbar in the stability field of Qz+Pl+Grt+Bt+Ilm+St+Sil (M_{AN3} stage; Fig. 11b). The Ti-in-biotite thermometer map (supplementary figure A3c) displays temperatures ranging from 630 to 560 °C, in agreement with the retrograde temperature conditions obtained by ITM.

3.4 EMPA monazite petrochronology

To constrain the timing of the metamorphic and deformation events, *in-situ* U-(Th)-Pb monazite chemical dating was carried out by EMPA (e.g., Dumond et al., 2015; Williams and Jercinovic, 2002, 2012). The analytical procedures are described in appendix A.

3.4.1 Sample NESG-388 – Liberdade Nappe

Monazites from sample NESG-388 are between quartz, plagioclase, white mica, and biotite from the matrix. Ten crystals were chosen to perform X-ray maps and trace element analysis. The results are illustrated in Fig. 12 and supplementary table A2. Most of the crystals display an elongated shape parallel to the mylonitic foliation, varying in size from 70 to 250 µm, except the Mnz 4, associated with ilmenite which shows an irregular lobate shape. In some crystals, small quartz (e.g., Mnz 4, Mnz 5, and Mnz 6) inclusions were observed, but most of the monazites are inclusions free. The monazites display a sectorial core-rim internal zoning (e.g., Mnz 1, 2, 6 and 7). A remarkable feature that might be highlighted is the core and rim zonation pattern that is well-aligned (e.g., Mnz1, 2, 6, 8, and 10) with the main foliation, suggesting a pre-to syn-mylonitic growth related to the rock fabric. In addition, the Mnz 7 occurred on the S-plane of a *S-C* fabric.

Three chemical domains are distinguished based on the X-ray maps, mainly of Y and Th distribution (Fig. 12a, b, and c). Domain 1, characterized by high-Th and low-Y cores, is small patchy (e.g., Mnz 9), and straight (e.g., Mnz 2). The Y_2O_3 content (wt%) varies from 1.02 to 1.39, and the ThO_2 (wt%) values are very spread, ranging from 4.00 to 6.95. Domain 2 is related to core characterized by low-Y and -Th. The Y_2O_3 (wt%) and ThO_2 (wt%) amounts vary respectively in a narrow range of 0.93-1.22 and 2.29-3.80. The third domain (domain 3) is associated with monazite rims showing high-Y, in which the Y_2O_3 (wt%) amounts are spread in a broad range from 1.62 up to 2.61, and ThO_2 (wt%) variation is concentrated between 3.18-3.59.

In total, 84 EMPA spot analyses were acquired in the different chemical domains for chemical dating calculation. Obtained dates span from 640 to 540 Ma. Domain 1, characterized by high-Th and low-Y core, dates range from 640±21Ma to 588±19 Ma. Domain 2, with low-Th and Y cores, has dates spread from 613 Ma±36 Ma to 550±33 Ma. Owing to the dates from domains 1 and domain 2 are relative to core, they were plotted in the same weighted average diagram (Fig. 12d) and yielded a mean age of 609±4 Ma (n=55; MSWD=1.6). Domain 3, related to high-Y rims, has dates from 590±28 Ma to 540±26 Ma and yields a mean weighted average age of 567±5 Ma (n=33; MSWD=1.19; Fig. 12e).

3.4.2 Sample NESG-401 – Andrelândia Nappe

Fig. 13a displays the mapped monazite crystals (n=8) from sample NESG-401, the elements analysis spots position, and the results of chemical dating. The monazites occur between the matrix minerals, hosted in quartz, plagioclase, biotite, and white mica (Mnz 1, 3 and 5), one crystal is enclosed in kyanite (Mnz 4), and three are located in apatite rims (Mnz 2, 5 and 8). The size of crystals varies from 50 µm up to 100 µm. Monazite shape varies from rounded to elongated. Quartz inclusions are observed in Mnz 1 and Mnz 7. Regarding the monazite compositional zoning, they are very homogenous. The crystals display intermediate Y_2O_3 contents varying from 1.3 to 2.9 wt% and variable Th amounts, varying the ThO_2 between 1.9 and 5.4 wt% (Fig. 13a, b, and c). The exception is represented by rims significantly enriched in Th (with ThO_2 content between 6.7-13.1 wt%) observed in crystals associated with apatite (Fig. 13c).

A total of 56 EMPA spot analyses were carried out. The obtained U-(Th)-Pb chemical dates range from 612±23 Ma to 535±28 Ma. The dates are plotted in the weighted average diagram (Fig. 13d), and they yield a mean age of 579±6 Ma (MSWD=3.5). Of particular interest is the crystal enclosed in kyanite (Mnz 4), which can report worthy information about tectonic and metamorphic events undergone by this rock since the kyanite is considered coeval with the S_2 foliation. The dates vary from 605±22 Ma to 558±25 Ma and yield a mean age of 589±19 Ma (MSWD=2.3; Fig. 13e).

4. DISCUSSION

4.1 Monazite chemical dating interpretation

The in-situ monazite dating combined with the X-ray maps (e.g., Y and Th) allows correlating monazite growth episodes with metamorphic reactions and deformation stages

(Bosse and Villa, 2019; Spear and Pyle, 2002; Williams and Jercinovic, 2002, 2012). The Y and HREE concentration in monazite mostly depend on the garnet presence in the system, once this mineral is the preferential sink for these elements (Spear and Pyle, 2002). Whereas the Th concentration is controlled by a Th-rich phase breakdown responsible for releasing this element in the system, preferentially partitioned into monazite structure (Benetti et al., 2021; Kohn and Malloy, 2004; Williams et al., 2022). Moreover, monazite can be a fabric-forming mineral in deformed rocks and behaves as a porphyroclast rotated and with inclusion trails (Dumond et al., 2008, 2022). Therefore, the *in-situ* dating allows us to relate the monazite chemical zonation with its microstructural position, providing means to constrain the deformation time.

At sub-solidus conditions, two main metamorphic reactions will control the monazite chemistry. Firstly, the allanite breakdown is responsible for releasing most of the REE necessary for the monazite precipitation (Gasser et al., 2012; Janots et al., 2008; Kohn and Malloy, 2004; Spear and Pyle, 2010). This reaction occurs between the greenschist-to amphibolite facies transition, at temperature conditions around 550°C (Gasser et al., 2012; Janots et al., 2008; Spear and Pyle, 2010). If monazite grows at these conditions before garnet growth, the monazite will display intermediate- to high-Y and HREE content. In contrast, when monazite grows in equilibrium with garnet, the monazite tends to be depleted in Y and HREE since these elements are strongly partitioned in garnet. In addition, due to allanite being a Th-rich mineral, the monazite that grows soon after its breakdown tends to be Th-enriched (Benetti et al., 2021; Kohn and Malloy, 2004). Another monazite generation is expected during the rock decompression path, in which garnet breakdown releases Y and HREE in the system, and the monazite precipitating from this reaction will display enriched signatures in these elements (Gasser et al., 2012; Kohn et al., 2005).

Considering the monazite behavior during the sub-solidus metamorphism and deformation described above, two episodes of monazite growth can be identified in the sample NESG-388 from the Liberdade Nappe. The first episode is correlated with Y-depleted cores and a wide range of Th amounts (domains 1 and 2). These dates are associated with prograde metamorphism (M_{LN1} stage) in which monazite grew after garnet crystallization in the system and yielded mean chemical age of 609±4 Ma. The Th-enriched domains (domain 1) can likely be linked to the early prograde metamorphism (early M_{LN1} stage), soon after the allanite-to-monazite transition, releasing Th in the system and reproducing the oldest dates. The weighted mean age of 567±5 Ma, represented by Y-enriched monazite rims (domain 3), is interpreted as linked with garnet resorption during the rock decompression (M_{LN2} and M_{LN3}). Furthermore, the growth orientation of some high-Y rims aligned with the S_2 foliation (e.g., Mnz 1 and 2), and the crystal in the S-C band (Mnz 7) rotated during the shearing suggest that the decompression was coeval with the development of the S_2 fabric related with the SE tectonic transport.

The monazites grains from the sample NESG-401 of the Andrelândia Nappe are homogenous with intermediate Y and Th-depleted. They are interpreted as growing coeval with the garnet during the prograde metamorphism (M_{AN}2 stage), at a minimum age of 579±6 Ma. The Mnz 4 is enclosed in kyanite and parallel to the AN S_2 fabric, providing time constraint for the foliation-forming deformation coeval with kyanite growth during the *P-T* path. This single crystal yields mean age of 589±19 (n=6), consequently interpreted as corresponding to the time of the S_2 deformation, and taking into account the age standard deviation, is considered contemporary to the prograde metamorphism ($M_{AN}2$ stage). Rims highly enriched in Th (Mnz 2, 5, and 8) are attributable to exchange reactions between apatite and monazite and have no signatures that can associate them with any significant tectono-metamorphic event.

4.2 Tectono-metamorphic evolution of the Andrelândia Nappe System (ANS)

The microstructural descriptions, *P-T* path traced through thermodynamic metamorphic modeling, and monazite petrochronological data presented here help elucidate the complex ANS framework in the southern sector of the SBO. The Liberdade and Andrelândia Nappes evolved from a clockwise sub-solidus *P-T* path characterized by burial and heating, followed by nearly isothermal decompression, and lastly, cooling and decompression. The Liberdade Nappe (NESG-388) M_{LN1} stage assemblage (Qz-Pl-Grt-Bt-Ms-Ilm) records peak conditions at *ca.* 650°C and 9.5-10 kbar and has a minimum age of 609±4 Ma (Fig. 14a). The peak conditions indicate that the LN rocks were buried by 36 km, corresponding to the middle and lower depth of a thickened crust with an apparent geothermal gradient of 18ºC/km (Fig. 14a). The further stages, M_{LN2} (Qz-Pl-Grt-Bt-Ms-Ilm-Ky(?)) and the M_{LN3} (Qz-Pl-Grt-Bt-Ms-Ilm-Sil-St), represent respectively the isothermal decompression and decompression/cooling episodes related to the LN migration toward SE, whose the minimum age is constrained at 567±5 Ma (Fig. 14a).

The Andrelândia Nappe sample (NESG-401) records a burial and heating episode in the kyanite stability field during the prograde metamorphism, from ~550°C and 9.0-9.5 kbar up to ~680 °C and 11-12 kbar (M_{AN2} stage; Fig. 14a). The *P-T* data suggest an apparent geothermal gradient of 16ºC/km and burial into crustal depths of 43 km (Fig. 14a). The minimum age for the prograde metamorphism was estimated at 579±6 Ma, and within the uncertainties is considered coeval with the S_2 deformation event underwent by this rock. It was followed by an almost isothermal decompression, in which the pressure conditions decreased from 12 kbar down to 8.0-7.0 kbar (Fig.14a). Lastly, the M_{AN3} stage related to staurolite and sillimanite appearance in the system was constrained in the *P-T* range of 670-550°C and 8.0-4.5 kbar (Fig. 14a).

A compilation of literature *P-T* paths from the Andrelândia and Liberdade Nappes is provided in Fig. 14a. Different approaches were adopted by Coelho et al. (2017), Motta and Moraes (2017), Reno et al. (2012), and Santos et al. (2004), such as inverse and forward thermodynamic modeling. Considering the different methods-related uncertainties, peak conditions constrained for the Andrelândia and Liberdade Nappes in this contribution agree with those previously reported. However, there are differences between the *P-T* path traced here and those interpreted by these authors. For instance, Reno et al. (2021) suggested two episodes of isobaric cooling separated by a near-isothermal decompression phase to the Carmo da Cachoeira Nappe, the Andrelândia Nappe equivalent in the SBO northern sector. Moreover, Santos et al. (2004) considered that Andrelândia Nappe underwent heating during decompression, while the Liberdade Nappe evolved from an isothermal decompression. These *P-T* path contrasts can be assigned to different interpretations regarding blastesis-deformation relationships and distinct approaches used by each of the authors and the present work.

Fig. 14b is a summary of the available metamorphic ages for the Andrelândia and Liberdade Nappes using monazite and zircon U-Pb geochronology techniques. The oldest ages of the Liberdade Nappe, at *ca.* 680-670 Ma, reported by Campos Neto et al. (2011) and Reno et al. (2009), are related to metamafic rocks and interpreted as the HP metamorphism age experienced by these rocks. Regarding the LN and AN micaschits and gneisses, the previously published ages by Coelho et al. (2017), Frugis et al. (2018), Marimon et al (2022), Motta and Moraes (2017), and Westin et al. (2021) and those reported in this work are widespread in a time range *ca.* 60 Ma, from 630 to 570 Ma. The geochronology data from the literature, calculated by different methods (e.g., isocron age, concordia age, and weighted average age), are comprised within the spread of chemical dates acquired here. However, in this study, the monazite petrochronology results indicate that each nappe experienced episodic growth during a single metamorphic cycle of burial (prograde metamorphism) and decompression (retrograde metamorphism), rather than being affected by polymetamorphism events.

4.3 Tectonic implications

Our present findings shed new light on some critical points regarding the tectono-metamorphic events experienced by the ANS. The first point is related to the Andrelândia and Liberdade Nappes *P-T* paths. Microstructural observations and thermodynamic modeling show that the staurolite and sillimanite in the matrix are related to decompression and cooling stages. Furthermore, the suggested metamorphic paths to the LN and AN pointed out that the baric and thermic peaks occur almost simultaneously. These information in conjunction with monazite petrochronology indicate that likely each one of the nappes underwent a single metamorphic loop of burial and decompression.

The second critical point concerns the timing constraints of metamorphism and deformation. The Liberdade Nappe attained prograde, amphibolite facies, within the kyanite stability field at minimum age of *ca.* 610 Ma, nearly 30 Ma before the Andrelândia Nappe (Fig. 15 b, c, and d). Although the sample from Andrelândia Nappe does not have dates related to exhumation, the spread dates from the Liberdade Nappe linked with the exhumation mostly overlap the prograde monazite dates in the Andrelândia Nappe, structurally below. Hence, it is possible to claim that when the Liberdade Nappe onset its decompression path, the Andrelândia Nappe was still experiencing prograde conditions and was likely exhumed afterward compared to the Liberdade Nappe (Fig. 15c). In other words, the dates younger than 610 Ma in the Liberdade Nappe are related to its exhumation and tectonic transport toward SE (Fig. 15c and d). In contrast, this time span is linked with prograde burial metamorphic conditions (coeval with kyanite growth) in the Andrelândia Nappe (Fig. 15c). The Pouso Alto Nappe, the upper structural level of the ANS in the southern part of the SBO, yields a minimums age of *ca.* 620 Ma and of *ca.* 610 Ma, for respectively the prograde metamorphism, and melt crystallization related to cooling and decompression (Fig. 15a and b; Benetti et al., in prep; Benetti, 2022). Therefore, the spread of ages from 630 Ma to 570 Ma (Fig. 15) within the ANS records a pattern of age decrease, toward lower structural levels, of the prograde and retrograde metamorphic ages during the protracted metamorphism of the SBO (Fig 15). The spatial arrangement and decrease of the metamorphic ages toward the bottom of the ANS stack outline an in-sequence fold-and-thrust architecture of the orogenic wedge (Fig. 15). This framework would have been developed through the inner material incorporated at the wedge being detached, shortened, and propagated over the incoming material, similar to what is proposed by Platt (1986) to the dynamics of orogenic wedges. Then, the rocks from the older nappes (i.e., Liberdade Nappe) were decompressed via thrust and folding over the younger ones (i.e., Andrelândia Nappe) that likely experienced their peak metamorphism as a consequence of loading of the overlying nappe. Analogue in-sequence fold-and-thrust architectures are described in other orogenic belts such as the Caledonian, Trans-Hudson, Grenville, Himalayan, and

Appalachian orogens (Beaumont et al., 2006; Carosi et al., 2016; Weller et al., 2021). This suggests that the mechanism described above is an important mechanism controlling the structural and metamorphic style of collisional wedges. Fig. 15 illustrates the proposed tectono-metamorphic evolution for the nappes of the Southern Brasília Orogen. The collision-related metamorphic event evolved from 630 to 570 Ma based on zircon, monazite, and titanite U-Pb ages and monazite-EPMA ages (Campos Neto et al., 2010; Coelho et al., 2017; Frugis et al., 2018; Fumes et al., 2021; Li et al. 2021; Marimon et al., 2020, 2022; Motta et al., 2021; Rocha et al., 2017; Westin et al., 2021). The Andrelândia Nappe System underwent high-pressure metamorphic conditions during the collision between the São Francisco (passive margin) and Paranapanema (active margin) paleoplates (Fig. 15). The crustal material was stored and sunk within the orogenic wedge hinterland until 620 Ma when the first nappe of the system, the Pouso Alto, started its decompression path with tectonic transport toward northeast (Fig. 15a and b). After *ca.* 610 Ma, the Liberdade Nappe follows an upward flow toward east/southeast, laterally to the south margin of the São Francisco Craton, over the Andrelândia Nappe (Fig. 15c). The final stage of the SBO continental collision took place after 580-570 Ma, coeval with the decompression and exhumation path of the Andrelândia and Carrancas Nappes (Fig., 15d; Campos Neto et al., 2010, 2020; Carvalho et al., 2020; Cioffi et al., 2019; Coelho et al., 2017; Frugis et al., 2018; Reno et al., 2009, 2012, Tedeschi et al., 2017; Westin et al., 2021).

5. CONCLUSION

The *P-T-t-D* data provided here document the metamorphic and deformation history of the Andrelândia and Liberdade Nappes. The Liberdade Nappe experienced prograde burial metamorphism at *ca.* 610 Ma and achieved peak conditions at ~650°C and 9.5-10 kbar. This stage was followed by a near-isothermal decompression and further cooling with a minimum age of *ca.* 570 Ma. Meanwhile, the Andrelândia Nappe structurally below the Liberdade Nappe underwent prograde metamorphism nearly 30 Ma later, at *ca.* 580 Ma, reaching the peak condition at *ca.* 680°C and 11.5-12 kbar. The data document an in-sequence fold-and-thrust architecture, in which the metamorphic ages decrease toward lower structural levels of the stack. This framework would have evolved through older material incorporated into the inner parts of the orogenic wedge has been detached and propagated via thrust-and-fold nappes upon recently accreted rocks, leading to a younger metamorphism event on the footwall of the ductile thrust.

APPENDIX A – ANALYTICAL METHODS

The equipment employed in the trace elements, quantitative mineral analyses, and compositional maps is a JEOL JXA-8230 Electron Probe Micro Analyzer (EPMA) equipped with five wavelengths dispersive spectrometry (WDS) detectors hosted at the Department of Geology at the State of São Paulo University (UNESP). The compositional maps were obtained through X-rays maps, which were further classified and calibrated using the internal standardization procedure and the pseudo-background correction available in the XMapTools 3.4 (Lanari et al., 2014, 2019). The X-ray maps for Mg, Na, Ca, K, and Fe were acquired by the WDS detectors, whereas for Al, Si, P, S, Ti, Mn, and Zr by the energy dispersive-spectrometry (EDS). The x-ray maps were carried out with an accelerating voltage of 15Kv, a current beam of 100nA, and a dwell of 100 ms. Representative analysis of silicates obtained within the X-maps perimeter used for the calibrations are available in the supplementary table file A1.

Monazite U-(Th)-Pb chemistry dating was performed using the same equipment cited above. The crystals were first identified through full thin-sections maps acquired using the Scanning Electron Microscopy and Mineral Liberation Analyzer (SEM-MLA). Considering the monazite structural position and textural relationships some crystals were selected to perform high-resolution compositional X-ray maps of Y, Al, Th, U, Pb, Si, Ca, Fe, La, and Ce. The acquisition conditions were 15 kV, 100 nA, 100 ms dwell time, and 10 μm electron beam size and step. Trace elements spots analyses were performed in the different domains identified with helping of the X-ray maps. The analytical procedure follows the strategies of Fumes et al. (2021). The moacyr monazite standard was used after each 10 to 20 punctual analyses, and their results are displayed in the supplementary figure file A7. The background was estimated in all analyzed spots. Spectral interference corrections considered matrix correction factors and were performed offline. Interference corrections and age calculations were performed using the Age_Cor program (Vlach, 2010). The dates were plotted in the weighted average diagram using the Isoplot program (Ludwig, 2008).

ACKNOWLEDGEMENTS

This research was supported by funds of "Ricerca Locale" of the Università di Torino (resp. Iaccarino S. and Montomoli C.) and the São Paulo Research Foundation (FAPESP grant 2015/03737-0). The authors would like to thank Gregory Dumond and an anonymous reviewer for their suggestions and careful revisions to improve this paper.

6. REFERENCES

Andrade, V. De, Vidal, O., Lewin, E., O'Brien, P., Agard, P., 2006. Quantification of electron microprobe compositional maps of rock thin sections: an optimized method and examples. Journal of Metamorphic Geology 24, 655–668. https://doi.org/10.1111/J.1525-1314.2006.00660.X

Baldwin, J.A., Powell, R., Brown, M., Moraes, R., Fuck, R.A., 2005. Modelling of mineral equilibria in ultrahigh-temperature metamorphic rocks from the Anápolis–Itauçu Complex, central Brazil. Journal of Metamorphic Geology 23, 511–531. https://doi.org/10.1111/J.1525-1314.2005.00591.X

Beaumont, C., Jamieson, R., Nguyen, M. H., Lee, B., 2001. Himalayan tectonics explained by extrusion of a low-viscosity crustal channel coupled to focused surface denudation. Nature, 738–742.

Beaumont, C., Nguyen, M. H., Jamieson, R. A., Ellis, S., 2006. Crustal flow modes in large hot orogens. Geological Society Special Publication, 268, 91–145. https://doi.org/10.1144/GSL.SP.2006.268.01.05

Benetti, B., 2022. Kinematics and P-T-t evolution in hot collisional frameworks – a comparison between a Neoproterozoic and a Phanerozoic large hot orogens. University of Turin.

Benetti, B., Montomoli, C., Iaccarino, S., Langone, A., Carosi, R., 2021. Mapping tectono-metamorphic discontinuities in orogenic belts: implications for mid-crust exhumation in NW Himalaya. Lithos 392–393, 106129. https://doi.org/10.1016/j.lithos.2021.106129

Bosse, V., Villa, I.M., 2019. Petrochronology and hygrochronology of tectono-metamorphic events. Gondwana Research 71, 76–90. https://doi.org/10.1016/j.gr.2018.12.014

Caddick, M.J., Konopásek, J., Thompson, A.B., 2010. Preservation of Garnet Growth Zoning and the Duration of Prograde Metamorphism. Journal of Petrology 51, 2327–2347. https://doi.org/10.1093/PETROLOGY/EGQ059

Campos Neto, M. da C., 2000. Orogenic systems from SW-Gondwana: an approach to Brasiliano-Pan African cycle and orogenic collage in SE-Brazil, in: Tectonic Evolution of South America. pp. 335–365.

Campos Neto, M. da C., Basei, M.A.S., Assis Janasi, V. de, Moraes, R., 2011. Orogen migration and tectonic setting of the Andrelândia Nappe system: An Ediacaran western Gondwana collage, south of São Francisco craton. Journal of South America Earth Science 32, 393–406. https://doi.org/10.1016/j.jsames.2011.02.006

Campos Neto, M. da C., Caby, R., 2000. Terrane accretion and upward extrusion of high-pressure granulites in the Neoproterozoic nappes of southeast Brazil: Petrologic and structural constraints. Tectonics 19, 669–687. https://doi.org/10.1029/1999TC900065

Campos Neto, M. da C., Cioffi, C.R., Moraes, R., da Motta, R.G., Siga, O., Basei, M.A.S., 2010. Structural and metamorphic control on the exhumation of high-P granulites: The Carvalhos Klippe example, from the oriental Andrelândia Nappe System, southern portion of the Brasília Orogen, Brazil. Precambrian Research 180, 125–142. https://doi.org/10.1016/j.precamres.2010.05.010

Campos Neto, M. da C., Cioffi, C.R., Westin, A., Rocha, B.C., Frugis, G.L., Tedeschi, M., Pinheiro, M.A.P., 2020. O Orógeno Brasília Meridional, in: Geocronologia e Evolução Tectônica Do Continente Sul-Americano: A Contribuição de Umberto Giuseppe Cordani.

Campos Neto, M.D.C., Caby, R., 1999. Neoproterozoic high-pressure metamorphism and tectonic constraint from the nappe system south of the Sao Francisco Craton, southeast Brazil. Precambrian Research 97, 3–26. https://doi.org/10.1016/S0301-9268(99)00010-8

Carosi, R., Montomoli, C., Iaccarino, S., Massonne, H. J., Rubatto, D., Langone, A., Gemignani, L., Visonà, D., 2016. Middle to late Eocene exhumation of the Greater Himalayan Sequence in the Central Himalayas: Progressive accretion from the Indian plate. Geological Society of America Bulletin, 128(11–12), 1571–1592. https://doi.org/10.1130/B31471.1

Carosi, R., Montomoli, C., Iaccarino, S., 2018. 20 years of geological mapping of the metamorphic core across Central and Eastern Himalayas. Earth Science Reviews 177, 124–138. https://doi.org/10.1016/j.earscirev.2017.11.006

Carvalho, B.R.B.M., Trouw, R.A.J., Costa, R.V.C. da, Ribeiro, A., Heilbron, M., Marimon, R.S., 2020. Microstructural and metamorphic evolution of the Carrancas Klippe, interference zone of the Neoproterozoic southern Brasilia and Ribeira orogens, SE Brazil. Journal of South America Earth Science 103, 102744. https://doi.org/10.1016/j.jsames.2020.102744

Cioffi, C.R., Campos Neto, M. da C., Möller, A., Rocha, B.C., 2019. Titanite petrochronology of the southern Brasília Orogen basement: Effects of retrograde net-transfer reactions on titanite trace element compositions. Lithos 344–345, 393–408. https://doi.org/10.1016/j.lithos.2019.06.035

Cioffi, C.R., Campos Neto, M. da C., Möller, A., Rocha, B.C., 2016. Paleoproterozoic continental crust generation events at 2.15 and 2.08Ga in the basement of the southern

Brasília Orogen, SE Brazil. Precambrian Research 275, 176–196. https://doi.org/10.1016/j.precamres.2016.01.007

Cioffi, C.R., Campos Neto, M. da C., Rocha, B.C. da, Moraes, R., Henrique-Pinto, R., 2012. Geochemical signatures of metasedimentary rocks of high-pressure granulite facies and their relation with partial melting: Carvalhos Klippe, Southern Brasília Belt, Brazil. Journal of South America Earth Science 40, 63–76. https://doi.org/10.1016/j.jsames.2012.09.007

Coelho, M.B., Trouw, R.A.J., Ganade, C.E., Vinagre, R., Mendes, J.C., Sato, K., 2017. Constraining timing and P-T conditions of continental collision and late overprinting in the Southern Brasília Orogen (SE-Brazil): U-Pb zircon ages and geothermobarometry of the Andrelândia Nappe System. Precambrian Research 292, 194–215. https://doi.org/10.1016/j.precamres.2017.02.001

Coggon, R., Holland, T.J.B., 2002. Mixing properties of phengitic micas and revised garnet-phengite thermobarometers. Journal of Metamorphic Geology 20, 683–696. https://doi.org/10.1046/J.1525-1314.2002.00395.X

Cordani, U.G., D’agrella-Filho, M.S., Brito-Neves, B.B., Trindade, R.I.F., 2003. Tearing up Rodinia: the Neoproterozoic palaeogeography of South American cratonic fragments. Terra Nova 15, 350–359. https://doi.org/10.1046/j.1365-3121.2003.00506.x

Davis, D., Suppe, J., Dahlen, F. A. (1983). Mechanics of fold-and-thrust belts and accretionary wedges. Journal of Geophysical Research, 88(B2), 1153–1172. https://doi.org/10.1029/JB088IB02P01153 de Capitani, C., Brown, T. H., 1987. The computation of chemical equilibrium in complex systems containing non-ideal solutions. Geochimica et Cosmochimica Acta, 51(10), 2639–2652. https://doi.org/10.1016/0016-7037(87)90145-1

de Capitani, C., Petrakakis, K., 2010. The computation of equilibrium assemblage diagrams with Theriak/Domino software. American Mineralogist, 95(7), 1006–1016. https://doi.org/10.2138/AM.2010.3354

Duesterhoeft, E., Lanari, P., 2020. Iterative thermodynamic modelling—Part 1: A theoretical scoring technique and a computer program (Bingo-Antidote). Journal of Metamorphic Geology 38, 527–551. https://doi.org/10.1111/JMG.12538

Dumond, G., Goncalves, P., Williams, M.L., Jercinovic, M.J., 2015. Monazite as a monitor of melting, garnet growth and feldspar recrystallization in continental lower crust. Journal of Metamorphic Geology 33, 735–762. https://doi.org/10.1111/jmg.12150

Dumond, G., Mahan, K.H., Goncalves, P., Williams, M.L., Jercinovic, M.J., 2022. Monazite as a monitor of shear strain in orogenic crust. Journal of Structural Geology 161, 104672. https://doi.org/10.1016/J.JSG.2022.104672

Dumond, G., McLean, N., Williams, M.L., Jercinovic, M.J., Bowring, S.A., 2008. High-resolution dating of granite petrogenesis and deformation in a lower crustal shear zone: Athabasca granulite terrane, western Canadian Shield. Chemical Geology 254, 175–196. https://doi.org/10.1016/j.chemgeo.2008.04.014

England, P.C., Thompson, A.B., 1984. Pressure-Temperature-Time Paths of Regional Metamorphism I. Heat Transfer during the Evolution of Regions of Thickened Continental Crust. Journal of Petrology 25, 894–928. https://doi.org/10.1093/petrology/25.4.894

England, P., Molnar, P., 1990. Surface uplift, uplift of rocks, and exhumation of rocks . Geology, 18(12), 1173–1177.

England, P., Molnar, P., 1993. The interpretation of inverted metamorphic isograds using simple physical calculations. Tectonics, 12(1), 145–157.

Fontainha, M.V.F., Trouw, R.A.J., Peternel, R., de Paula, R.R., Polo, H.J.O., Negrão, A.P., Furtado, P.C., Telles, R.C.M., 2020. A case study of superposed structures in the tectonic interference zone between the Southern Brasília and Ribeira orogens, southeastern Brazil. Journal of South America Earth Science 104, 102718. https://doi.org/10.1016/j.jsames.2020.102718

Frugis, G.L., Campos Neto, M. da C., Lima, R.B., 2018. Eastern Paranapanema and southern São Francisco orogenic margins: Records of enduring Neoproterozoic oceanic convergence and collision in the southern Brasília Orogen. Precambrian Research 308, 35–57. https://doi.org/10.1016/j.precamres.2018.02.005

Fumes, R.A., Luvizotto, G.L., Moraes, R., Lanari, P., Valeriano, C. de M., Zack, T., Caddick, M.J., Simões, L.S.A., 2021. Petrochronology of high-pressure granulite facies rocks from Southern Brasília Orogen, SE Brazil: Combining quantitative compositional mapping, single-element thermometry and geochronology. Journal of Metamorphic Geology 1–36. https://doi.org/10.1111/JMG.12637

Ganade De Araujo, C.E., Rubatto, D., Hermann, J., Cordani, U.G., Caby, R., Basei, M.A.S., 2014. Ediacaran 2,500-km-long synchronous deep continental subduction in the West Gondwana Orogen. Nat Commun 5, 1–8. https://doi.org/10.1038/ncomms6198

Garcia, M. da G.M., Campos Neto, M. da C., 2003. Contrasting metamorphic conditions in the Neoproterozoic collision-related Nappes south of São Francisco Craton, SE Brazil. Journal of South America Earth Science 15, 853–870. https://doi.org/10.1016/S0895-9811(02)00147-5

Gasser, D., Bruand, E., Rubatto, D., Stüwe, K., 2012. The behavior of monazite from greenschist facies phyllites to anatectic gneisses: An example from the Chugach Metamorphic Complex, southern Alaska. Lithos 134–135, 108–122. https://doi.org/10.1016/j.lithos.2011.12.003

Heilbron, M., Machado, R., Figueiredo, M., 2017. Lithogeochemistry of paleoproterozoic orthogranulites from the Rio Preto (MG)-vassouras (RJ) region, central Ribeira Belt, SE Brazil. Revista Brasileira de Geociências 27 (1). http://www.ppegeo.igc.usp.br/index.php/rbg/article/view/11274

Henry, D.J., Guidotti, C. V., Thomson, J.A., 2005. The Ti-saturation surface for low-to-medium pressure metapelitic biotites: Implications for geothermometry and Ti-substitution mechanisms. American Mineralogist 90, 316–328. https://doi.org/10.2138/AM.2005.1498

Holland, T.J.B., Powell, R., 1998. An internally consistent thermodynamic data set for phases of petrological interest. Journal of Metamorphic Geology 16, 309–343. https://doi.org/10.1111/J.1525-1314.1998.00140.X

Jamieson, R.A., Beaumont, C., 2013. On the origin of orogens. Bulletin of the Geological Society of America 125, 1671–1702. https://doi.org/10.1130/B30855.1

Janots, E., Engi, M., Berger, A., Allaz, J., Schwarz, J.-O., Spandler, C., 2008. Prograde metamorphic sequence of REE minerals in pelitic rocks of the Central Alps: implications for allanite–monazite–xenotime phase relations from 250 to 610 °C. Journal of Metamorphic Geology 26, 509–526. https://doi.org/10.1111/j.1525-1314.2008.00774.x

Kohn, M.J., Engi, M., Lanari, P., 2017. Petrochronology: Methods and applications, Petrochronology. Reviews in Mineralogy & Geochemistry, vol 83. https://doi.org/10.1515/9783110561890/HTML

Kohn, M.J., Malloy, M.A., 2004. Formation of monazite via prograde metamorphic reactions among common silicates: Implications for age determinations. Geochimica et Cosmochimica Acta 68, 101–113. https://doi.org/10.1016/S0016-7037(03)00258-8

Kohn, M.J., Wieland, M.S., Parkinson, C.D., Upreti, B.N., 2005. Five generations of monazite in Langtang gneisses: Implications for chronology of the Himalayan metamorphic core. Journal of Metamorphic Geology 23, 399–406. https://doi.org/10.1111/j.1525-1314.2005.00584.x

Lanari, P., Engi, M., 2017. on Metamorphic Mineral Assemblages. Reviews in Mineralogy and Geochemistry 83, 55–102.

Lanari, P., Hermann, J., 2021. Iterative thermodynamic modelling-Part 2: Tracing equilibrium relationships between minerals in metamorphic rocks. Journal of Metamorphic Geology 39, 651–674. https://doi.org/10.1111/jmg.12575

Lanari, P., Vho, A., Bovay, T., Airaghi, L., Centrella, S., 2019. Quantitative compositional mapping of mineral phases by electron probe micro-analyser. Geological Society, London, Special Publications 478, 39–63. https://doi.org/10.1144/SP478.4

Lanari, P., Vidal, O., de Andrade, V., Dubacq, B., Lewin, E., Grosch, E.G., Schwartz, S., 2014. XMapTools: A MATLAB©-based program for electron microprobe X-ray image processing and geothermobarometry. Computers & Geosciences 62, 227–240. https://doi.org/10.1016/J.CAGEO.2013.08.010

Law, R.D., 2014. Deformation thermometry based on quartz c-axis fabrics and recrystallization microstructures: A review. Journal of Structural Geology 66, 129–161. https://doi.org/10.1016/j.jsg.2014.05.023

Le Fort, P., 1975. Himalayas: the collided range. Present knowledge of the continental arc. American Journal of Science, 275(1), 1–44.

Li, B., Massonne, H.J., Hartmann, L.A., Zhang, J., Luo, T., 2021. Kyanite-garnet granulite from the Andrelândia nappe system, Brasília belt, registers two late Neoproterozoic metamorphic cycles. Precambrian Research 355, 106086. https://doi.org/10.1016/j.precamres.2020.106086

Ludwig, K.R., 2008. User’s manual for Isoplot/Ex version 3.70: a geochronology toolkit for Microsoft Excel: No. 4. Berkeley Geochronological Center, Special Publication 1–76.

Marimon, R.S., Hawkesworth, C.J., Trouw, R.A.J., Trouw, C., Dantas, E.L., Ribeiro, A., Vinagre, R., Hackspacher, P., Ávila, C., Motta, R., Moraes, R., 2022. Subduction and continental collision in the Neoproterozoic: Sanukitoid-like magmatism and paired metamorphism in SE Brazil. Precambrian Research 383, 106888. https://doi.org/10.1016/J.PRECAMRES.2022.106888

Marimon, R.S., Trouw, R.A.J., Dantas, E.L., 2020. Significance of age periodicity in the continental crust record: The São Francisco Craton and adjacent Neoproterozoic orogens as a case study. Gondwana Research 86, 144–163. https://doi.org/10.1016/J.GR.2020.05.010

Motta, R.G., Fitzsimons, I.C.W., Moraes, R., Johnson, T.E., Schuindt, S., Benetti, B.Y., 2021. Recovering P–T–t paths from ultra-high temperature (UHT) felsic orthogneiss: An example from the Southern Brasília Orogen, Brazil. Precambrian Research 359, 106222. https://doi.org/10.1016/j.precamres.2021.106222

Motta, R.G., Moraes, R., 2017. Pseudo- and real-inverted metamorphism caused by the superposition and extrusion of a stack of nappes: a case study of the Southern Brasília Orogen, Brazil. International Journal of Earth Sciences 106, 2407–2427. https://doi.org/10.1007/s00531-016-1436-7

Passchier, C.W., Trouw, R.A.J., 2005. Microtectonics, 2nd ed. Berlin:Springer Verlag.

Peternel, R., Allard, R., Trouw, J., Da, R., Schmitt, S., Xavier, F., 2005. Interferência entre duas faixas móveis Neoproterozóicas: O caso das faixas Brasília e Ribeira no sudeste do Brasil. Revista Brasileira de Geociências 35, 297–310.

Platt, J.P., 1986. Dynamics of orogenic wedges and the uplift of high-pressure metamorphic rocks. GSA Bulletin 9, 1037–1053.

Powell, R., Holland, T.J.B., 2008. On thermobarometry. Journal of Metamorphic Geology 26, 155–179. https://doi.org/10.1111/j.1525-1314.2007.00756.x

Ramsay, J.G., 1962. Interference Patterns Produced by the Superposition of Folds of Similar Type. The Journal of Geology 70, 466–481. https://doi.org/10.1086/626837

Reno, B.L., Brown, M., Kobayashi, K., Nakamura, E., Piccoli, P.M., Trouw, R.A.J., 2009. Eclogite-high-pressure granulite metamorphism records early collision in West Gondwana: New data from the Southern Brasília Belt, Brazil. Journal of the Geological Society of London 166, 1013–1032. https://doi.org/10.1144/0016-76492008-140

Reno, B.L., Piccoli, P.M., Brown, M., Trouw, R.A.J., 2012. In situ monazite (U-Th)-Pb ages from the Southern Brasília Belt, Brazil: constraints on the high-temperature retrograde evolution of HP granulites. Journal of Metamorphic Geology 30, 81–112. https://doi.org/10.1111/j.1525-1314.2011.00957.x

Ring, U., Brandon, M. T., Willett, S. D., Lister, G. S., 1999. Exhumation processes. Geological Society Special Publication, 154, 1–27. https://doi.org/10.1144/GSL.SP.1999.154.01.01

Rocha, B.C., Moraes, R., Möller, A., Cioffi, C.R., Jercinovic, M.J., 2017. Timing of anatexis and melt crystallization in the Socorro–Guaxupé Nappe, SE Brazil: Insights from trace element composition of zircon, monazite and garnet coupled to UPb geochronology. Lithos 277, 337–355. https://doi.org/10.1016/J.LITHOS.2016.05.020

Rodrigues, S.W. de O., Martins-Ferreira, M.A.C., Faleiros, F.M., Campos Neto, M. da C., Yogi, M.T.A.G., 2019. Deformation conditions and quartz c-axis fabric development along nappe boundaries: The Andrelândia Nappe System, Southern Brasília Orogen (Brazil). Tectonophysics 766, 283–301. https://doi.org/10.1016/J.TECTO.2019.06.014

Rudnick, R.L., Fountain, D.M., 1995. Nature and composition of the continental crust: A lower crustal perspective. Reviews of Geophysics 33, 267. https://doi.org/10.1029/95RG01302

Santos, L.P., da Costa Campos Neto, M., Grohmann, C.H., 2004. Metamorphic path constrained by metapelitic rocks from the inner Aiuruoca-Andrelândia nappe, south of the São Francisco craton, SE Brazil. Journal of South America Earth Science 16, 725–741. https://doi.org/10.1016/j.jsames.2003.12.006

Spear, F.S., Kohn, M.J., Cheney, J.T., 1999. P-T paths from anatectic pelites. Contributions to Mineralogy and Petrology 1999 134:1 134, 17–32. https://doi.org/10.1007/S004100050466

Spear, F.S., Pyle, J.M., 2010. Theoretical modeling of monazite growth in a low-Ca metapelite. Chemical Geology 273, 111–119. https://doi.org/10.1016/j.chemgeo.2010.02.016

Spear, F.S., Pyle, J.M., 2002. Apatite, monazite, and xenotime in metamorphic rocks. Reviews in Mineralogy and Geochemistry 48, 293–335. https://doi.org/10.2138/rmg.2002.48.7

Tedeschi, M., Lanari, P., Rubatto, D., Pedrosa-Soares, A., Hermann, J., Dussin, I., Pinheiro, M.A.P., Bouvier, A.S., Baumgartner, L., 2017. Reconstruction of multiple P-T-t stages from retrogressed mafic rocks: Subduction versus collision in the Southern Brasília orogen (SE Brazil). Lithos 294–295, 283–303. https://doi.org/10.1016/j.lithos.2017.09.025

Tedeschi, M., Pedrosa-Soares, A., Dussin, I., Lanari, P., Novo, T., Pinheiro, M.A.P., Lana, C., Peters, D., 2018. Protracted zircon geochronological record of UHT garnet-free granulites in the Southern Brasília orogen (SE Brazil): Petrochronological constraints on magmatism and metamorphism. Precambrian Research 316, 103–126. https://doi.org/10.1016/j.precamres.2018.07.023

Trouw, R.A.J., Heilbron, M., Ribeiro, A., Paciullo, F., Valeriano, C.M., Almeida, J.C.H., Tupinambá, M., Andreis, R.R., 2000. The central segment of the Ribeira Belt, in: Tectonic Evolution of South America. pp. 287–310.

Trouw, R.A.J., Paciullo, F.V.P., Ribeiro, A., 1998. Tectonic significance of Neoproterozoic high-pressure granulites in southern Minas Gerais., in: 14th International Conference on Basement Tectonics,. Ouro Preto, MG, pp. 69–71.

Trouw, R.A.J., Peternel, R., Ribeiro, A., Heilbron, M., Vinagre, R., Duffles, P., Trouw, C.C., Fontainha, M., Kussama, H.H., 2013. A new interpretation for the interference zone between the southern Brasília belt and the central Ribeira belt, SE Brazil. Journal of South America Earth Science 48, 43–57. https://doi.org/10.1016/j.jsames.2013.07.012

Vanderhaeghe, O., 2012. The thermal-mechanical evolution of crustal orogenic belts at convergent plate boundaries: A reappraisal of the orogenic cycle. Journal of Geodynamics 56–57, 124–145. https://doi.org/10.1016/j.jog.2011.10.004

Vanderhaeghe, O., Medvedev, S., Fullsack, P., Beaumont, C., Jamieson, R.A., 2003. Evolution of orogenic wedges and continental plateaux: insights from crustal thermal–mechanical models overlying subducting mantle lithosphere. Geophysical Journal International 153, 27–51. https://doi.org/10.1046/J.1365-246X.2003.01861.X

Vlach, S. R. F., 2010. Th-U-Pb_T dating by electron probe microanalysis, part I. Monazite: analytical procedures and data treatment. Geologia USP: Série Científica, 10(1), 61–85. https://doi. org/10.5327/Z1519-874X2010000100006

Waters, D.J., 2019. Metamorphic constraints on the tectonic evolution of the high Himalaya in Nepal: The art of the possible. Geological Society of London Special Publication 483, 325–375. https://doi.org/10.1144/SP483-2018-187

Weller, O. M., Mottram, C. M., St-Onge, M. R., Möller, C., Strachan, R., Rivers, T., Copley, A., 2021. The metamorphic and magmatic record of collisional orogens. Nature Reviews Earth & Environment 2021, 1–19. https://doi.org/10.1038/s43017-021-00218-z

Westin, A., Campos Neto, M.C., Hawkesworth, C.J., Cawood, P.A., Dhuime, B., Delavault, H., 2016. A paleoproterozoic intra-arc basin associated with a juvenile source in the Southern Brasilia Orogen: Application of U-Pb and Hf-Nd isotopic analyses to provenance studies of complex areas. Precambrian Research 276, 178–193. https://doi.org/10.1016/j.precamres.2016.02.004

Westin, A., Campos Neto, M.C., Hollanda, M.H.B.M., Salazar-Mora, C.A., Queiroga, G.N., Frugis, G.L., de Castro, M.P., 2021. The fast exhumation pattern of a Neoproterozoic nappe system built during West Gondwana amalgamation: Insights from thermochronology. Precambrian Research 355, 106115. https://doi.org/10.1016/j.precamres.2021.106115

Whipple, K. X., 2009. The influence of climate on the tectonic evolution of mountain belts. Nature Geoscience, 2(2), 97–104.

White, R.W., Pomroy, N.E., Powell, R., 2005. An in situ metatexite–diatexite transition in upper amphibolite facies rocks from Broken Hill, Australia. Journal of Metamorphic Geology 23, 579–602. https://doi.org/10.1111/J.1525-1314.2005.00597.X

White, R.W., Powell, R., Holland, T.J.B., 2007. Progress relating to calculation of partial melting equilibria for metapelites. Journal of Metamorphic Geology 25, 511–527. https://doi.org/10.1111/J.1525-1314.2007.00711.X

Whitney, D.L., Evans, B.W., 2010. Abbreviations for names of rock-forming minerals. American Mineralogist 95, 185–187. https://doi.org/10.2138/am.2010.3371

Willett, S. D., 1999. Orogeny and orography: The effects of erosion on the structure of mountain belts. Journal of Geophysical Research: Solid Earth, 104(B12), 28957–28981. https://doi.org/10.1029/1999JB900248

Williams, M.A., Kelsey, D.E., Rubatto, D., 2022. Thorium zoning in monazite: a case study from the Ivrea–Verbano Zone, NW Italy. Journal of Metamorphic Geology 1–28. https://doi.org/10.1111/JMG.12656

Williams, M.L., Jercinovic, M.J., 2012. Tectonic interpretation of metamorphic tectonites: Integrating compositional mapping, microstructural analysis and in situ monazite dating. Journal of Metamorphic Geology 30, 739–752. https://doi.org/10.1111/j.1525-1314.2012.00995.x

Williams, M.L., Jercinovic, M.J., 2002. Microprobe monazite geochronology: Putting absolute time into microstructural analysis. Journal of Structural Geology 24, 1013–1028. https://doi.org/10.1016/S0191-8141(01)00088-8

Zuquim, M. P. S., Trouw, R. A. J., Trouw, C. C., Tohver, E., 2011. Structural evolution and U–Pb SHRIMP zircon ages of the Neoproterozoic Maria da Fé shear zone, central Ribeira Belt – SE Brazil. Journal of South American Earth Sciences, 31(2–3), 199–213. https://doi.org/10.1016/J.JSAMES.2011.02.002

FIGURES CAPTIONS

Figure 1 - a) Western Gondwana reconstruction by Westin et al. (2021). The blue square marks the cratonic blocks involved in the Southern Brasilia Orogen (SBO) development.

(1) Transbrasiliano-Kandi Lineament. Continental cratons: A-Amazon; CC- Congo; KA-Kazai; LA- Luis Alves; P- Pampia; Pp- Paranapanema; Pb- Parnaíba; WA-RA- Ria Apa; RP- Rio de la Plata; SH- Sahara; SF- São Francisco; SL- São Luis; b) Orogenic belts of Central and Southeast Brazil (Westin et al., 2021). Red square is the SBO position.

Figure 2 - Southern Brasilia Orogen (SBO) tectonic map modified after Campos Neto et al. (2020). The black square marks the study area location.

Figure 3 – Cross-section A-B (see Fig. 2) illustrating the tectonic architecture of the south sector of the Southern Brasilia Orogen.

Figure 4 - a) Geological map of Pouso Alto county; b) Geological cross-section of the area and stereographic projections of collected structural data.

Figure 5 - Blastesis-deformation relationships in the Liberdade and Andrelândia Nappes.

Figure 6 - Liberdade Nappe (LN) photomicrographs. a) Spaced disjunctive schistosity (S_2) defined by biotite and white mica shape preferential orientation (SPO). Quartz displays moderately irregular contacts (UTM 521535/7560145); b) Skeletal garnet and decussate fibrolite (UTM 521535/7560145); c) Garnet porphyroblast with S-shaped internal foliation (UTM 521535/7560145); d) Garnet pseudomorph replaced completely by fibrolite (UTM 521535/7560145); e) Isoclinal fold marked by fibrolite orientation (UTM 519472/ 7549550); f) Kyanite relic overgrown by white mica (UTM 5110028/7561820).

Figure 7 - Quantitative compositional maps for the sample NESG-388 of the Liberdade Nappe: a) Mineral map of the investigated thin-section area showing the mineral phases in the mapped area; b) Anorthite (XAn) content in plagioclase map; c)-f) Almandine (XAlm),

grossular (XGrs), pyrope (XPrp) and spessartine (XSps) zoning in garnet. The red circles indicate the area used to perform the Q_{cmp} maps for garnet, and plagioclase (core and rim).

Figure 8 - Andrelândia Nappe (AN) photomicrographs. a) Compositional banding, alternating layers made by quartz and plagioclase, and those constituted by white mica and biotite with subordinate garnet and kyanite (UTM 513937/7565930); b) Garnet porphyroblast with opaque inclusion trails defying the internal foliation (Pre-S_2), and kyanite aligned according to the external S_2 foliation (UTM 516960/7565691); c) Fibrolite growth along a shear bands (UTM 516960/7565691); d) Garnet with opaque inclusion trails oblique to the external foliation (post-S_2) made by sillimanite, quartz, and biotite. Staurolite with internal foliation continuous with the external one. Note the fibrolite replacing biotite crystals (UTM 516960/7565691).

Figure 9 - Quantitative compositional maps for sample NESG-401 of the Andrelândia Nappe; a) Mineral map of the investigated thin-section area showing the mineral phases in the mapped area; b) Anorthite (XAn) content in plagioclase map; c)-f) Almandine (XAlm), grossular (XGrs), pyrope (XPrp) and spessartine (XSps) zoning in garnet. The red circles indicate the area used to perform the Q_{cmp} maps for garnet (mantle and rim), and plagioclase (core and rim).

Figure 10 – a) *P-T* isochemical phase diagram in the MnNCKFMASHT system for the Liberdade Nappe (NESG-388); b) *P-T* path based on optimal conditions of mineral chemistry composition (Q_{cmp}) and mode (Q_{mode}) maps. The red star corresponds to the optimal *P-T* conditions obtained by the antidote.

Figure 11 – a) *P-T* isochemical phase diagram in the MnNCKFMASHT system for the Andrelândia Nappe (NESG-401); b) *P-T* path based on optimal conditions for mineral chemistry composition (Q_{cmp}) and mode (Q_{mode}) maps. The red star corresponds to the optimal P-T conditions obtained by the antidote.

Figure 12– Liberdade Nappe (sample NESG-388): a) BSE images, X-ray maps (Y and Th) of monazites showing structural position, textural relationships, and internal zoning; b) Y_2O_3 (wt%) *vs.* age plot; c) ThO_2 (wt%) *vs.* age plot; d) weighted average diagram for monazite core dates (domain 1 and 2); e) weighted average diagram for monazite rim dates (domain 3).

Figure 13 – Andrelândia Nappe (sample NESG-401): a) BSE images, X-ray maps (Y and Th) of monazites showing structural position, textural relationships, and internal zoning; b) Y_2O_3 (wt%) *vs.* age plot; c) ThO_2 (wt%) *vs.* age plot; d) weighted average diagram for monazite core dates; e) weighted average diagram for monazite enclosed in Ky.

Figure 14 – a) Summary of Andrelândia Nappe System (ANS) *P-T* paths. Grey dotted lines display different geothermal gradients trends. Solidus curve from Spear et al. (1999) in the NaKFMASH system; b) summary of the monazite and zircon U-Pb metamorphic ages from the Liberdade and Andrelândia Nappes.

Figure 15 – Tectono-metamorphic model for the evolution of the SBO nappes. a) 630 to 620 Ma: Early prograde metamorphism in the collisional wedge and Pouso Alto Nappe burial and heating stage; b) 620 to 610 Ma: Onset of the decompression path in the collisional wedge. Pouso Alto Nappe decompression and melt crystallization stage, while the Liberdade Nappe was buried and heated; c) 610 to 580 Ma: Liberdade Nappe onset its

upward isothermal decompression path over the Andrelândia Nappe, which was heated and buried; d) <580-570 Ma: Final stage of the SBO continental collision coeval with the Andrelândia and Carrancas Nappes decompression and cooling stages. The *P-T-t* paths are based on Benetti. (2022), Campos Neto et al. (2021), Coelho et al. (2017), Fumes et al., (2021), Li et al. (2021), Marimon et al. (2020, 2022), Motta and Moraes (2017), Motta et al. (2021), Rocha et al. (2017), Westin et al. (2021).

SUPPLEMENTARY FIGURE FILE A

Figure A1 - Full thin-sections maps acquired using the Scanning Electron Microscopy and Mineral Liberation Analyzer (SEM-MLA). The black square represents the local bulk composition (LBC) investigated. a) Sample NESG-388 from Liberdade Nappe; b) Sample NESG-401 from Andrelândia Nappe.

Figure A2 – Quantitative compositional maps for the sample NESG-388 from Liberdade Nappe. a) Map of Ti content in biotite (a.p.f.u); b) Map of #Mg in biotite; c) Map of Ti in biotite thermometer of Henry et al. (2005); d) Map of Si^{+4} content in white mica (a.p.f.u). Red circle indicates the area used to perform the Q_{cmp} maps.

Figure A3 – Quantitative compositional maps for the sample NESG-401 from Andrelândia Nappe. a) Map of Ti content in biotite (a.p.f.u); b) Map of #Mg in biotite; c) Map of Ti in biotite thermometer of Henry et al. (2005); d) Map of Si^{+4} content in white mica (a.p.f.u). Red circle indicates the area used to perform the Q_{cmp} maps.

Figure A4- Maps of quality factors by Antidote for Liberdade Nappe. a) Q_{asm}; b)Q_{mode}; c) Q_{cmp} for the LBC bulk composition; d)Q_{cmp} for garnet composition; e) Q_{cmp} for plagioclase core composition; f) Q_{cmp} for plagioclase rim composition; g) Q_{cmp} for white mica composition; h) Q_{cmp} for biotite composition.

Figure A5- a) *P-T* isochemical phase diagram in the MnNCKFMASHT system for the Andrelândia Nappe (NESG-401) for LBC including garnet core composition; b) Map of quality factor Q_{cmp} by Antidote for AN garnet core composition.

Figure A6 - Maps of quality factors by Antidote for Andrelândia Nappe. a) Q_{asm}; b) Q_{mode}; c) Q_{cmp} for the LBC bulk composition; d) Q_{cmp} for garnet mantle composition; e) Q_{cmp} for garnet rim composition; f) Q_{cmp} for white mica composition; g) Q_{cmp} for plagioclase core composition; h) Q_{cmp} for plagioclase rim composition; i) Q_{cmp} for biotite composition.

Figure A7 – Weighted mean plot for Moacyr monazite standard.

SUPPLEMENTARY TABLE FILE A

Table A1- Representative Electron Microprobe (EMP) analyses of minerals from samples NESG-388 and NESG-401. (b.d.l. - below detection limit).

Table A2 - Monazite chemical composition from sample NESG-388 and NESG-401 (normalized to 4O), (b.d.l- below detection limit).

In-sequence tectonic evolution of Ediacaran nappes in the southeastern branch of the Brasília Orogen (SE Brazil): constraints from metamorphic iterative thermodynamic modeling and monazite petrochronology

Beatriz Benetti[a,b*], Mario da Costa Campos Neto[b], Rodolfo Carosi[a], George Luvizotto[c], Salvatore Iaccarino[a], Chiara Montomoli[a,d]

Corresponding author:

*Beatriz Benetti – beatrizyuri.benettisilva@unito.it - ORCID: 0000-0001-5698-3075

Present address: Geological Survey of Brazil – SGB/CPRM, Av Pasteur 404, Rio de Janeiro - RJ, Brazil

Affiliations:

a Dipartimento di Scienze della Terra, Università degli Studi di Torino, Turin, Italy

b Instituto de Geociências, Universidade de São Paulo, São Paulo, Brazil

c Departamento de Geologia, Universidade do Estado de São Paulo

d Istituto di Geoscienze e Georisorse, IGG-CNR, Pisa, Italy

ABSTRACT

The metamorphic and kinematic evolution of medium-high grade rocks of~~forming the hinterland of the orogenic wedge are able to record pressure (*P*) and temperature (*T*) changes during the orogen development, as well as its kinematic history.~~ ~~T~~the Andrelândia Nappe System (ANS), ~~is~~ the ~~hinterland~~ orogenic wedge of the Southern Brasilia Orogen (SBO), was investigated in this work ~~and its tectono-metamorphic evolution has been a~~

~~subject of intense debate in the past decades~~. Field and microstructural observations were combined with metamorphic petrology (i.e., iterative thermodynamic modeling) and monazite petrochronology to reconstruct the tectono-metamorphic history of the ANS rocks. The Liberdade Nappe ~~attained~~ experienced prograde metamorphism at *ca.* 610 Ma, achieving peak metamorphic conditions of ~~∼~~*ca.* 650°C and 9.5-10 kbar. This stage was followed by isothermal decompression linked to tectonic transport toward SE, at *ca.* 570 Ma. On the contrary, the Andrelândia Nappe experienced prograde metamorphism later, at *ca.* 580 Ma, reaching peak metamorphic conditions of *ca.* 680°C and 11-12 kbar. The obtained results indicate that each~~the~~ nappe of the Andrelândia System ~~record~~records a single metamorphic cycle of burial and decompression, although it took place at different ages over a period of *ca.* 60 ~~Ma~~myr, from 630 to 570 Ma. The nappes experienced prograde and retrograde metamorphism whose ages progressively decreased toward the bottom of the nappe stack. ~~The different ages of when the nappes experienced prograde and retrograde metamorphism followed a progressive decrease toward the bottom of the stack.~~ We attribute this pattern ~~This would have occurred owing~~ to propagation of older buried material from ~~inner parts of~~ the orogenic wedge (i.e., Liberdade Nappe), via thrust-and-fold, upon recently accreted rocks (i.e., Andrelândia Nappe), conducting a younger metamorphism event on the footwall of the ductile thrusted nappes ~~external parts of the wedge~~. This mechanism is consistent with the ANS~~would be responsible to outline an the~~ in-sequence fold-and-thrust architecture ~~of the ANS~~.

KEYWORDS:

Monazite petrochronology, iterative thermodynamic modeling, Brasília Orogen metamorphism, P-T-t-D paths

1. INTRODUCTION

The growth of a mountain belt is controlled by the balance among accretion of crustal material, such as sediments and magma addition as well as thrust stacking, and removal by erosion, ~~tectonic~~ delamination, and post-orogenic ~~thinning~~ extension (Beaumont et al., 2001; Davies et al., 1983; Jamieson and Beaumont, 2013; Vanderhaeghe, 2012; Whipple, 2009; Willett, 1999). ~~External (e.g., climate) and internal (e.g., structure and geodynamic) factors, controlling mountain building, play a main role in modifying the architecture of the orogenic wedge of a collisional belt (DeCelles and Mitra, 1995).~~ An orogenic wedge is constituted by crustal material mainly detached from the subducted lithosphere, accreted, and stored within the orogenic system (Vanderhaeghe, 2012; Vanderhaeghe et al., 2003). During orogenesis, erosion, normal faulting, and ductile flow can lead ~~balance of the orogen active forces leads~~ to exhumation of the deep-seated rocks at the front of the crustal wedge (DeCelles and Mitra, 1995; England & Molnar, 1990; Ring et al., 1999; Vanderhaeghe et al., 2003). Deformation and ductile flow can follow an in-sequence pattern when they present progressive age decreases in the same direction of the tectonic transport (Weller et al., 2021). ~~Moreover, t~~The accumulation of crustal material within an orogen enriched in radioactive heat-production elements, such as U, Th, and K, modifies its crustal geothermal gradient (England and Thompson, 1984; Rudnick and Fountain, 1995). Moreover, thrust stacking of hot rocks upon colder ones can also be a heat source for metamorphism in the footwall ("the hot iron model"; England & Molnar, 1993; Le Fort, 1975). Therefore, ~~The aforementioned observations demonstrate that~~ the deep-seated crustal rocks~~, stored within an orogenic wedge,~~ are able to record pressure (*P*) and temperature (*T*) changes during the development of an orogen as recorded by its kinematic and internal structure, providing valuable information to understand the deep dynamics of collisional wedges.~~an orogen development as well as its kinematics history and crust internal structure~~. ~~Hence, the study of the deformation and metamorphic conditions of deep-seated crustal rocks stored in an orogenic wedge is fundamental to comprehending the tectonic and geodynamic evolution of ancient and young orogenic belts.~~

The Andrelândia Nappe System (ANS) is regarded as the Southern Brasilia Orogen (SBO) hinterland of an orogenic wedge. Its tectono-metamorphic evolution has been a target of intense debate ~~in~~ during the past several decades. ~~Indeed,~~ Some researchers (Coelho et al., 2017; Fontainha et al., 2020; Li et., 2021; Trouw et al., 2013) argue that the ANS evolution was due to polymetamorphism related to two separate tectonic events during different orogenic cycles.~~results of a polymetamorphic evolution related to two separate tectono-metamorphic events from different orogenic cycles~~. The first event ~~is~~ was related to high-P metamorphic conditions testified by the HP-granulites and E/NE nappe stacking, owing to the Paranapanema and São Francisco Cratons collision in the period from *ca.* 630 to 600 Ma (Coelho et al., 2017; Li et al., 2021; Reno et al., 2012; Trouw et al., 2013). It was followed by a second orogenic event, characterized by medium pressure, greenschist- to amphibolite-facies conditions in the staurolite and sillimanite zones, during NW-SE contraction at 600-560 Ma (Coelho et al., 2017; Fontainha et al., 2020; Heilbron et al., 2017; Trouw et al., 2013; Zuquim et al., 2011).~~, with NW-SE shortening direction, and ages from 600 to 560 Ma~~. ~~This second episode would be related~~ This tectonic event is attributed to the Central Ribeira Orogeny (Fig. 1b). The second ~~viewpoint~~ model proposes that the ANS evolution ~~results~~ was due to ~~from~~ a single orogenic cycle. ~~According to them,~~ The ANS tectono-metamorphic evolution is linked to the Paranapanema block collision against the São Francisco Craton (Campos Neto et al., 2011; Frugis et al., 2018; Westin et al., 2021). In this hypothesis, the sillimanite and staurolite presence documented by the ANS rocks would result from the decompression/exhumation of the nappe pile rather than testify a second tectono-thermal event. The available metamorphic ages, from 630 to 580 Ma, indicate a thrust propagation from WSW to ENE toward the São Francisco Craton southern edge (Westin et al., 2021 and references therein).

The reconstruction of Pressure-Temperature-time-Deformation (*P-T-t-D*) paths provide ~~elementary~~ fundamental information to understand the tectonic and metamorphic events experienced by rocks accreted to the orogenic wedge. Primarily, the application of internally consistent databases to create phase equilibria models that can be ~~to build pseudosection has been~~ used to constrain metamorphic conditions (Powell and Holland, 2008; Waters, 2019). This data can be linked with microstructural observations to set up the rock fabric relationships with the metamorphic mineral assemblage, i.e., the so-called blastesis-deformation relationships ~~(Passchier & Trouw, 2005)~~. In addition, the in-situ dating of accessory minerals, such as monazite, zircon, or titanite can provide ages for specific metamorphic reactions and deformation events~~, can be bound to metamorphic reactions and deformation events~~ (e.g., Bosse and Villa, 2019; Kohn et al., 2017; Williams and Jercinovic, 2012). This approach is ~~has been~~ ~~proven to be~~ one of the most effective ways to understand the complex frameworks of collisional belts ~~complex frameworks~~ (Carosi et al., 2018; Waters, 2019). In this contribution, we combine field and microstructural observations with iterative metamorphic thermodynamic modeling~~modern techniques in metamorphic petrology~~ and *in-situ* monazite geochronology. This integrative approach provides ~~the necessary~~ information about the timing of tectonic processes that drove the build of the ANS fold-and-thrust belt, such as tectonic burial and exhumation, and allowed the reconstruction of the tectono-metamorphic history of the ANS rocks.

2. GEOLOGICAL SETTING

The Brazilian-Pan African event is the name given to a series of diachronic collisions in the São Francisco-Congo Craton side of the West Gondwana paleocontinent (Cordani et al., 2003; Ganade De Araujo et al., 2014; Fig. 1). The Southern Brasilia Orogen (SBO) is one of the orogenic belts built during this tectonic event (Cordani et al., 2003; Fig. 1 and 2). The SBO evolved from the lateral collision between the Paranapanema paleocontinent, the active margin, against the São Francisco paleocontinent, representing the SBO passive margin (Campos Neto, 2000; Campos Neto et al., 2011; Trouw et al., 2013, 2000).

The SBO final architecture resulted in an almost flat-lying fold-nappe pile, with top-to-the-east/northeast tectonic transport (Fig. 3). Three tectonic domains are recognized within the SBO (Campos Neto, 2000; Campos Neto et al., 2011, 2021; Trouw et al., 2013, 2000; Fig. 2 and 3): (1) the active margin of the Paranapanema paleocontinent, constituted by the granulites and migmatites of the Socorro-Guaxupé Nappe, (2) the orogenic wedge hinterland, a pile of metasedimentary nappes of the Andrelândia Nappe System, (3) the passive margin related to the São Francisco paleocontinent, made by the psamo-pelitic sequences of the Carrancas and Lima Duarte Nappes. These tectonics domains are intruded by leucogranites (Fig. 3) and A-type granitic rocks (i.e., Itu Granite Province, Pedra Branca, and Capituva Plutons; Fig. 2) interpreted as post-orogenic plutons~~bodies~~.

The SBO is split into two segments by a tectonic window (Fig. 2) exposing the Archean-Paleoproterozoic migmatitic orthogneiss from the basement complexes (Cioffi et al., 2019, 2016; Westin et al., 2016). The Andrelândia Nappe System (ANS) is sandwiched among the UHT-HT metamorphic rocks of the Socorro-Guaxupé Nappe (Campos Neto and Caby, 1999; Motta et al., 2021; Rocha et al., 2017a; Tedeschi et al., 2018; Fig. 3) at the top and, by the low- to medium temperature metasedimentary rocks of the passive margin covers (Fig. 2 and Fig. 3), at the bottom. Internally, the ANS is divided from its uppermost structural level to the bottom by the Três Pontas-Varginha and Carmo da Cachoeira Nappes in the northern sector. In the southern sector, the ANS is segmented into the Pouso Alto (or Aiuruoca, Carvalhos, and Serra da Natureza Klippes equivalent), Liberdade, and Andrelândia Nappes (Fig. 3). Two characteristics are remarkable in the ANS: i) its inverted metamorphic pattern, in which rocks in the high-P granulite metamorphic facies structurally overlap those in amphibolite facies conditions (Campos Neto and Caby, 2000, 1999; Garcia and Campos Neto, 2003; Motta and Moraes, 2017; Trouw et al., 2000, 1998); ii) the decrease of metamorphic ages eastward, which is the same sense of the non-coaxial ductile flow (Campos Neto et al., 2011; Westin et al., 2021).

The Três Pontas-Varginha, Pouso Alto Nappe, and the Auiruoca, Carvalhos, and Serra da Natureza Klippes, lay on the top of the ANS stack. They are made of K-feldspar+garnet+kyanite+rutile-bearing gneiss. These rocks attained metamorphic conditions of *ca.* 830°-900°C and 12-16 kbar in the high-pressure granulite facies conditions (Campos Neto et al., 2010; Campos Neto and Caby, 2000; Cioffi et al., 2012; Fumes et al., 2021; Garcia and Campos Neto, 2003; Li et al., 2021; Reno et al., 2009).

The Liberdade Nappe (LN), the intermediate unit of the ANS, is composed of garnet+kyanite+ilmenite(±sillimanite±rutile)-bearing micaschist and paragneiss with subordinate quartzite, metabasite, and calc-silicate lenses. Metamorphic conditions, in metapelites, are constrained in the *P-T* range of 642-715°C and 6-10 kbar (Coelho et al., 2017; Motta and Moraes, 2017; Rodrigues et al., 2019; Santos et al., 2004). Zircon and monazite U-Pb dating retrieved ages around 620-615 Ma (Coelho et al., 2017; Motta and Moraes, 2017; Westin et al., 2021). Moreover, the metamafic rocks, interpreted as retroeclogites (Campos Neto and Caby, 1999; Coelho et al., 2017; Reno et al., 2009; Trouw et al., 2013), experienced *P-T* conditions around 700°-800°C and 12-16 kbar (Coelho et al., 2017; Reno et al., 2009; Tedeschi et al., 2017). The metamafic rocks present two clusters of metamorphic ages, the first around 680-660 Ma (Campos Neto et al., 2011; Reno et al., 2009), and the other around 630-625 Ma (Coelho et al., 2017; Tedeschi et al., 2017).

The Andrelândia (AN) and Carmo da Cachoeira Nappes are at the bottom of the ANS stack. They are internally constituted by~~, divided into three lithostratigraphic units.~~ ~~F~~from the top to the base, ~~they are:~~ micaschists intercalated with metapsamites ~~Rio Capivari~~, metawackes ~~from the Santo Antonio~~, and micaschists ~~from the Serra da Boa Vista~~. The AN displays an inverted metamorphic gradient in which "peak" mineral assemblages vary from garnet+~~biotie~~biotite+staurolite at its bottom to the kyanite+garnet+melt at the top. The Andrelândia and Carmo da Cachoeira Nappes attained peak conditions around 650-670°C and 9-10 kbar in *ca.* 600 Ma, followed by almost isothermal decompression in the time span of 600-575 Ma (Frugis et al., 2018; Marimon et al., 2022; Motta and Moraes, 2017; Reno et al., 2012; Santos et al., 2004; Westin et al., 2021).

3. RESULTS

3.1 Field observations

The study area is located in southeast Brazil, in the Minas Gerais state around Pouso Alto County. It comprises a geological section from SW to NE in the Andrelândia Nappe System southern sector (Figs. 2 and 4), highlighting all of its allochthonous units along with the basement ~~nucleus~~ cores of the nappe system.

The Pouso Alto Nappe has a spoon-shaped cylindrical SW-oriented synform, with W-SW plunging of the mineral and stretched lineations, and a general transport toward NE evidenced by asymmetric mafic boudin and *S-C* fabric kinematic indicators (Fig. 4a and b). The main lithotype described is a medium- to coarse-grained K-feldspar+garnet+kyanite+rutile(±ilmenite±biotite)-bearing gneiss.

The Liberdade Nappe is represented by fine- to medium-grained garnet+ilmenite (±sillimanite ±rutile±kyanite±staurolite)-bearing micaschist interlayered with quartzite. Micaschist displays a main spaced disjunctive schistosity, defined by biotite, white mica, and aluminum silicates shape preferred orientation (SPO). Intrafolial stretched isoclinal passive folds are observed. The ensemble of the foliation describes a large cylindrical synform with an SW-oriented B-axis in a type-3 superposition pattern (Ramsay, 1962) over recumbent isoclinal folding between the basement nucleus and the metasedimentary sequence (Fig. 3). The mineral (sillimanite/fibrolite and micas) lineations are mainly oriented to SE, which, coupled with some kinematics indicators (*S-C* fabric and asymmetrical ~~pressure~~ strain shadow structures), point to an eastward transport of the nappe. The Pouso Alegre Complex is made by orthogneisses of a tonalite-granite series related to the Paleoproterozoic basement (Cioffi et al., 2016). A leucogranite body intrudes micaschist of the Liberdade Nappe, the Alagoa migmatite, and the Pouso Alegre Complex (Fig. 3, 4a, and b).

The Andrelândia Nappe crops out in the north of the study area (Fig. 4a and b). It is made of grayish metawackes, and at its lithostratigraphic boundaries metapelites associations prevail. The main lithology described is a garnet+kyanite(±staurolite)-bearing gneiss. The main foliation is a spaced disjunctive schistosity identified by SPO on white mica, biotite, and kyanite. The schistosity strikes ENE-WNW with dips varying from low to high angles, between 20°-80° toward the north. White mica, biotite, quartz, and kyanite are responsible for outlining the mineral and stretching lineation, which trends between N90°-N120° and plunges 10°-50° to E/SE. A kinematic change between the Pouso Alto Nappe, and the Liberdade and Andrelândia is noticed in the area. Whereas the upper nappe points to northeastward tectonic transport, the middle and lower suggest an east-southeastward direction.

3.2 Petrography, microstructural relationships, and mineral chemistry

In order to constrain the relationships between mineral growth and deformation (Fig. 5), several samples from Liberdade and Andrelândia Nappes were petrographically studied. One representative sample of each nappe was selected for performing full thin-sections maps acquired using the Scanning Electron Microscopy and Mineral Liberation Analyzer (SEM-MLA) (supplementary figures A1). The location of samples is given in Fig. 4a. An area of each thin-section mapped containing the inferred peak mineral assemblage, avoiding retrometamorphic textures where possible, was investigated using X-ray maps acquired by an electron probe micro-analyzer (EMPA). The analytical procedure employed for EMPA analysis is described in Appendix A. The X-ray maps were converted into oxide weight percentage maps applying internal standards (Andrade et al., 2006) in the software XMapTools 3.4 (Lanari et al., 2014, 2019). Such areas were the basis for estimating the Local Bulk Composition (LBC) needed for petrological modeling (see section 5). The mineral abbreviations follow Whitney and Evans (2010).

3.2.1 Liberdade Nappe (LN)

The Liberdade Nappe micaschist is made up of quartz+plagioclase+white mica+biotite+garnet+ilmenite(±sillimanite±rutile+kyanite±staurolite). The LN displays a spaced disjunctive schistosity (S_2, Fig. 6a), and in some portions presents microstructures of tectonic transport such as a *S*-*C* fabric and isoclinal folds, made up mainly of white mica and sillimanite, denoting top-to-the-SE motion. Quartz has slightly lobate contacts (Fig. 6a), and plagioclase has undulose extinction. The quartz features reveal that this mineral was recrystallized due to the grain boundary migration (GBM) regime and underwent the grain boundary area reduction (GBAR; Passchier and Trouw, 2005). Garnet porphyroblast has in several circumstances a skeletal microstructure (Fig. 6b). It also shows S-shaped inclusions made of quartz (Fig. 6c), defining an internal foliation that is not continuous with the external one. Then, garnet is regarded as a pre- to early-syn-tectonic mineral with respect to the S_2 schistosity. Sillimanite is present as fibrolite, it replaces partial to completely garnet porphyroblasts, forming pseudomorphs (Fig. 6d), and also occurs along intrafolial isoclinal folds (Fig. 6e). Subidiomorphic relic of kyanite wrapped by white mica is observed (Fig. 6f). Staurolite, in a very low modal amount, is fine-grained and often related to garnet rims. Rutile is enclosed in garnet and in the matrix is usually rimmed by ilmenite.

The relationships among minerals suggest three metamorphic stages, here referred as M_{LN1}, M_{LN2}, and M_{LN3}, for the Liberdade Nappe micaschist (Fig. 5). The M_{LN1} stage is pre-S_2, related to prograde/peak metamorphism and it is characterized by quartz+plagioclase+white mica+biotite+garnet+rutile+kyanite(?) as the equilibrium assemblage in the rock. The M_{LN2} stage, in which quartz+plagioclase+white mica+biotite+garnet+kyanite(?)+ilmenite is inferred to be stable, represents a post-peak mineral assemblage. Finally, sillimanite and staurolite are regarded as phases that grew during the late stages of the metamorphic path (M_{LN3} and Syn-S_2).

Sample NESG-388 (Fig. 4a, supplementary figure A1) was selected for the LN mineral chemistry investigation and petrological modeling. The NESG-388 is a white mica+biotite+garnet+ilmenite-bearing mylonitic schist with minor sillimanite, rutile, and staurolite (Fig. 7a). Plagioclase is compositionally zoned, and its anorthite content increases from core to rim (XAn –0.20-0.32) (Fig. 7b). Garnet end-members vary slightly from core to rim: almandine (XAlm)=0.81-0.79, pyrope (XPrp)=0.11-0.07, spessartine (XSps) =0.05-0.06 and grossular (XGrs)=0.05-0.06 (Fig. 7c-f). The Ti (a.p.f.u) in biotite decreases toward the rim, ranging from 0.14 to 0.09, whereas the #Mg (Mg/Fe^{+2}+Mg) ratio displays an inverse correlation, increasing toward the rims, varying from 0.37 to 0.43 (supplementary figures A2a and b). The Si^{4+} (a.p.f.u) of white mica varies from 3.04 to 3.12 (supplementary figure A2d).

3.2.2 *Andrelândia Nappe*

The Andrelândia Nappe is constituted by the major phases: quartz+plagioclase+biotite+white mica+garnet+kyanite+ilmenite(±sillimanite±staurolite) and tourmaline+apatite+monazite+zircon+rutile as accessories. The AN has a S_2 foliation characterized by discontinuous millimetric compositional layers of granoblastic, made by quartz and plagioclase, and lepidoblastic, constituted by white mica and biotite with subordinate garnet and kyanite (Fig. 8a). The AN close to the contact with the Liberdade Nappe is affected by shearing and displays a mylonitic fabric (post-S_2). The kinematic indicators described in the sheared gneisses are S-C fabric and white mica-fish, which point to a top-to-the-E/ESE tectonic transport. Quartz is a medium- to coarse-grained mineral with irregular and lobate ~~contacts~~boundaries, typical of the GBM recrystallization mechanism (Law, 2014).

Garnet is present as porphyroblast (≤2 cm in size) (Fig. 8b). Discontinuous inclusion trails of opaque minerals within garnet, with respect to the S_2 fabric, testify to the inter-tectonic nature of this mineral (Fig. 8b and d). Thin graphite crystals, ilmenite, and rutile are the typical inclusions in garnet, and staurolite, quartz, plagioclase, biotite, and white mica are subordinate. Kyanite is a coarse-grained subidiomorphic crystal with a long axis aligned along the S_2 foliation (Fig. 8b). Twinning in kyanite is observed. Late fibrolite growth (post-S_2) along shear bands and replacing biotite crystals are observed (Fig. 8c and d). Two generations of staurolite were observed, the first is characterized by tiny crystals enclosed in garnet, ~~Whereas~~ whereas the second one is in the matrix, often around garnet rims. A staurolite with biotite and sillimanite inclusions aligned with the external foliation, made by sillimanite, quartz, and biotite, denotes a syn-tectonic origin regarding the post-S_2 fabric (Fig. 8d). The contact between staurolite and garnet, as well as the abrupt change of the internal foliation of both minerals, suggest a pattern of porphyroblasts amalgamated (Fig. 8d, e.g., Passchier and Trouw, 2005).

Based on the above description, three main stages of mineral equilibration were recognized (Fig. 5). The early prograde assemblage (M_{AN1}), preserved in garnet core, is constituted by ~~Grt(core)+Qz+Pl+Bt+Ms+St+Rt~~garnet(core)+quartz+plagioclase+biotite+white mica+staurolite+rutile. The peak assemblage (M_{AN2}) is coeval with the S_2 foliation and is marked by the appearance of kyanite and ilmenite and the consumption of staurolite and rutile. The M_{AN3} assemblage corresponds to retrograde metamorphic ~~path~~assemblage, characterized by a second growth of staurolite around garnet rims together with the late fibrolite appearance, and structures related to the tectonic transport (post-S_2 foliation).

Sample NESG-401 was chosen for a detailed chemical investigation (Fig. 4a, supplementary figure A1). The gneiss is composed of quartz+plagioclase+biotite+white mica+garnet+ilmenite~~Qz+Pl+Bt+Ms+Grt+Ilm~~ and minor apatite (Fig. 9a). This sample is white mica-poor, which is restricted to the garnet strain shadow zones (supplementary figure A1 and Fig. 9a). The plagioclase is zoned, displaying Ca-poor cores (XAn -0.22) and Ca-rich rims (XAn -0.32). The highest Ca-content (XAn -0.34) occurs in crystals that bound garnet (Fig. 9b). There are two garnet crystals in the X-ray mapped area. The large garnet porphyroblast displays a bell shape profile, whereas the smaller one presents an almost flat profile (Fig. 9c, d, e, and f). The garnet porphyroblast shows an increase in almandine and pyrope toward the rim, whereas spessartine and grossular display the inverse pattern (Core- XAlm-0.6, XPrp-0.06, XSps -0.1, XGrs-0.22; Rim- XAlm-0.72, XPrp-0.13, XSps-0.03, XGrs-0.08) (Fig. 9c, d, e, and f). Spessartine displays a sharp increase in the outermost rim (XSps-0.09/0.1) in both garnet crystals. The biotite composition varies according to its structural position. Crystals close to garnet have higher #Mg and lower Ti (a.p.f.u) compared to grains far from garnet (Bt near garnet XMg- 0.54-0.52 and Ti(a.p.f.u)- 0.8-0.10; Bt in matrix XMg-0.5-0.51 and Ti(a.p.f.u)- 0.11-0.12) (supplementary figure A3a and b). The Si^{4+} content in white mica is close to the muscovite end-member, between 3.00-3.08 a.p.f.u. (supplementary figure A3d).

3.3 Iterative Thermodynamic Modeling (ITM) and P-T path

The iterative thermodynamic modeling (ITM) integrated with quantitative compositional mapping was applied as the strategy for setting up the metamorphic history of the Andrelândia and Liberdade Nappes using the software Bingo-Antidote a XMapTools add-on (Duesterhoeft and Lanari, 2020; Lanari and Hermann, 2021). This approach provides a means of investigating rocks that were not fully re-equilibrated during their metamorphic paths. Through the quantitative compositional maps, areas\phases within a sample that best represents the reactive phases can be selected for the local bulk composition (LBC) calculation. Furthermore, the Bingo-Antidote software provides series of statistics routines that compare the model results with the observed mineral assemblage, modes, and phase compositions for the LBC studied. The bingo routines calculate the model quality, assessing as much as it matches with the LBC mineral assemblage (Q_{asm}), mineral modes (Q_{mode}), and mineral compositions (Q_{cmp}). The quality factors Q_{asm}, Q_{mode}, and Q_{cmp} vary from 0%, which means there is no match between the model and LBC observations, and 100%, meaning that the model perfectly reproduces the LBC features. In addition, the antidote provides routines, for instance the recipe 14, to evaluate how the quality factors change within the model P-T(-X). The Andrelândia and Liberdade Nappes thin-section areas investigated for obtaining LBCs and mineral compositions (Q_{cmp}) quality factors are displayed in Fig. 7a, 9a, supplementary figures A1, A2, and A3. The maps of quality factors from both samples are shown in supplementary figures A4, A5, and A6.

The isochemical diagrams were calculated for the local bulk composition (LBC) obtained by the Bingo-Antidote using the Theriak-Domino software (de Capitani and Petrakakis, 2010; de Capitani and Brown, 1987) to illustrate the stability of mineral fields. The calculations were performed in the chemical system MnO-Na_2O-CaO-K_2O-FeO-MgO-Al_2O_3-TiO_2-SiO_2-H_2O. The water amount was chosen using recipe 14 of the antidote, a statistical routine that asses how the quality factors (Q_{asm}, Q_{mode}, and Q_{cmp}), the mineral chemistry, and mode would vary along a given range of H_2O~~0~~, at fixed *P-T* conditions. The diagrams were calculated for the *P-T* range of 4-12 kbar and 550-725 °C. The database tc55 (Holland and Powell, 1998), provided and employed in the Bingo-Antidote software, was used for the isochemical diagrams calculations. The respective solution models were utilized: feldspar (Baldwin et al., 2005), garnet (White et al., 2005), biotite (White et al., 2005), staurolite (Holland and Powell, 1998), cordierite (Holland and Powell, 1998), white mica (Coggon and Holland, 2002), ilmenite (White et al., 2007) and melt (White et al., 2007).

3.3.1 Sample NESG-388 - Liberdade Nappe

The calculated isochemical diagram for the Liberdade Nappe LBC is presented in Fig. 10a. The observed peak mineral assemblage, quartz+plagioclase+white mica+biotite+ilmenite, is stable in the penta-variant field constrained in the *P-T* range of 6.5-12 kbar and 600-670°C. Assuming the mineral phase equilibrium, the optimal *P-T* condition is expected to be achieved at 628°C and 7.5 kbar. At this condition, the quality factors for the mode (Q_{mode}) is 92%, and the system mineral chemistry (Q_{cmp}) is 86% (Fig. 10b).

The mineral *P-T* chemistry composition maps are presented in supplementary figure A4. They display a more complex story used to trace the *P-T* path (Fig. 10b). The An-poor plagioclase core compositions (Q_{cmp}=100%) are stable in higher pressure, 8.5 kbar up to 11.5 kbar, and in large temperature conditions, from 500°C to 700°C. On the contrary, plagioclase rim composition records a lower pressure condition, down to 8 kbar, and temperatures from 590°C to 660°C. Although the optimal *P-T* conditions obtained by the antidote, peak conditions are better constrained by plagioclase rim composition (Q_{cmp} =100%), around 650°C and 9.5-10 kbar. The Na-Ca diffusion in plagioclase is considered slower than garnet Ca-Fe-Mg-Mn in temperatures above 600°C (Caddick et al., 2010; Lanari and Hermann, 2021). These described diffusional behaviors are the likely causes of plagioclase core records better the prograde conditions rather than garnet.

Plagioclase rim (Q_{cmp} =100%), and garnet (Q_{cmp} =90-100%) mineral chemistry compositions in addition with the mineral modes (Q_{mode} =100%) intersect at the hexa-variant field in which Qz+Pl+Bt+Grt+Ms+Ky+Ilm are the stable phases. The intersection is around 650°C and 7-7.5 kbar, suggesting an almost isothermal decompression path. Relics of kyanite are described in the LN (Fig. 6f), supporting that this mineral was stable at some moment of the LN *P-T* path. Lastly, the *P-T* path later stage is recorded by the compositional match between the plagioclase rim and muscovite (Pl-Q_{cmp} =100%; Ms-Q_{cmp} =95%) in the hexa-variant field where Qz+Pl+Grt+Bt+Ms+Ilm+Sil+H_2O are stable. A *P-T* path (Fig. 10b) is suggested based on the above mineral chemistry and mode optimal quality factors fields, and the M_{LN1}, M_{LN2}, and M_{LN3} metamorphic stages described in section 4.1. The quantitative map of the Ti-in-biotite thermometer (Henry et al., 2005) was applied (supplementary figure A2c). It displays values from 650 to 580°C consistent with the findings obtained by the ITM approach.

3.3.2 Sample NESG-401 – Andrelândia Nappe

Fig. 11a displays the isochemical diagram built for the Andrelândia Nappe LBC that better represents the peak-to post-peak conditions. Bulk compositions that consider phases that are not fully equilibrated in the system, such as minerals relics or displaying compositional zoning, can affect the thermodynamic models quality (Lanari and Engi, 2017). Once one garnet of the LBC is strongly zoned and likely its core was unreactive at peak condition, for avoiding the question described above, the garnet core area was subtracted and is not considered in the bulk composition. Although, the isochemical diagram taking into account the garnet core composition and the *P-T* stability field map for garnet core composition (garnet core Q_{cmp}) are provided in the supplementary figure A5. Therefore, the M_{AN1} stage, which corresponds to a mineral assemblage preserved in the garnet core, does not appear in the suggested *P-T* path.

The peak mineral assemblage, Qz+Pl+Bt+Grt+Ky+Ms+Ilm+H_2O, was constrained in the quadri-variant field delimitated in the *P-T* range of 620°C-675°C and 7-10 kbar. The optimal *P-T* condition obtained is 676°C and 8.1 kbar with Q_{cmp}= 92% and Q_{mode}=95% (Fig. 11b). The mineral phases chemical composition of sample NESG-401 preserves three stages of the metamorphic path, the prograde, decompression, and cooling (Fig. 11b), which were traced using *P-T* stability field maps (supplementary figure A6). The prograde path was traced taking into account the compositions of garnet mantle (Q_{cmp} =100%), which records early stages of amphibolite facies around 550-570°C and 8-9 kbar, plagioclase core (Q_{cmp} =100%), and white mica (Q_{cmp} =85-80%). Indeed, the antidote optimal conditions calculations seem to underestimate the peak condition. The plagioclase core and white mica chemical composition provide a better constrain, crossing at *ca.* 660°C-670°C and 11.5-12 kbar, at these conditions, Qz+Pl+Bt+Grt+Ky+Ms+Ilm are the stable phases (M_{AN2} stage). An almost isothermal decompression is suggested based on the mineral modes (Q_{mode}= 95-100%) field of stability, which is at lower pressure of 6-8 kbar but at almost the same temperature range, from 625 to 680 °C. At last, garnet rim chemical composition (Q_{cmp} =80%) provided information about the AN cooling stage. It is equilibrated at 550°C and 4.5 kbar in the stability field of Qz+Pl+Grt+Bt+Ilm+St+Sil (M_{AN3} stage; Fig. 11b). The Ti-in-biotite thermometer map (supplementary figure A3c) displays temperatures ranging from 630 to 560 °C, in agreement with the retrograde temperature conditions obtained by ITM.

3.4 EMPA monazite petrochronology

To constrain the timing of the metamorphic and deformation events, *in-situ* U-(Th)-Pb monazite chemical dating was carried out by EMPA (e.g., Dumond et al., 2015; Williams and Jercinovic, 2002, 2012). The analytical procedures are described in appendix A.

3.4.1 Sample NESG-388 – Liberdade Nappe

Monazites from sample NESG-388 are between quartz, plagioclase, white mica, and biotite from the matrix. Ten crystals were chosen to perform X-ray maps and trace element analysis. The results are illustrated in Fig. 12 and supplementary table A2. Most of the crystals display an elongated shape parallel to the mylonitic foliation, varying in size from 70 to 250 µm, except the Mnz 4, associated with ilmenite which shows an irregular lobate shape. In some crystals, small quartz (e.g., Mnz 4, Mnz 5, and Mnz 6) inclusions were observed, but most of the monazites are inclusions free. The monazites display a sectorial core-rim internal zoning (e.g., Mnz 1, 2, 6 and 7). A remarkable feature that might be highlighted is the core and rim zonation pattern that is well-aligned (e.g., Mnz1, 2, 6, 8, and 10) with the main foliation, suggesting a pre-to syn-mylonitic growth related to the rock fabric. In addition, the Mnz 7 occurred on the S-plane of a *S-C* fabric.

Three chemical domains are distinguished based on the X-ray maps, mainly of Y and Th distribution (Fig. 12a, b, and c). Domain 1, characterized by high-Th and low-Y cores, is small patchy (e.g., Mnz 9), and straight (e.g., Mnz 2). The Y_2O_3 content (wt%) varies from 1.02 to 1.39, and the ThO_2 (wt%) values are very spread, ranging from 4.00 to 6.95. Domain 2 is related to core characterized by low-Y and -Th. The Y_2O_3 (wt%) and ThO_2 (wt%) amounts vary respectively in a narrow range of 0.93-1.22 and 2.29-3.80. The third domain (domain 3) is associated with monazite rims showing high-Y, in which the Y_2O_3 (wt%) amounts are spread in a broad range from 1.62 up to 2.61, and ThO_2 (wt%) variation is concentrated between 3.18-3.59.

In total, 84 ~~punctual~~ EMPA spot analyses were acquired in the different chemical domains for chemical dating calculation. Obtained dates span from 640 to 540 Ma. Domain 1, characterized by high-Th and low-Y core, dates range from 640±21Ma to 588±19 Ma. Domain 2, with low-Th and Y cores, has dates spread from 613 Ma±36 Ma to 550±33 Ma. Owing to the dates from domains 1 and domain 2 are relative to core, they were plotted in the same weighted average diagram (Fig. 12d) and yielded a mean age of 609±4 Ma (n=55; MSWD=1.6). Domain 3, related to high-Y rims, has dates from 590±28 Ma to 540±26 Ma and yields a mean weighted average age of 567±5 Ma (n=33; MSWD=1.19; Fig. 12e).

3.4.2 Sample NESG-401 – Andrelândia Nappe

Fig. 13a displays the mapped monazite crystals (n=8) from sample NESG-401, the elements analysis spots position, and the results of chemical dating. The monazites occur between the matrix minerals, hosted in quartz, plagioclase, biotite, and white mica (Mnz 1, 3 and 5), one crystal is enclosed in kyanite (Mnz 4), and three are located in apatite rims (Mnz 2, 5 and 8). The size of crystals varies from 50 µm up to 100 µm. Monazite shape varies from rounded to elongated. Quartz inclusions are observed in Mnz 1 and Mnz 7. Regarding the monazite compositional zoning, they are very homogenous. The crystals display intermediate Y_2O_3 contents varying from 1.3 to 2.9 wt% and variable Th amounts, varying the ThO_2 between 1.9 and 5.4 wt% (Fig. 13a, b, and c). The exception is represented by rims significantly enriched in Th (with ThO_2 content between 6.7-13.1 wt%) observed in crystals associated with apatite (Fig. 13c).

A total of 56 ~~chemical spots of~~ EMPA spot analyses were carried out. The obtained U-(Th)-Pb chemical dates range from 612±23 Ma to 535±28 Ma. The dates are plotted in the weighted average diagram (Fig. 13d), and they yield a mean age of 579±6 Ma (MSWD=3.5). Of particular interest is the crystal enclosed in kyanite (Mnz 4), which can report worthy information about tectonic and metamorphic events undergone by this rock since the kyanite is considered coeval with the S_2 foliation. The dates vary from 605±22 Ma to 558±25 Ma and yield a mean age of 589±19 Ma (MSWD=2.3; Fig. 13e).

4. DISCUSSION

4.1 Monazite chemical dating interpretation

The in-situ monazite dating combined with the X-ray ~~trace elements~~ maps (e.g., Y and Th) allows correlating monazite growth episodes with metamorphic reactions and deformation stages (Bosse and Villa, 2019; Spear and Pyle, 2002; Williams and Jercinovic, 2002, 2012). The Y and HREE concentration in monazite mostly depend~~s~~ on the garnet presence in the system, once this mineral is the preferential sink for these elements (Spear and Pyle, 2002). Whereas the Th concentration is controlled by a Th-rich phase breakdown responsible for releasing this element in the system, preferentially partitioned into monazite structure (Benetti et al., 2021; Kohn and Malloy, 2004; Williams et al., 2022). Moreover, monazite can be a fabric-forming mineral in deformed rocks and behaves as a porphyroclast rotated and with inclusion trails (Dumond et al., 2008, 2022). Therefore, the *in-situ* dating allows us to relate the monazite chemical zonation with its microstructural position, providing means to constrain the deformation time.

At sub-solidus conditions, two main metamorphic reactions will control the monazite chemistry. Firstly, the allanite breakdown is responsible for releasing most of the REE necessary for the monazite precipitation (Gasser et al., 2012; Janots et al., 2008; Kohn and Malloy, 2004; Spear and Pyle, 2010). This reaction occurs between the greenschist-to amphibolite facies transition, at temperature conditions around 550°C (Gasser et al., 2012; Janots et al., 2008; Spear and Pyle, 2010). If monazite grows at these conditions before garnet growth, the monazite will display ~~At these conditions, if monazite grows coeval or previous than garnet is a stable phase, the monazite will display~~ intermediate- to high-Y and HREE content. In contrast, when monazite grows in equilibrium with garnet, the monazite tends to be depleted in Y and HREE since these elements are strongly partitioned in garnet. ~~if garnet is already a reactive phase, the Y will be partitioned toward it, and the monazite will be Y-depleted~~ In addition, due to allanite being a Th-rich mineral, the monazite that grows soon after its breakdown tends to be Th-enriched (Benetti et al., 2021;

Kohn and Malloy, 2004). Another monazite generation is expected during the rock decompression path, in which garnet breakdown releases Y and HREE in the system, and the monazite precipitating from this reaction will display enriched signatures in these elements (Gasser et al., 2012; Kohn et al., 2005).

Considering the monazite behavior during the sub-solidus metamorphism and deformation described above, two episodes of ~~its~~ monazite growth can be identified in the sample NESG-388 from the Liberdade Nappe. The first episode is correlated with Y-depleted cores and a wide range of Th amounts (domains 1 and 2). These dates are associated with prograde metamorphism (M_{LN1} stage) in which monazite grew after ~~post-~~ garnet crystallization in the system and yielded mean chemical age of 609~~8~~±4 Ma. The Th-enriched domains (domain 1) can likely be linked to the early prograde metamorphism~~path~~ (early M_{LN1} stage), soon after the allanite-to-monazite transition, releasing Th in the system and reproducing the oldest dates. The weighted mean age of 567±5 Ma, represented by Y-enriched monazite rims (domain 3), is interpreted as linked with garnet resorption during the rock decompression (M_{LN2} and M_{LN3}). Furthermore, the growth orientation of some high-Y rims aligned with the S_2 foliation (e.g., Mnz 1 and 2), and the crystal in the S-C band (Mnz 7) rotated during the shearing suggest that the decompression was coeval with the development of the S_2 fabric related with the SE tectonic transport.

The monazites grains from the sample NESG-401 of the Andrelândia Nappe are homogenous with intermediate Y and Th-depleted. They are interpreted as growing coeval with the garnet during the prograde metamorphism ($M_{AN}2$ stage), at a minimum age of 579±6 Ma. The Mnz 4 is enclosed in kyanite and parallel to the AN S_2 fabric, providing time constraint for the foliation-forming deformation coeval with kyanite growth during the

P-T path. This single crystal yields mean age of 589±19 (n=6), consequently interpreted as corresponding to the time of the S_2 deformation, and taking into account the age standard deviation, is considered contemporary to the prograde metamorphism ($M_{AN}2$ stage). Rims highly enriched in Th (Mnz 2, 5, and 8) are attributable to exchange reactions between apatite and monazite and have no signatures that can associate them with any significant tectono-metamorphic event.

4.2 Tectono-metamorphic evolution of the Andrelândia Nappe System (ANS)

The microstructural descriptions, *P-T* path traced through thermodynamic metamorphic modeling, and monazite petrochronological data presented here help ~~contribute to~~ elucidate the complex ANS framework in the southern sector of the SBO. The Liberdade and Andrelândia Nappes evolved from a clockwise sub-solidus *P-T* path characterized by burial and heating, followed by nearly isothermal decompression, and lastly, cooling and decompression. The Liberdade Nappe (NESG-388) M_{LN1} stage assemblage (Qz-Pl-Grt-Bt-Ms-Ilm) records peak conditions at *ca.* 650°C and 9.5-10 kbar and has a minimum age of 609±4 Ma (Fig. 14a). The peak conditions indicate that the LN rocks were buried by 36 km, corresponding to the middle and lower depth of a thickened crust with apparent geothermal gradient of 18ºC/km (Fig. 14a). The further stages, M_{LN2} (Qz-Pl-Grt-Bt-Ms-Ilm-Ky(?)) and the M_{LN3} (Qz-Pl-Grt-Bt-Ms-Ilm-Sil-St), represent respectively the isothermal decompression and decompression/cooling episodes related to the LN migration toward SE, whose the minimum age is constrained at 567±5 Ma (Fig. 14a).

The Andrelândia Nappe sample (NESG-401) records a burial and heating episode in the kyanite stability field during the prograde metamorphism, from ~550°C and 9.0-9.5

kbar up to ~680 °C and 11-12 kbar (M_{AN2} stage; Fig. 14a). The *P-T* data suggest an apparent geothermal gradient of 16ºC/km and burial into crustal depths of 43 km (Fig. 14a). The minimum age for the prograde metamorphism was estimated at 579±6 Ma, and within the uncertainties is considered coeval with the S_2 deformation event underwent by this rock. It was followed by an almost isothermal decompression, in which the pressure conditions decreased from 12 kbar down to 8.0-7.0 kbar (Fig.14a). Lastly, the M_{AN3} stage related to staurolite and sillimanite appearance in the system was constrained in the *P-T* range of 670-550°C and 8.0-4.5 kbar (Fig. 14a).

A compilation of literature *P-T* paths from the Andrelândia and Liberdade Nappes is provided in Fig. 14a. ~~Even though the~~ Different approaches were adopted by Coelho et al. (2017), Motta and Moraes (2017), Reno et al. (2012), and Santos et al. (2004) ~~the other authors~~, such as~~(e.g.,~~ inverse and forward thermodynamic modeling. ~~and~~Considering the different methods-related uncertainties, peak conditions constrained for the Andrelândia and Liberdade Nappes in this contribution agree with those previously reported ~~by Coelho et al. (2017), Motta and Moraes (2017), Reno et al. (2012), and Santos et al. (2004)~~. However, there are differences between the *P-T* path traced here and those interpreted by these authors. For instance, Reno et al. (2021) suggested two episodes of isobaric cooling separated by a near-isothermal decompression phase to the Carmo da Cachoeira Nappe, the Andrelândia Nappe equivalent in the SBO northern sector. Moreover, Santos et al. (2004) considered that Andrelândia Nappe underwent heating during decompression~~exhumation~~, while the Liberdade Nappe evolved from an isothermal decompression. These *P-T* path contrasts can be assigned to different interpretations regarding blastesis-deformation relationships and distinct approaches used by each of the authors and the present work.

Fig. 14b is a summary of the available metamorphic ages for the Andrelândia and Liberdade Nappes using monazite and zircon U-Pb geochronology techniques. The oldest ages of the Liberdade Nappe, at *ca*. 680-670 Ma, reported by Campos Neto et al. (2011) and Reno et al. (2009), are related to metamafic rocks and interpreted as the HP metamorphism age experienced by these rocks. Regarding the LN and AN micaschits and gneisses, the previously published ages by Coelho et al. (2017), Frugis et al. (2018), Marimon et al (2022), Motta and Moraes (2017), and Westin et al. (2021) and those reported in this work are widespread in a time range *ca*. 60 Ma, from 630 to 570 Ma. The geochronology data from the literature, calculated by different methods (e.g., isocron age, concordia age, and weighted average age), are comprised within the spread of chemical dates acquired here. However, in this study, the monazite petrochronology results indicate that each nappe experienced episodic growth during a single metamorphic cycle of burial (prograde metamorphism) and decompression (retrograde metamorphism), rather than being affected by polymetamorphism events.

4.3 Tectonic implications

Our present findings shed new light on some critical points regarding the tectono-metamorphic events experienced by the ANS. The first point is related to the Andrelândia and Liberdade Nappes *P-T* paths. Microstructural observations and thermodynamic modeling show that the staurolite and sillimanite in the matrix are related to decompression and cooling stages. Furthermore, the suggested metamorphic paths to the LN and AN pointed out that the baric and thermic peaks occur almost simultaneously. These information in conjunction with monazite petrochronology indicate that likely each one of the nappes ~~those rocks~~ underwent a single metamorphic ~~cycle~~ loop of burial and decompression.

The second critical point concerns the ~~time~~timing constraints of metamorphism and deformation. The Liberdade Nappe attained prograde, amphibolite facies, within the kyanite stability field at minimum age of *ca.* 610 Ma, nearly 30 Ma before the Andrelândia Nappe (Fig. 15 b, c, and d). Although the sample from Andrelândia Nappe does not have dates related to exhumation, the spread dates from the Liberdade Nappe linked with the exhumation mostly overlap the prograde monazite dates in the Andrelândia Nappe, structurally below. Hence, it is possible to claim that when the Liberdade Nappe onset its decompression path, the Andrelândia Nappe was still experiencing prograde conditions and was likely exhumed afterward compared to the Liberdade Nappe (Fig. 15c). In other words, the dates younger than 610 Ma in the Liberdade Nappe are related to its exhumation and tectonic transport toward SE (Fig. 15c and d). In contrast, this time span is linked with prograde burial metamorphic conditions (coeval with kyanite growth) in the Andrelândia Nappe (Fig. 15c). The Pouso Alto Nappe, the upper structural level of the ANS in the southern part of the SBO, yields a minimums age of *ca.* 620 Ma and of *ca.* 610 Ma, for respectively the prograde metamorphism, and melt crystallization related to cooling and decompression (Fig. 15a and b; Benetti et al., in prep; Benetti, 2022). Therefore, the spread of ages from 630 Ma to 570 Ma (Fig. 15) within the ANS records a ~~temporal~~ pattern of age decrease, toward lower structural levels, ~~variation~~ of ~~when the nappes attended their~~ prograde and retrograde metamorphic ages ~~stage~~ during the protracted metamorphism of the SBO ~~and follow a pattern of progressive decrease toward lower structural levels of the system~~ (Fig 15). The spatial arrangement and decrease of the metamorphic ages toward the bottom of the ANS stack outline an in-sequence fold-and-thrust architecture of the orogenic wedge (Fig. 15). This ~~ANS~~ framework would have been developed through the inner material incorporated at the wedge being detached, shortened, and propagated over the incoming material, similar to what is proposed by Platt (1986) to the dynamics of orogenic wedges. Then, the rocks from the older nappes (i.e., Liberdade Nappe) were decompressed via thrust and folding over the younger ones (i.e., Andrelândia Nappe) that likely experienced their peak metamorphism as a consequence of loading of the overlying nappe. Analogue in-sequence fold-and-thrust architectures are described in other orogenic belts such as the Caledonian, Trans-Hudson, Grenville, Himalayan, and Appalachian orogens (Beaumont et al., 2006; Carosi et al., 2016; Weller et al., 2021). This suggests that the mechanism described above is an important mechanism controlling the structural and metamorphic style of collisional wedges. Fig. 15 illustrates the proposed tectono-metamorphic evolution for the nappes of the Southern Brasília Orogen. The collision-related metamorphic event evolved from 630 to 570 Ma based on zircon, monazite, and titanite U-Pb ages and monazite-EPMA ages (Campos Neto et al., 2010; Coelho et al., 2017; Frugis et al., 2018; Fumes et al., 2021; Li et al. 2021; Marimon et al., 2020, 2022; Motta et al., 2021; Rocha et al., 2017; Westin et al., 2021~~, submitted~~). The Andrelândia Nappe System underwent high-pressure metamorphic conditions during the collision between the São Francisco (passive margin) and Paranapanema (active margin) paleoplates (Fig. 15). The crustal material was stored and sunk within the orogenic wedge hinterland until 620 Ma when the first nappe of the system, the Pouso Alto, started its decompression path with tectonic transport toward northeast (Fig. 15a and b). After *ca.* 610 Ma, the Liberdade Nappe follows an upward flow toward east/southeast, laterally to the south margin of the São Francisco Craton, over the Andrelândia Nappe (Fig. 15c). The final stage of the SBO continental collision took place after 580-570 Ma, coeval with the decompression and exhumation path of the Andrelândia and Carrancas Nappes (Fig., 15d; Campos Neto et al., 2010, 2020; Carvalho et al., 2020; Cioffi et al., 2019; Coelho et al., 2017; Frugis et al., 2018; Reno et al., 2009, 2012, Tedeschi et al., 2017; Westin et al., 2021, ~~submitted~~).

5. CONCLUSION

The *P-T-t-D* data provided here document the metamorphic and deformation history of the Andrelândia and Liberdade Nappes. The Liberdade Nappe experienced prograde burial metamorphism at *ca.* 610 Ma and achieved peak conditions at ~650°C and 9.5-10 kbar. This stage was followed by a near-isothermal decompression and further cooling with a minimum age of *ca.* 570 Ma. Meanwhile, the Andrelândia Nappe structurally below the Liberdade Nappe underwent prograde metamorphism nearly 30 Ma later, at *ca.* 580 Ma, reaching the peak condition at *ca.* 680°C and 11.5-12 kbar. The data document an in-sequence fold-and-thrust architecture, in which the metamorphic ages decrease toward lower structural levels of the stack. This framework would have evolved through older material incorporated into the inner parts of the orogenic wedge has been detached and propagated via thrust-and-fold nappes upon recently accreted rocks, leading to a younger metamorphism event on the footwall of the ductile thrust~~external parts of the wedge~~.

APPENDIX A – ANALYTICAL METHODS

The equipment employed in the trace elements, quantitative mineral analyses, and compositional maps is a JEOL JXA-8230 Electron Probe Micro Analyzer (EPMA) equipped with five wavelengths dispersive spectrometry (WDS) detectors hosted at the Department of Geology at the State of São Paulo University (UNESP). The compositional maps were obtained through X-rays maps, which were further classified and calibrated using the internal standardization procedure and the pseudo-background correction available in the XMapTools 3.4 (Lanari et al., 2014, 2019). The X-ray maps for Mg, Na, Ca, K, and Fe were acquired by the WDS detectors, whereas for Al, Si, P, S, Ti, Mn, and Zr by the energy dispersive-spectrometry (EDS). The x-ray maps were carried out with an accelerating voltage of 15Kv, a current beam of 100nA, and a dwell of 100 ms. Representative analysis of silicates obtained within the X-maps perimeter used for the calibrations are available in the supplementary table file A1.

Monazite U-(Th)-Pb chemistry dating was performed using the same equipment cited above. The crystals were first identified through full thin-sections maps acquired using the Scanning Electron Microscopy and Mineral Liberation Analyzer (SEM-MLA). Considering the monazite structural position and textural relationships some crystals were selected to perform high-resolution compositional X-ray maps of Y, Al, Th, U, Pb, Si, Ca, Fe, La, and Ce. The acquisition conditions were 15 kV, 100 nA, 100 ms dwell time, and 10 μm electron beam size and step. Trace elements spots analyses were performed in the different domains identified with helping of the X-ray maps. The analytical procedure follows the strategies of Fumes et al. (2021). The moacyr monazite standard was used after each 10 to 20 punctual analyses, and their results are displayed in the supplementary figure file A7. The background was estimated in all analyzed spots. Spectral interference corrections considered matrix correction factors and were performed offline. Interference corrections and age calculations were performed using the Age_Cor program (Vlach, 2010). The dates were plotted in the weighted average diagram using the Isoplot program (Ludwig, 2008).

ACKNOWLEDGEMENTS

This research was supported by funds of "Ricerca Locale" of the Università di Torino (resp. Iaccarino S. and Montomoli C.) and the São Paulo Research Foundation (FAPESP grant 2015/03737-0). The authors would like to thank Gregory Dumond and an anonymous reviewer for their suggestions and careful revisions to improve this paper.

6. REFERENCES

Andrade, V. De, Vidal, O., Lewin, E., O'Brien, P., Agard, P., 2006. Quantification of electron microprobe compositional maps of rock thin sections: an optimized method and examples. Journal of Metamorphic Geology 24, 655–668. https://doi.org/10.1111/J.1525-1314.2006.00660.X

Baldwin, J.A., Powell, R., Brown, M., Moraes, R., Fuck, R.A., 2005. Modelling of mineral equilibria in ultrahigh-temperature metamorphic rocks from the Anápolis–Itauçu Complex, central Brazil. Journal of Metamorphic Geology 23, 511–531. https://doi.org/10.1111/J.1525-1314.2005.00591.X

Beaumont, C., Jamieson, R., Nguyen, M. H., Lee, B., 2001. Himalayan tectonics explained by extrusion of a low-viscosity crustal channel coupled to focused surface denudation. Nature, 738–742.

Beaumont, C., Nguyen, M. H., Jamieson, R. A., & Ellis, S., 2006. Crustal flow modes in large hot orogens. Geological Society Special Publication, 268, 91–145. https://doi.org/10.1144/GSL.SP.2006.268.01.05

Benetti, B., 2022. Kinematics and P-T-t evolution in hot collisional frameworks – a comparison between a Neoproterozoic and a Phanerozoic large hot orogens. University of Turin.

Benetti, B., Montomoli, C., Iaccarino, S., Langone, A., Carosi, R., 2021. Mapping tectono-metamorphic discontinuities in orogenic belts: implications for mid-crust exhumation in NW Himalaya. Lithos 392–393, 106129. https://doi.org/10.1016/j.lithos.2021.106129

Bosse, V., Villa, I.M., 2019. Petrochronology and hygrochronology of tectono-metamorphic events. Gondwana Research 71, 76–90. https://doi.org/10.1016/j.gr.2018.12.014

Caddick, M.J., Konopásek, J., Thompson, A.B., 2010. Preservation of Garnet Growth Zoning and the Duration of Prograde Metamorphism. Journal of Petrology 51, 2327–2347. https://doi.org/10.1093/PETROLOGY/EGQ059

Campos Neto, M. da C., 2000. Orogenic systems from SW-Gondwana: an approach to Brasiliano-Pan African cycle and orogenic collage in SE-Brazil, in: Tectonic Evolution of South America. pp. 335–365.

Campos Neto, M. da C., Basei, M.A.S., Assis Janasi, V. de, Moraes, R., 2011. Orogen migration and tectonic setting of the Andrelândia Nappe system: An Ediacaran western Gondwana collage, south of São Francisco craton. Journal of South America Earth Science 32, 393–406. https://doi.org/10.1016/j.jsames.2011.02.006

Campos Neto, M. da C., Caby, R., 2000. Terrane accretion and upward extrusion of high-pressure granulites in the Neoproterozoic nappes of southeast Brazil: Petrologic and structural constraints. Tectonics 19, 669–687. https://doi.org/10.1029/1999TC900065

Campos Neto, M. da C., Cioffi, C.R., Moraes, R., da Motta, R.G., Siga, O., Basei, M.A.S., 2010. Structural and metamorphic control on the exhumation of high-P granulites: The Carvalhos Klippe example, from the oriental Andrelândia Nappe System, southern portion of the Brasília Orogen, Brazil. Precambrian Research 180, 125–142. https://doi.org/10.1016/j.precamres.2010.05.010

Campos Neto, M. da C., Cioffi, C.R., Westin, A., Rocha, B.C., Frugis, G.L., Tedeschi, M., Pinheiro, M.A.P., 2020. O Orógeno Brasília Meridional, in: Geocronologia e Evolução Tectônica Do Continente Sul-Americano: A Contribuição de Umberto Giuseppe Cordani.

Campos Neto, M.D.C., Caby, R., 1999. Neoproterozoic high-pressure metamorphism and tectonic constraint from the nappe system south of the Sao Francisco Craton, southeast Brazil. Precambrian Research 97, 3–26. https://doi.org/10.1016/S0301-9268(99)00010-8

Carosi, R., Montomoli, C., Iaccarino, S., Massonne, H. J., Rubatto, D., Langone, A., Gemignani, L., Visonà, D., 2016. Middle to late Eocene exhumation of the Greater Himalayan Sequence in the Central Himalayas: Progressive accretion from the Indian plate. Geological Society of America Bulletin, 128(11–12), 1571–1592. https://doi.org/10.1130/B31471.1

Carosi, R., Montomoli, C., Iaccarino, S., 2018. 20 years of geological mapping of the metamorphic core across Central and Eastern Himalayas. Earth Science Reviews 177, 124–138. https://doi.org/10.1016/j.earscirev.2017.11.006

Carvalho, B.R.B.M., Trouw, R.A.J., Costa, R.V.C. da, Ribeiro, A., Heilbron, M., Marimon, R.S., 2020. Microstructural and metamorphic evolution of the Carrancas Klippe, interference zone of the Neoproterozoic southern Brasilia and Ribeira orogens, SE Brazil.

Journal of South America Earth Science 103, 102744. https://doi.org/10.1016/j.jsames.2020.102744

Cioffi, C.R., Campos Neto, M. da C., Möller, A., Rocha, B.C., 2019. Titanite petrochronology of the southern Brasília Orogen basement: Effects of retrograde net-transfer reactions on titanite trace element compositions. Lithos 344–345, 393–408. https://doi.org/10.1016/j.lithos.2019.06.035

Cioffi, C.R., Campos Neto, M. da C., Möller, A., Rocha, B.C., 2016. Paleoproterozoic continental crust generation events at 2.15 and 2.08Ga in the basement of the southern Brasília Orogen, SE Brazil. Precambrian Research 275, 176–196. https://doi.org/10.1016/j.precamres.2016.01.007

Cioffi, C.R., Campos Neto, M. da C., Rocha, B.C. da, Moraes, R., Henrique-Pinto, R., 2012. Geochemical signatures of metasedimentary rocks of high-pressure granulite facies and their relation with partial melting: Carvalhos Klippe, Southern Brasília Belt, Brazil. Journal of South America Earth Science 40, 63–76. https://doi.org/10.1016/j.jsames.2012.09.007

Coelho, M.B., Trouw, R.A.J., Ganade, C.E., Vinagre, R., Mendes, J.C., Sato, K., 2017. Constraining timing and P-T conditions of continental collision and late overprinting in the Southern Brasília Orogen (SE-Brazil): U-Pb zircon ages and geothermobarometry of the Andrelândia Nappe System. Precambrian Research 292, 194–215. https://doi.org/10.1016/j.precamres.2017.02.001

Coggon, R., Holland, T.J.B., 2002. Mixing properties of phengitic micas and revised garnet-phengite thermobarometers. Journal of Metamorphic Geology 20, 683–696. https://doi.org/10.1046/J.1525-1314.2002.00395.X

Cordani, U.G., D'agrella-Filho, M.S., Brito-Neves, B.B., Trindade, R.I.F., 2003. Tearing up Rodinia: the Neoproterozoic palaeogeography of South American cratonic fragments. Terra Nova 15, 350–359. https://doi.org/10.1046/j.1365-3121.2003.00506.x

Davis, D., Suppe, J., Dahlen, F. A., 1983. Mechanics of fold-and-thrust belts and accretionary wedges. Journal of Geophysical Research, 88(B2), 1153–1172. https://doi.org/10.1029/JB088IB02P01153

de Capitani, C., Brown, T. H., 1987. The computation of chemical equilibrium in complex systems containing non-ideal solutions. Geochimica et Cosmochimica Acta, 51(10), 2639–2652. https://doi.org/10.1016/0016-7037(87)90145-1

de Capitani, C., Petrakakis, K., 2010. The computation of equilibrium assemblage diagrams with Theriak/Domino software. American Mineralogist, 95(7), 1006–1016. https://doi.org/10.2138/AM.2010.3354

~~DeCelles, P.G., Mitra, G., 1995. History of the Sevier orogenic wedge in terms of critical taper models, northeast Utah and southwest Wyoming . GSA Bulletin 107, 454–462.~~

Duesterhoeft, E., Lanari, P., 2020. Iterative thermodynamic modelling—Part 1: A theoretical scoring technique and a computer program (Bingo-Antidote). Journal of Metamorphic Geology 38, 527–551. https://doi.org/10.1111/JMG.12538

Dumond, G., Goncalves, P., Williams, M.L., Jercinovic, M.J., 2015. Monazite as a monitor of melting, garnet growth and feldspar recrystallization in continental lower crust. Journal of Metamorphic Geology 33, 735–762. https://doi.org/10.1111/jmg.12150

Dumond, G., Mahan, K.H., Goncalves, P., Williams, M.L., Jercinovic, M.J., 2022. Monazite as a monitor of shear strain in orogenic crust. Journal of Structural Geology 161, 104672. https://doi.org/10.1016/J.JSG.2022.104672

Dumond, G., McLean, N., Williams, M.L., Jercinovic, M.J., Bowring, S.A., 2008. High-resolution dating of granite petrogenesis and deformation in a lower crustal shear zone: Athabasca granulite terrane, western Canadian Shield. Chemical Geology 254, 175–196. https://doi.org/10.1016/j.chemgeo.2008.04.014

England, P.C., Thompson, A.B., 1984. Pressure-Temperature-Time Paths of Regional Metamorphism I. Heat Transfer during the Evolution of Regions of Thickened Continental Crust. Journal of Petrology 25, 894–928. https://doi.org/10.1093/petrology/25.4.894

England, P., Molnar, P., 1990. Surface uplift, uplift of rocks, and exhumation of rocks . Geology, 18(12), 1173–1177.

England, P., & Molnar, P., 1993. The interpretation of inverted metamorphic isograds using simple physical calculations. Tectonics, 12(1), 145–157.

Fontainha, M.V.F., Trouw, R.A.J., Peternel, R., de Paula, R.R., Polo, H.J.O., Negrão, A.P., Furtado, P.C., Telles, R.C.M., 2020. A case study of superposed structures in the tectonic interference zone between the Southern Brasília and Ribeira orogens, southeastern Brazil. Journal of South America Earth Science 104, 102718. https://doi.org/10.1016/j.jsames.2020.102718

Frugis, G.L., Campos Neto, M. da C., Lima, R.B., 2018. Eastern Paranapanema and southern São Francisco orogenic margins: Records of enduring Neoproterozoic oceanic convergence and collision in the southern Brasília Orogen. Precambrian Research 308, 35–57. https://doi.org/10.1016/j.precamres.2018.02.005

Fumes, R.A., Luvizotto, G.L., Moraes, R., Lanari, P., Valeriano, C. de M., Zack, T., Caddick, M.J., Simões, L.S.A., 2021. Petrochronology of high-pressure granulite facies rocks from Southern Brasília Orogen, SE Brazil: Combining quantitative compositional mapping, single-element thermometry and geochronology. Journal of Metamorphic Geology 1–36. https://doi.org/10.1111/JMG.12637

Ganade De Araujo, C.E., Rubatto, D., Hermann, J., Cordani, U.G., Caby, R., Basei, M.A.S., 2014. Ediacaran 2,500-km-long synchronous deep continental subduction in the West Gondwana Orogen. Nat Commun 5, 1–8. https://doi.org/10.1038/ncomms6198

Garcia, M. da G.M., Campos Neto, M. da C., 2003. Contrasting metamorphic conditions in the Neoproterozoic collision-related Nappes south of São Francisco Craton, SE Brazil. Journal of South America Earth Science 15, 853–870. https://doi.org/10.1016/S0895-9811(02)00147-5

Gasser, D., Bruand, E., Rubatto, D., Stüwe, K., 2012. The behavior of monazite from greenschist facies phyllites to anatectic gneisses: An example from the Chugach Metamorphic Complex, southern Alaska. Lithos 134–135, 108–122. https://doi.org/10.1016/j.lithos.2011.12.003

Heilbron, M., Machado, R., Figueiredo, M., 2017. Lithogeochemistry of paleoproterozoic orthogranulites from the Rio Preto (MG)-vassouras (RJ) region, central Ribeira Belt, SE

Brazil. Revista Brasileira de Geociências 27 (1). http://www.ppegeo.igc.usp.br/index.php/rbg/article/view/11274

Henry, D.J., Guidotti, C. V., Thomson, J.A., 2005. The Ti-saturation surface for low-to-medium pressure metapelitic biotites: Implications for geothermometry and Ti-substitution mechanisms. American Mineralogist 90, 316–328. https://doi.org/10.2138/AM.2005.1498

Holland, T.J.B., Powell, R., 1998. An internally consistent thermodynamic data set for phases of petrological interest. Journal of Metamorphic Geology 16, 309–343. https://doi.org/10.1111/J.1525-1314.1998.00140.X

Jamieson, R.A., Beaumont, C., 2013. On the origin of orogens. Bulletin of the Geological Society of America 125, 1671–1702. https://doi.org/10.1130/B30855.1

Janots, E., Engi, M., Berger, A., Allaz, J., Schwarz, J.-O., Spandler, C., 2008. Prograde metamorphic sequence of REE minerals in pelitic rocks of the Central Alps: implications for allanite–monazite–xenotime phase relations from 250 to 610 °C. Journal of Metamorphic Geology 26, 509–526. https://doi.org/10.1111/j.1525-1314.2008.00774.x

Kohn, M.J., Engi, M., Lanari, P., 2017. Petrochronology: Methods and applications, Petrochronology. Reviews in Mineralogy & Geochemistry, vol 83. https://doi.org/10.1515/9783110561890/HTML

Kohn, M.J., Malloy, M.A., 2004. Formation of monazite via prograde metamorphic reactions among common silicates: Implications for age determinations. Geochimica et Cosmochimica Acta 68, 101–113. https://doi.org/10.1016/S0016-7037(03)00258-8

Kohn, M.J., Wieland, M.S., Parkinson, C.D., Upreti, B.N., 2005. Five generations of monazite in Langtang gneisses: Implications for chronology of the Himalayan metamorphic core. Journal of Metamorphic Geology 23, 399–406. https://doi.org/10.1111/j.1525-1314.2005.00584.x

Lanari, P., Engi, M., 2017. on Metamorphic Mineral Assemblages. Reviews in Mineralogy and Geochemistry 83, 55–102.

Lanari, P., Hermann, J., 2021. Iterative thermodynamic modelling-Part 2: Tracing equilibrium relationships between minerals in metamorphic rocks. Journal of Metamorphic Geology 39, 651–674. https://doi.org/10.1111/jmg.12575

Lanari, P., Vho, A., Bovay, T., Airaghi, L., Centrella, S., 2019. Quantitative compositional mapping of mineral phases by electron probe micro-analyser. Geological Society, London, Special Publications 478, 39–63. https://doi.org/10.1144/SP478.4

Lanari, P., Vidal, O., de Andrade, V., Dubacq, B., Lewin, E., Grosch, E.G., Schwartz, S., 2014. XMapTools: A MATLAB©-based program for electron microprobe X-ray image processing and geothermobarometry. Computers & Geosciences 62, 227–240. https://doi.org/10.1016/J.CAGEO.2013.08.010

Law, R.D., 2014. Deformation thermometry based on quartz c-axis fabrics and recrystallization microstructures: A review. Journal of Structural Geology 66, 129–161. https://doi.org/10.1016/j.jsg.2014.05.023

Le Fort, P., 1975. Himalayas: the collided range. Present knowledge of the continental arc. American Journal of Science, 275(1), 1–44.

Li, B., Massonne, H.J., Hartmann, L.A., Zhang, J., Luo, T., 2021. Kyanite-garnet granulite from the Andrelândia nappe system, Brasília belt, registers two late Neoproterozoic metamorphic cycles. Precambrian Research 355, 106086. https://doi.org/10.1016/j.precamres.2020.106086

Ludwig, K.R., 2008. User’s manual for Isoplot/Ex version 3.70: a geochronology toolkit for Microsoft Excel: No. 4. Berkeley Geochronological Center, Special Publication 1–76.

Marimon, R.S., Hawkesworth, C.J., Trouw, R.A.J., Trouw, C., Dantas, E.L., Ribeiro, A., Vinagre, R., Hackspacher, P., Ávila, C., Motta, R., Moraes, R., 2022. Subduction and continental collision in the Neoproterozoic: Sanukitoid-like magmatism and paired metamorphism in SE Brazil. Precambrian Research 383, 106888. https://doi.org/10.1016/J.PRECAMRES.2022.106888

Marimon, R.S., Trouw, R.A.J., Dantas, E.L., 2020. Significance of age periodicity in the continental crust record: The São Francisco Craton and adjacent Neoproterozoic orogens as a case study. Gondwana Research 86, 144–163. https://doi.org/10.1016/J.GR.2020.05.010

Motta, R.G., Fitzsimons, I.C.W., Moraes, R., Johnson, T.E., Schuindt, S., Benetti, B.Y., 2021. Recovering P–T–t paths from ultra-high temperature (UHT) felsic orthogneiss: An example from the Southern Brasília Orogen, Brazil. Precambrian Research 359, 106222. https://doi.org/10.1016/j.precamres.2021.106222

Motta, R.G., Moraes, R., 2017. Pseudo- and real-inverted metamorphism caused by the superposition and extrusion of a stack of nappes: a case study of the Southern Brasília Orogen, Brazil. International Journal of Earth Sciences 106, 2407–2427. https://doi.org/10.1007/s00531-016-1436-7

Passchier, C.W., Trouw, R.A.J., 2005. Microtectonics, 2nd ed. Berlin:Springer Verlag.

Peternel, R., Allard, R., Trouw, J., Da, R., Schmitt, S., Xavier, F., 2005. Interferência entre duas faixas móveis Neoproterozóicas: O caso das faixas Brasília e Ribeira no sudeste do Brasil. Revista Brasileira de Geociências 35, 297–310.

Platt, J.P., 1986. Dynamics of orogenic wedges and the uplift of high-pressure metamorphic rocks. GSA Bulletin 9, 1037–1053.

Powell, R., Holland, T.J.B., 2008. On thermobarometry. Journal of Metamorphic Geology 26, 155–179. https://doi.org/10.1111/j.1525-1314.2007.00756.x

Ramsay, J.G., 1962. Interference Patterns Produced by the Superposition of Folds of Similar Type. The Journal of Geology 70, 466–481. https://doi.org/10.1086/626837

Reno, B.L., Brown, M., Kobayashi, K., Nakamura, E., Piccoli, P.M., Trouw, R.A.J., 2009. Eclogite-high-pressure granulite metamorphism records early collision in West Gondwana: New data from the Southern Brasília Belt, Brazil. Journal of the Geological Society of London 166, 1013–1032. https://doi.org/10.1144/0016-76492008-140

Reno, B.L., Piccoli, P.M., Brown, M., Trouw, R.A.J., 2012. In situ monazite (U-Th)-Pb ages from the Southern Brasília Belt, Brazil: constraints on the high-temperature retrograde evolution of HP granulites. Journal of Metamorphic Geology 30, 81–112. https://doi.org/10.1111/j.1525-1314.2011.00957.x

Ring, U., Brandon, M. T., Willett, S. D., Lister, G. S., 1999. Exhumation processes. Geological Society Special Publication, 154, 1–27. https://doi.org/10.1144/GSL.SP.1999.154.01.01

Rocha, B.C., Moraes, R., Möller, A., Cioffi, C.R., Jercinovic, M.J., 2017. Timing of anatexis and melt crystallization in the Socorro–Guaxupé Nappe, SE Brazil: Insights from trace element composition of zircon, monazite and garnet coupled to UPb geochronology. Lithos 277, 337–355. https://doi.org/10.1016/J.LITHOS.2016.05.020

Rodrigues, S.W. de O., Martins-Ferreira, M.A.C., Faleiros, F.M., Campos Neto, M. da C., Yogi, M.T.A.G., 2019. Deformation conditions and quartz c-axis fabric development along nappe boundaries: The Andrelândia Nappe System, Southern Brasília Orogen (Brazil). Tectonophysics 766, 283–301. https://doi.org/10.1016/J.TECTO.2019.06.014

Rudnick, R.L., Fountain, D.M., 1995. Nature and composition of the continental crust: A lower crustal perspective. Reviews of Geophysics 33, 267. https://doi.org/10.1029/95RG01302

Santos, L.P., da Costa Campos Neto, M., Grohmann, C.H., 2004. Metamorphic path constrained by metapelitic rocks from the inner Aiuruoca-Andrelândia nappe, south of the São Francisco craton, SE Brazil. Journal of South America Earth Science 16, 725–741. https://doi.org/10.1016/j.jsames.2003.12.006

Spear, F.S., Kohn, M.J., Cheney, J.T., 1999. P-T paths from anatectic pelites. Contributions to Mineralogy and Petrology 1999 134:1 134, 17–32. https://doi.org/10.1007/S004100050466

Spear, F.S., Pyle, J.M., 2010. Theoretical modeling of monazite growth in a low-Ca metapelite. Chemical Geology 273, 111–119. https://doi.org/10.1016/j.chemgeo.2010.02.016

Spear, F.S., Pyle, J.M., 2002. Apatite, monazite, and xenotime in metamorphic rocks. Reviews in Mineralogy and Geochemistry 48, 293–335. https://doi.org/10.2138/rmg.2002.48.7

Tedeschi, M., Lanari, P., Rubatto, D., Pedrosa-Soares, A., Hermann, J., Dussin, I., Pinheiro, M.A.P., Bouvier, A.S., Baumgartner, L., 2017. Reconstruction of multiple P-T-t stages from retrogressed mafic rocks: Subduction versus collision in the Southern Brasília orogen (SE Brazil). Lithos 294–295, 283–303. https://doi.org/10.1016/j.lithos.2017.09.025

Tedeschi, M., Pedrosa-Soares, A., Dussin, I., Lanari, P., Novo, T., Pinheiro, M.A.P., Lana, C., Peters, D., 2018. Protracted zircon geochronological record of UHT garnet-free granulites in the Southern Brasília orogen (SE Brazil): Petrochronological constraints on magmatism and metamorphism. Precambrian Research 316, 103–126. https://doi.org/10.1016/j.precamres.2018.07.023

Trouw, R.A.J., Heilbron, M., Ribeiro, A., Paciullo, F., Valeriano, C.M., Almeida, J.C.H., Tupinambá, M., Andreis, R.R., 2000. The central segment of the Ribeira Belt, in: Tectonic Evolution of South America. pp. 287–310.

Trouw, R.A.J., Paciullo, F.V.P., Ribeiro, A., 1998. Tectonic significance of Neoproterozoic high-pressure granulites in southern Minas Gerais., in: 14th International Conference on Basement Tectonics,. Ouro Preto, MG, pp. 69–71.

Trouw, R.A.J., Peternel, R., Ribeiro, A., Heilbron, M., Vinagre, R., Duffles, P., Trouw, C.C., Fontainha, M., Kussama, H.H., 2013. A new interpretation for the interference zone between the southern Brasília belt and the central Ribeira belt, SE Brazil. Journal of South America Earth Science 48, 43–57. https://doi.org/10.1016/j.jsames.2013.07.012

Vanderhaeghe, O., 2012. The thermal-mechanical evolution of crustal orogenic belts at convergent plate boundaries: A reappraisal of the orogenic cycle. Journal of Geodynamics 56–57, 124–145. https://doi.org/10.1016/j.jog.2011.10.004

Vanderhaeghe, O., Medvedev, S., Fullsack, P., Beaumont, C., Jamieson, R.A., 2003. Evolution of orogenic wedges and continental plateaux: insights from crustal thermal–mechanical models overlying subducting mantle lithosphere. Geophysical Journal International 153, 27–51. https://doi.org/10.1046/J.1365-246X.2003.01861.X

Vlach, S. R. F., 2010. Th-U-Pb_T dating by electron probe microanalysis, part I. Monazite: analytical procedures and data treatment. Geologia USP: Série Científica, 10(1), 61–85. https://doi. org/10.5327/Z1519-874X2010000100006

Waters, D.J., 2019. Metamorphic constraints on the tectonic evolution of the high Himalaya in Nepal: The art of the possible. Geological Society of London Special Publication 483, 325–375. https://doi.org/10.1144/SP483-2018-187

Weller, O. M., Mottram, C. M., St-Onge, M. R., Möller, C., Strachan, R., Rivers, T., Copley, A., 2021. The metamorphic and magmatic record of collisional orogens. Nature Reviews Earth & Environment 2021, 1–19. https://doi.org/10.1038/s43017-021-00218-z

Westin, A., Campos Neto, M.C., Hawkesworth, C.J., Cawood, P.A., Dhuime, B., Delavault, H., 2016. A paleoproterozoic intra-arc basin associated with a juvenile source in the Southern Brasilia Orogen: Application of U-Pb and Hf-Nd isotopic analyses to provenance studies of complex areas. Precambrian Research 276, 178–193. https://doi.org/10.1016/j.precamres.2016.02.004

Westin, A., Campos Neto, M.C., Hollanda, M.H.B.M., Salazar-Mora, C.A., Queiroga, G.N., Frugis, G.L., de Castro, M.P., 2021. The fast exhumation pattern of a Neoproterozoic nappe system built during West Gondwana amalgamation: Insights from thermochronology. Precambrian Research 355, 106115. https://doi.org/10.1016/j.precamres.2021.106115

~~Westin, A., Tedeschi, M., Campos Neto, M.C., Luvizotto, G.L., Forshaw, J.B.; Nobre, A.G., Ando, R.A. Submitted. Orogenic front P-T-t paths reveal continental crust underthrusting at the southernmost edge of the Brasília Orogen. Journal of Metamorphic Geology.~~

Whipple, K. X., 2009. The influence of climate on the tectonic evolution of mountain belts. Nature Geoscience, 2(2), 97–104.

White, R.W., Pomroy, N.E., Powell, R., 2005. An in situ metatexite–diatexite transition in upper amphibolite facies rocks from Broken Hill, Australia. Journal of Metamorphic Geology 23, 579–602. https://doi.org/10.1111/J.1525-1314.2005.00597.X

White, R.W., Powell, R., Holland, T.J.B., 2007. Progress relating to calculation of partial melting equilibria for metapelites. Journal of Metamorphic Geology 25, 511–527. https://doi.org/10.1111/J.1525-1314.2007.00711.X

Whitney, D.L., Evans, B.W., 2010. Abbreviations for names of rock-forming minerals. American Mineralogist 95, 185–187. https://doi.org/10.2138/am.2010.3371

Willett, S. D., 1999. Orogeny and orography: The effects of erosion on the structure of mountain belts. Journal of Geophysical Research: Solid Earth, 104(B12), 28957–28981. https://doi.org/10.1029/1999JB900248

Williams, M.A., Kelsey, D.E., Rubatto, D., 2022. Thorium zoning in monazite: a case study from the Ivrea–Verbano Zone, NW Italy. Journal of Metamorphic Geology 1–28. https://doi.org/10.1111/JMG.12656

Williams, M.L., Jercinovic, M.J., 2012. Tectonic interpretation of metamorphic tectonites: Integrating compositional mapping, microstructural analysis and in situ monazite dating. Journal of Metamorphic Geology 30, 739–752. https://doi.org/10.1111/j.1525-1314.2012.00995.x

Williams, M.L., Jercinovic, M.J., 2002. Microprobe monazite geochronology: Putting absolute time into microstructural analysis. Journal of Structural Geology 24, 1013–1028. https://doi.org/10.1016/S0191-8141(01)00088-8

Zuquim, M. P. S., Trouw, R. A. J., Trouw, C. C., Tohver, E., 2011. Structural evolution and U–Pb SHRIMP zircon ages of the Neoproterozoic Maria da Fé shear zone, central Ribeira Belt – SE Brazil. Journal of South American Earth Sciences, 31(2–3), 199–213. https://doi.org/10.1016/J.JSAMES.2011.02.002

FIGURES CAPTIONS

Figure 1 - a) Western Gondwana reconstruction by Westin et al. (2021). The blue square marks the cratonic blocks involved in the Southern Brasilia Orogen (SBO) development. (1) Transbrasiliano-Kandi Lineament. Continental cratons: A-Amazon; CC- Congo; KA-Kazai; LA- Luis Alves; P- Pampia; Pp- Paranapanema; Pb- Parnaíba; WA-RA- Ria Apa; RP- Rio de la Plata; SH- Sahara; SF- São Francisco; SL- São Luis; b) Orogenic belts of Central and Southeast Brazil (Westin et al., 2021). Red square is the SBO position.

Figure 2 - Southern Brasilia Orogen (SBO) tectonic map modified after Campos Neto et al. (2020). The black square marks the study area location.

Figure 3 – Cross-section A-B (see Fig. 2) illustrating the tectonic architecture of the south sector of the Southern Brasilia Orogen.

Figure 4 - a) Geological map of Pouso Alto county; b) Geological cross-section of the area and stereographic projections of collected structural data.

Figure 5 - Blastesis-deformation relationships in the Liberdade and Andrelândia Nappes.

Figure 6 - Liberdade Nappe (LN) photomicrographs. a) Spaced disjunctive schistosity (S_2) defined by biotite and white mica shape preferential orientation (SPO). Quartz displays moderately irregular contacts (UTM 521535/7560145); b) Skeletal garnet and decussate fibrolite (UTM 521535/7560145); c) Garnet porphyroblast with S-shaped internal foliation (UTM 521535/7560145); d) Garnet pseudomorph replaced completely by fibrolite (UTM 521535/7560145); e) Isoclinal fold marked by fibrolite orientation (UTM 519472/ 7549550); f) Kyanite relic overgrown by white mica (UTM 5110028/7561820).

Figure 7 - Quantitative compositional maps for the sample NESG-388 of the Liberdade Nappe: a) Mineral map of the investigated thin-section area showing the mineral phases in the mapped area; b) Anorthite (XAn) content in plagioclase map; c)-f) Almandine (XAlm), grossular (XGrs), pyrope (XPrp) and spessartine (XSps) zoning in garnet. The red circles indicate the area used to perform the Q_{cmp} maps for garnet, and plagioclase (core and rim).

Figure 8 - Andrelândia Nappe (AN) photomicrographs. a) Compositional banding, alternating layers made by quartz and plagioclase, and those constituted by white mica and biotite with subordinate garnet and kyanite (UTM 513937/7565930); b) Garnet porphyroblast with opaque inclusion trails defying the internal foliation (Pre-S_2), and kyanite aligned according to the external S_2 foliation (UTM 516960/7565691); c) Fibrolite growth along a shear bands (UTM 516960/7565691); d) Garnet with opaque inclusion trails oblique to the external foliation (post-S_2) made by sillimanite, quartz, and biotite. Staurolite

with internal foliation continuous with the external one. Note the fibrolite replacing biotite crystals (UTM 516960/7565691).

Figure 9 - Quantitative compositional maps for sample NESG-401 of the Andrelândia Nappe; a) Mineral map of the investigated thin-section area showing the mineral phases in the mapped area; b) Anorthite (XAn) content in plagioclase map; c)-f) Almandine (XAlm), grossular (XGrs), pyrope (XPrp) and spessartine (XSps) zoning in garnet. The red circles indicate the area used to perform the Q_{cmp} maps for garnet (mantle and rim), and plagioclase (core and rim).

Figure 10 – a) *P-T* isochemical phase diagram in the MnNCKFMASHT system for the Liberdade Nappe (NESG-388); b) *P-T* path based on optimal conditions of mineral chemistry composition (Q_{cmp}) and mode (Q_{mode}) maps. The red star corresponds to the optimal *P-T* conditions obtained by the antidote.

Figure 11 – a) *P-T* isochemical phase diagram in the MnNCKFMASHT system for the Andrelândia Nappe (NESG-401); b) *P-T* path based on optimal conditions for mineral chemistry composition (Q_{cmp}) and mode (Q_{mode}) maps. The red star corresponds to the optimal P-T conditions obtained by the antidote.

Figure 12– Liberdade Nappe (sample NESG-388): a) BSE images, X-ray maps (Y and Th) of monazites showing structural position, textural relationships, and internal zoning; b) Y_2O_3 (wt%) *vs.* age plot; c) ThO_2 (wt%) *vs.* age plot; d) weighted average diagram for monazite core dates (domain 1 and 2); e) weighted average diagram for monazite rim dates (domain 3).

Figure 13 – Andrelândia Nappe (sample NESG-401): a) BSE images, X-ray maps (Y and Th) of monazites showing structural position, textural relationships, and internal zoning; b) Y_2O_3 (wt%) *vs.* age plot; c) ThO_2 (wt%) *vs.* age plot; d) weighted average diagram for monazite core dates; e) weighted average diagram for monazite enclosed in Ky.

Figure 14 – a) Summary of Andrelândia Nappe System (ANS) *P-T* paths. Grey dotted lines display different geothermal gradients trends. Solidus curve from Spear et al. (1999) in the NaKFMASH system; b) summary of the monazite and zircon U-Pb metamorphic ages from the Liberdade and Andrelândia Nappes.

Figure 15 – Tectono-metamorphic model for the evolution of the SBO nappes. a) 630 to 620 Ma: Early prograde metamorphism in the collisional wedge and Pouso Alto Nappe burial and heating stage; b) 620 to 610 Ma: Onset of the decompression path in the collisional wedge. Pouso Alto Nappe decompression and melt crystallization stage, while the Liberdade Nappe was buried and heated; c) 610 to 580 Ma: Liberdade Nappe onset its upward isothermal decompression path over the Andrelândia Nappe, which was heated and buried; d) <580-570 Ma: Final stage of the SBO continental collision coeval with the Andrelândia and Carrancas Nappes decompression and cooling stages. The *P-T-t* paths are based on Benetti. (2022), Campos Neto et al. (2021), Coelho et al. (2017), Fumes et al., (2021), Li et al. (2021), Marimon et al. (2020, 2022), Motta and Moraes (2017), Motta et al. (2021), Rocha et al. (2017), Westin et al. (2021~~, submitted~~).

SUPPLEMENTARY FIGURE FILE A

Figure A1 - Full thin-sections maps acquired using the Scanning Electron Microscopy and Mineral Liberation Analyzer (SEM-MLA). The black square represents the local bulk composition (LBC) investigated. a) Sample NESG-388 from Liberdade Nappe; b) Sample NESG-401 from Andrelândia Nappe.

Figure A2 – Quantitative compositional maps for the sample NESG-388 from Liberdade Nappe. a) Map of Ti content in biotite (a.p.f.u); b) Map of #Mg in biotite; c) Map of Ti in biotite thermometer of Henry et al. (2005); d) Map of Si^{+4} content in white mica (a.p.f.u). Red circle indicates the area used to perform the Q_{cmp} maps.

Figure A3 – Quantitative compositional maps for the sample NESG-401 from Andrelândia Nappe. a) Map of Ti content in biotite (a.p.f.u); b) Map of #Mg in biotite; c) Map of Ti in biotite thermometer of Henry et al. (2005); d) Map of Si^{+4} content in white mica (a.p.f.u). Red circle indicates the area used to perform the Q_{cmp} maps.

Figure A4- Maps of quality factors by Antidote for Liberdade Nappe. a) Q_{asm}; b)Q_{mode}; c) Q_{cmp} for the LBC bulk composition; d)Q_{cmp} for garnet composition; e) Q_{cmp} for plagioclase core composition; f) Q_{cmp} for plagioclase rim composition; g) Q_{cmp} for white mica composition; h) Q_{cmp} for biotite composition.

Figure A5- a) *P-T* isochemical phase diagram in the MnNCKFMASHT system for the Andrelândia Nappe (NESG-401) for LBC including garnet core composition; b) Map of quality factor Q_{cmp} by Antidote for AN garnet core composition.

Figure A6 - Maps of quality factors by Antidote for Andrelândia Nappe. a) Q_{asm}; b) Q_{mode}; c) Q_{cmp} for the LBC bulk composition; d) Q_{cmp} for garnet mantle composition; e) Q_{cmp} for garnet rim composition; f) Q_{cmp} for white mica composition; g) Q_{cmp} for plagioclase core composition; h) Q_{cmp} for plagioclase rim composition; i) Q_{cmp} for biotite composition.

Figure A7 – Weighted mean plot for Moacyr monazite standard.

SUPPLEMENTARY TABLE FILE A

Table A1- Representative Electron Microprobe (EMP) analyses of minerals from samples NESG-388 and NESG-401. (b.d.l. - below detection limit).

Table A2 - Monazite chemical composition from sample NESG-388 and NESG-401 (normalized to 4O), (b.d.l- below detection limit).

Figure

Click here to access/download;Figure;fig.1.tif

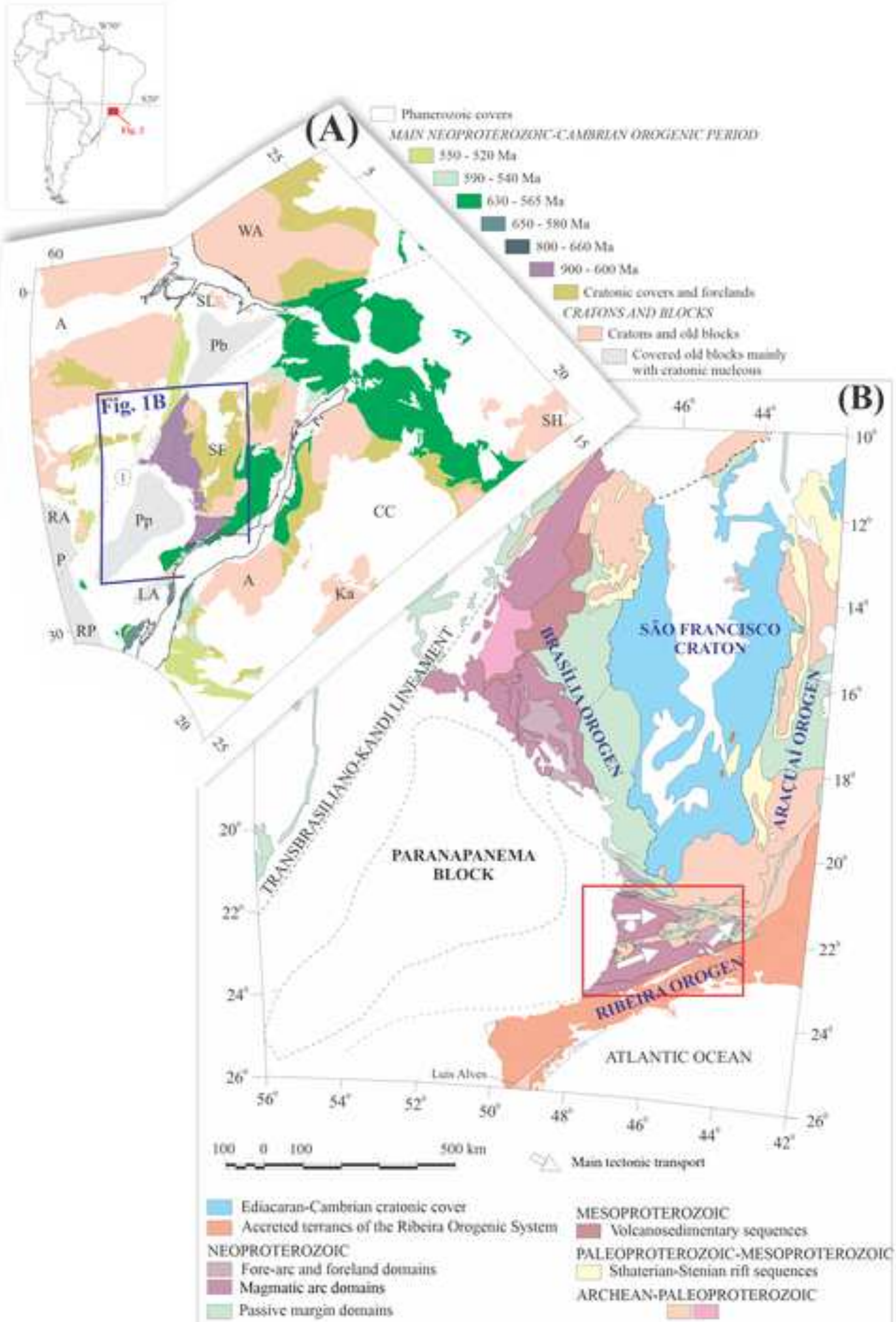

Figure

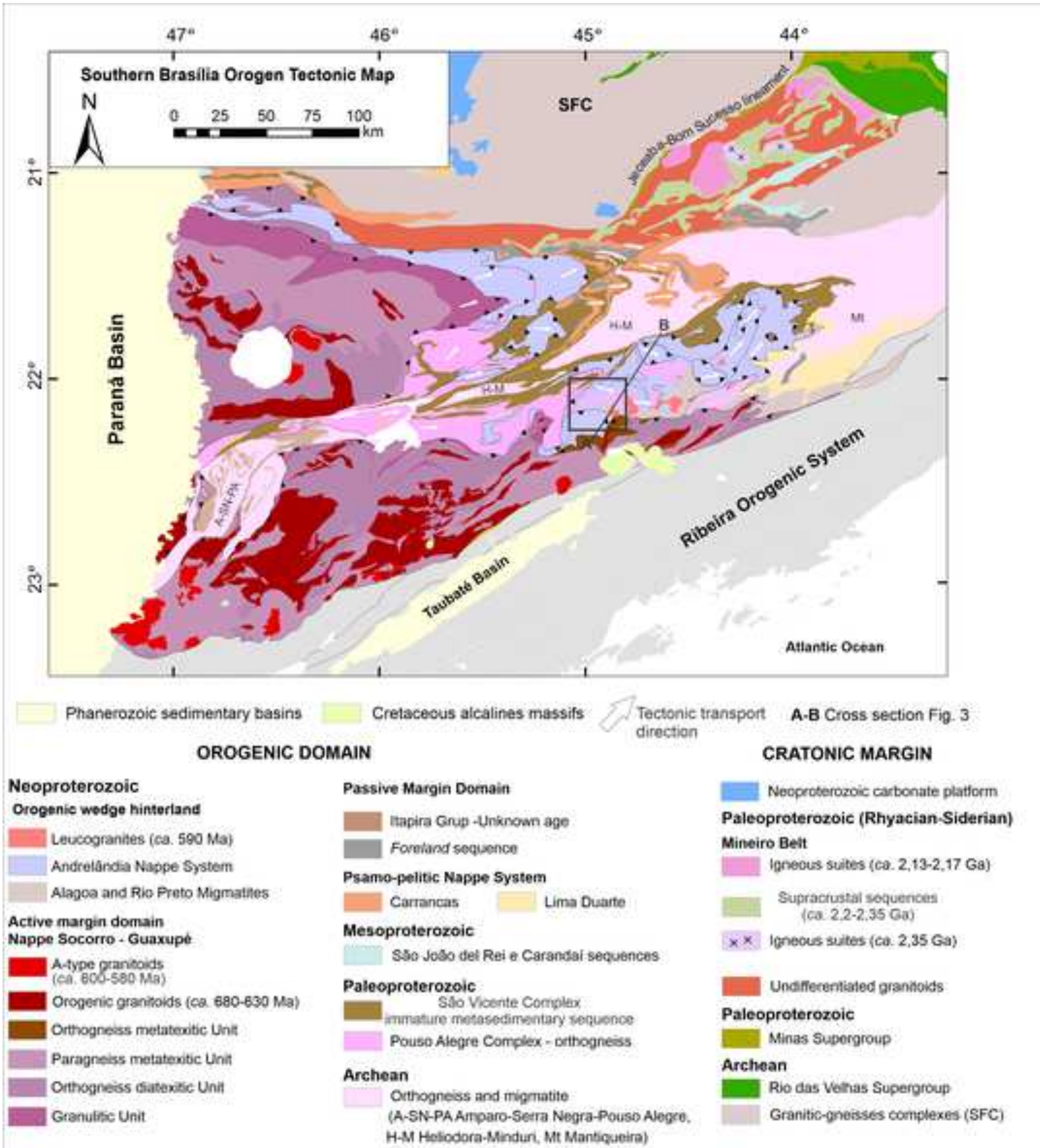
47°
46°
45°
44°
21°
22°
23°
Southern Brasília Orogen Tectonic Map
N
0 25 50 75 100
km
SFC
Jeceaba-Bom Sucesso lineament
Paraná Basin
H-M
B
Mt
A-SN-PA
Ribeira Orogenic System
Taubaté Basin
Atlantic Ocean
Phanerozoic sedimentary basins
Cretaceous alcalines massifs
Tectonic transport direction
A-B Cross section Fig. 3
OROGENIC DOMAIN
CRATONIC MARGIN
Neoproterozoic
Orogenic wedge hinterland
Leucogranites (ca. 590 Ma)
Andrelândia Nappe System
Alagoa and Rio Preto Migmatites
Active margin domain
Nappe Socorro - Guaxupé
A-type granitoids (ca. 600-580 Ma)
Orogenic granitoids (ca. 680-630 Ma)
Orthogneiss metatexitic Unit
Paragneiss metatexitic Unit
Orthogneiss diatexitic Unit
Granulitic Unit
Passive Margin Domain
Itapira Grup -Unknown age
Foreland sequence
Psamo-pelitic Nappe System
Carrancas
Lima Duarte
Mesoproterozoic
São João del Rei e Carandaí sequences
Paleoproterozoic
São Vicente Complex immature metasedimentary sequence
Pouso Alegre Complex - orthogneiss
Archean
Orthogneiss and migmatite
(A-SN-PA Amparo-Serra Negra-Pouso Alegre, H-M Heliodora-Minduri, Mt Mantiqueira)
Neoproterozoic carbonate platform
Paleoproterozoic (Rhyacian-Siderian)
Mineiro Belt
Igneous suites (ca. 2,13-2,17 Ga)
Supracrustal sequences (ca. 2,2-2,35 Ga)
Igneous suites (ca. 2,35 Ga)
Undifferentiated granitoids
Paleoproterozoic
Minas Supergroup
Archean
Rio das Velhas Supergroup
Granitic-gneisses complexes (SFC)

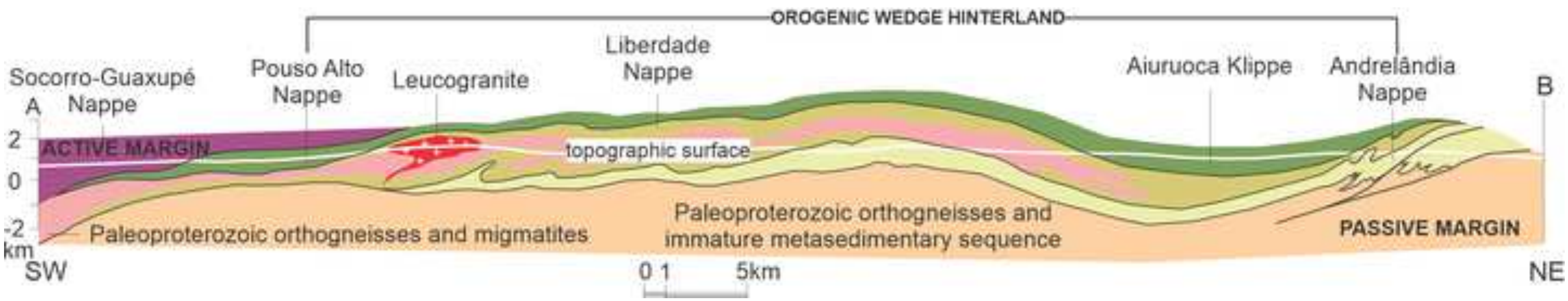
OROGENIC WEDGE HINTERLAND
Socorro-Guaxupé Nappe
Pouso Alto Nappe
Leucogranite
Liberdade Nappe
Aiuruoca Klippe
Andrelândia Nappe
A
B
2
0
-2
km
ACTIVE MARGIN
topographic surface
Paleoproterozoic orthogneisses and migmatites
Paleoproterozoic orthogneisses and immature metasedimentary sequence
PASSIVE MARGIN
SW
NE
0 1 5km

Figure

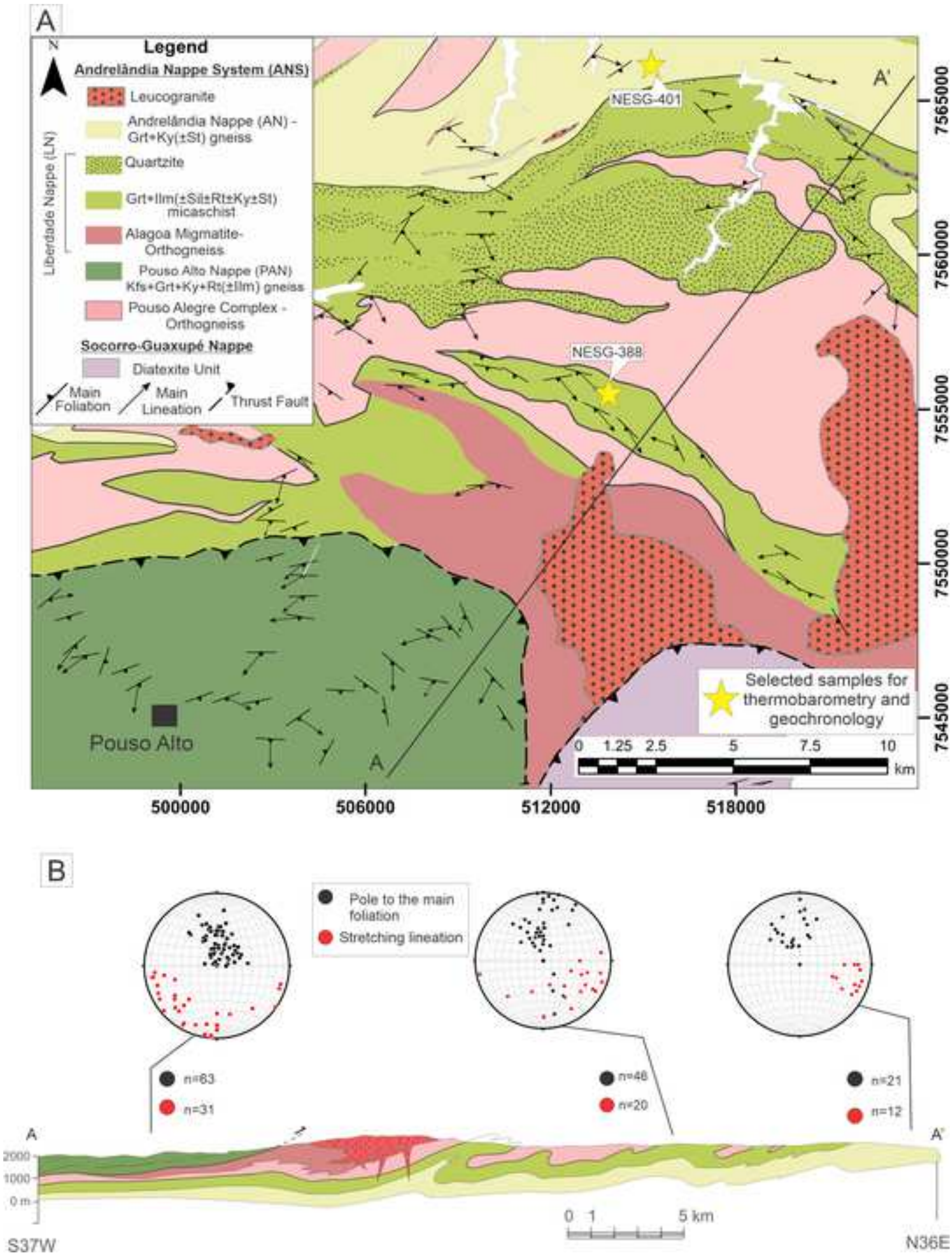

A
N
Legend
Andrelândia Nappe System (ANS)
Leucogranite
Andrelândia Nappe (AN) - Grt+Ky(±St) gneiss
Liberdade Nappe (LN)
Quartzite
Grt+Ilm(±Sil±Rt±Ky±St) micaschist
Alagoa Migmatite-Orthogneiss
Pouso Alto Nappe (PAN) Kfs+Grt+Ky+Rt(±Ilm) gneiss
Pouso Alegre Complex - Orthogneiss
Socorro-Guaxupé Nappe
Diatexite Unit
Main Foliation
Main Lineation
Thrust Fault
NESG-401
NESG-388
A'
A
Pouso Alto
Selected samples for thermobarometry and geochronology
0 1.25 2.5 5 7.5 10
km
7565000
7560000
7555000
7550000
7545000
500000
506000
512000
518000
B
Pole to the main foliation
Stretching lineation
n=63
n=31
n=48
n=20
n=21
n=12
A
A'
2000
1000
0 m
0 1 5 km
S37W
N36E

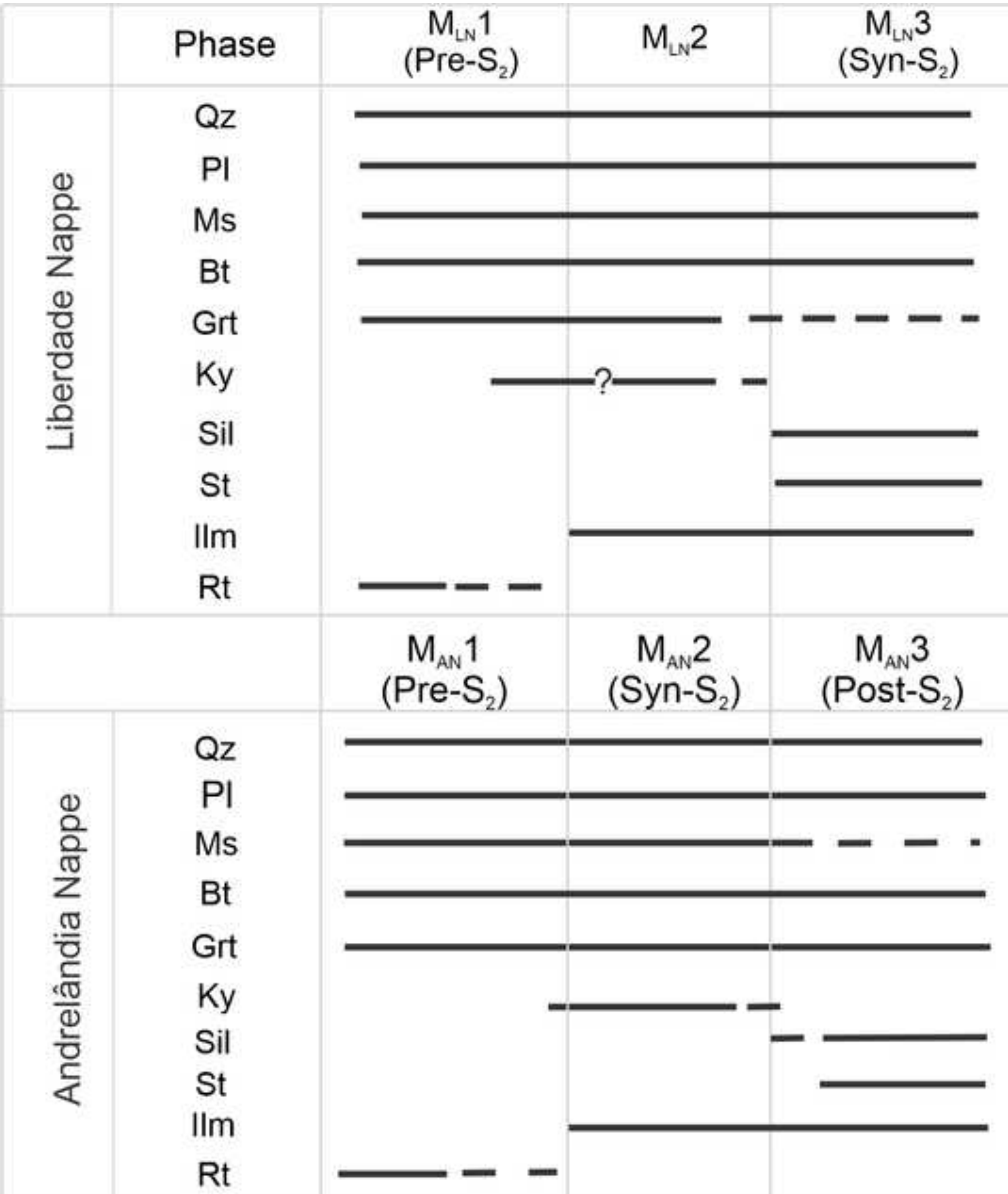
Phase
$M_{LN}1$ (Pre-S_2)
$M_{LN}2$
$M_{LN}3$ (Syn-S_2)
Liberdade Nappe
Qz
Pl
Ms
Bt
Grt
Ky
?
Sil
St
Ilm
Rt
$M_{AN}1$ (Pre-S_2)
$M_{AN}2$ (Syn-S_2)
$M_{AN}3$ (Post-S_2)
Andrelândia Nappe
Qz
Pl
Ms
Bt
Grt
Ky
Sil
St
Ilm
Rt

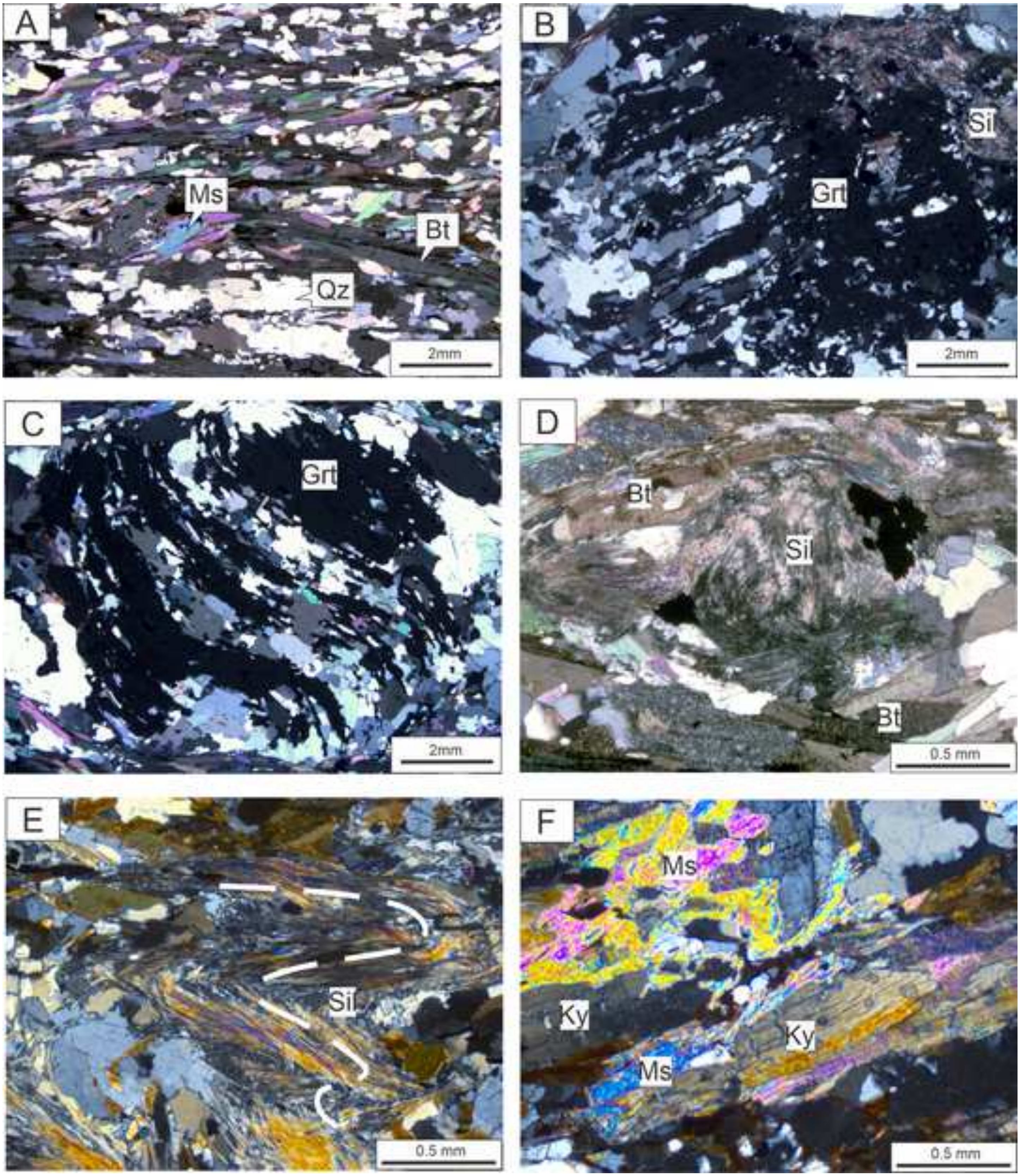
A
Ms
Bt
Qz
2mm
B
Si
Grt
2mm
C
Grt
2mm
D
Bt
Si
Bt
0.5 mm
E
Sil
0.5 mm
F
Ms
Ky
Ky
Ms
0.5 mm

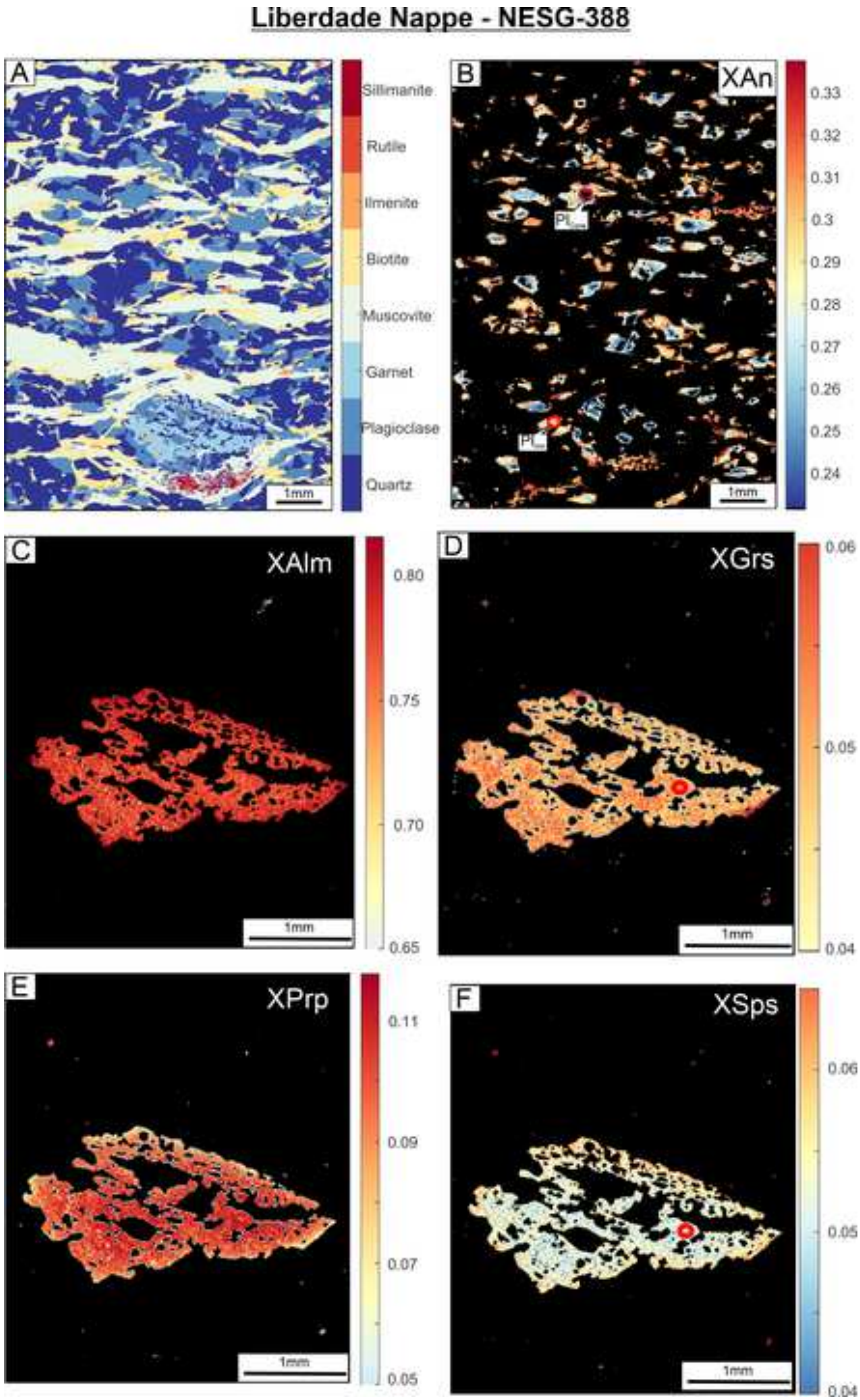
Liberdade Nappe - NESG-388
A
Sillimanite
Rutile
Ilmenite
Biotite
Muscovite
Garnet
Plagioclase
Quartz
1mm
B
XAn
0.33
0.32
0.31
0.3
0.29
0.28
0.27
0.26
0.25
0.24
1mm
C
XAlm
0.80
0.75
0.70
0.65
1mm
D
XGrs
0.06
0.05
0.04
1mm
E
XPrp
0.11
0.09
0.07
0.05
1mm
F
XSps
0.06
0.05
0.04
1mm

Figure

Click here to access/download;Figure;Fig.8.tif

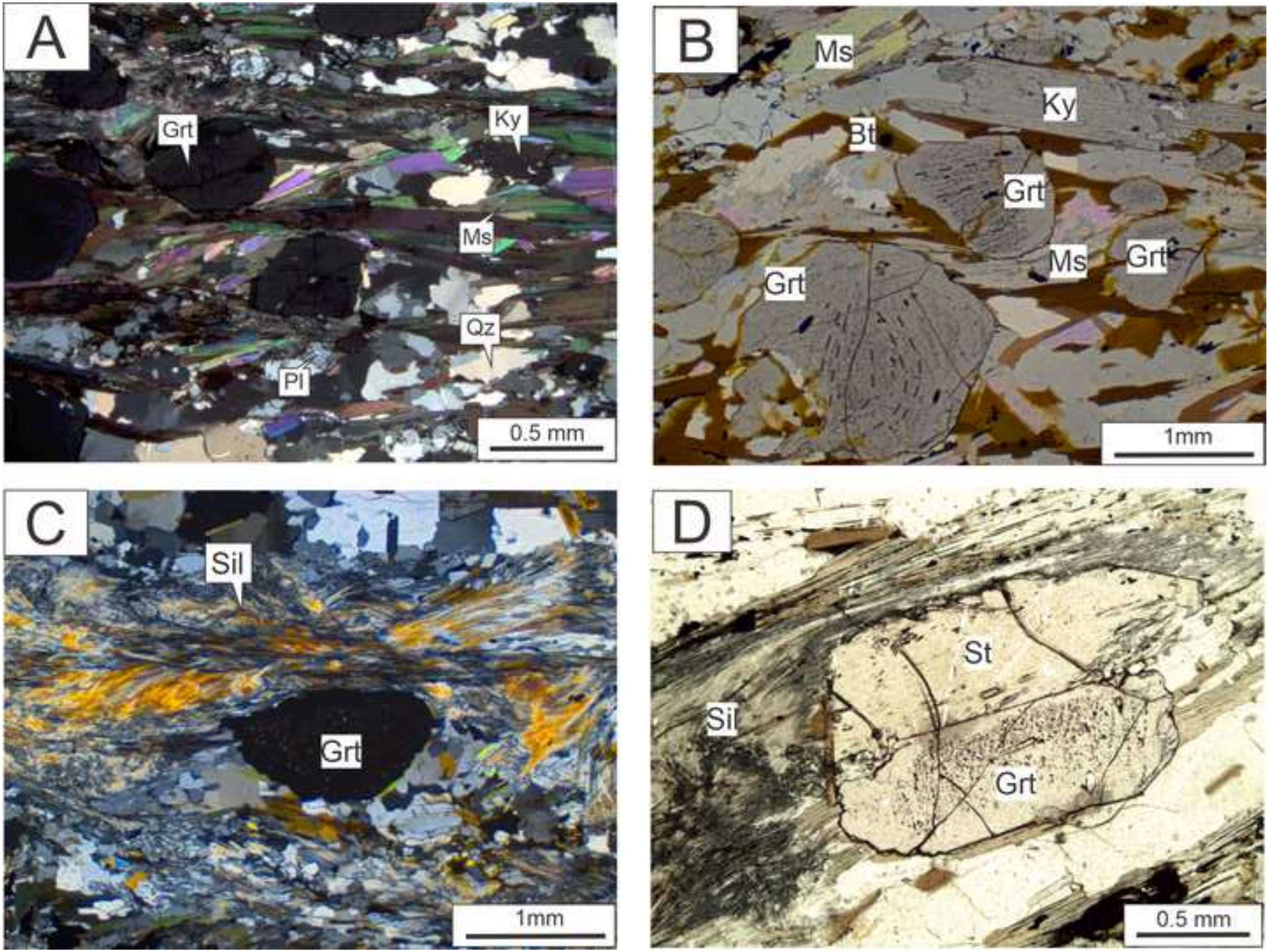

Figure

Click here to access/download;Figure;Fig.9.tif

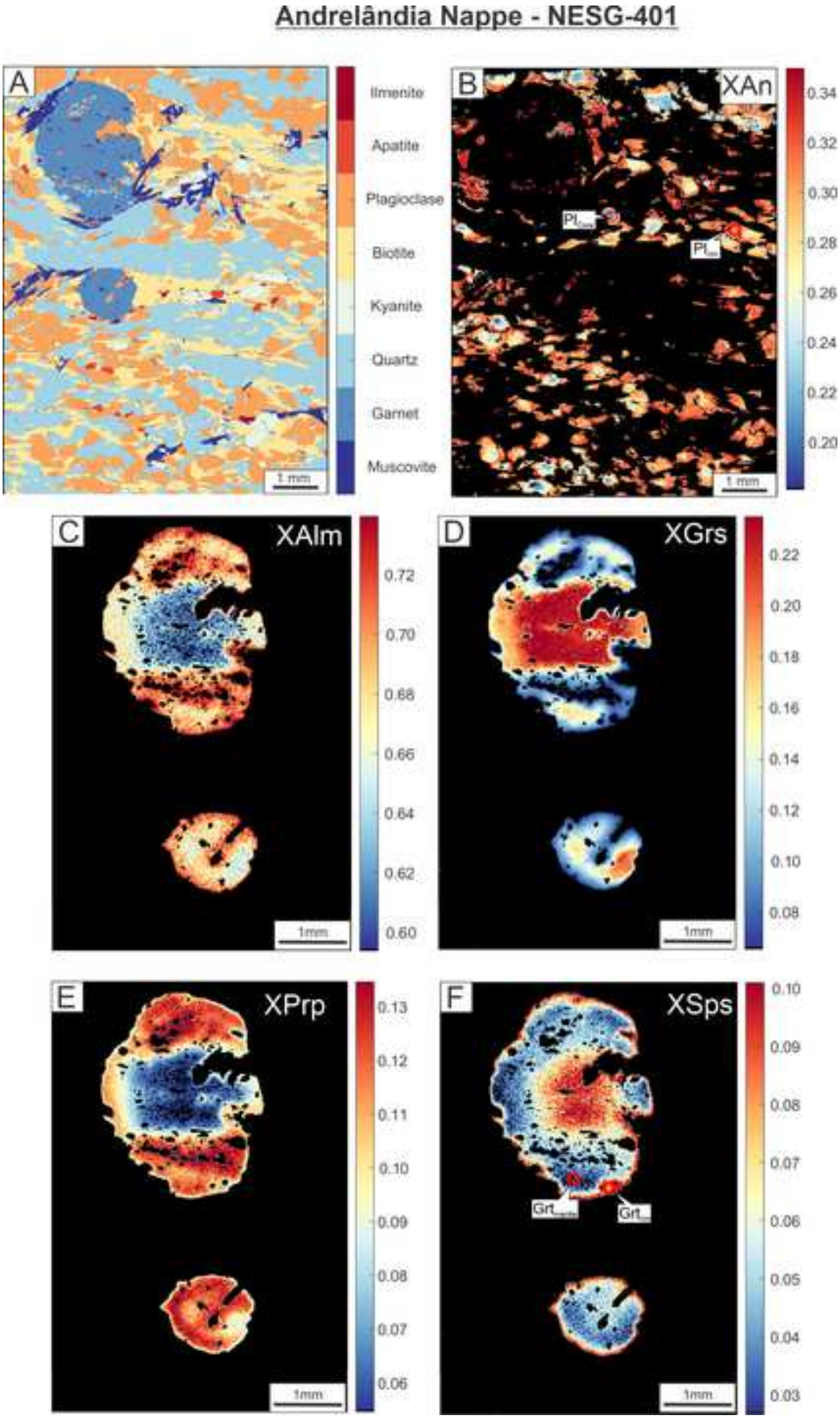

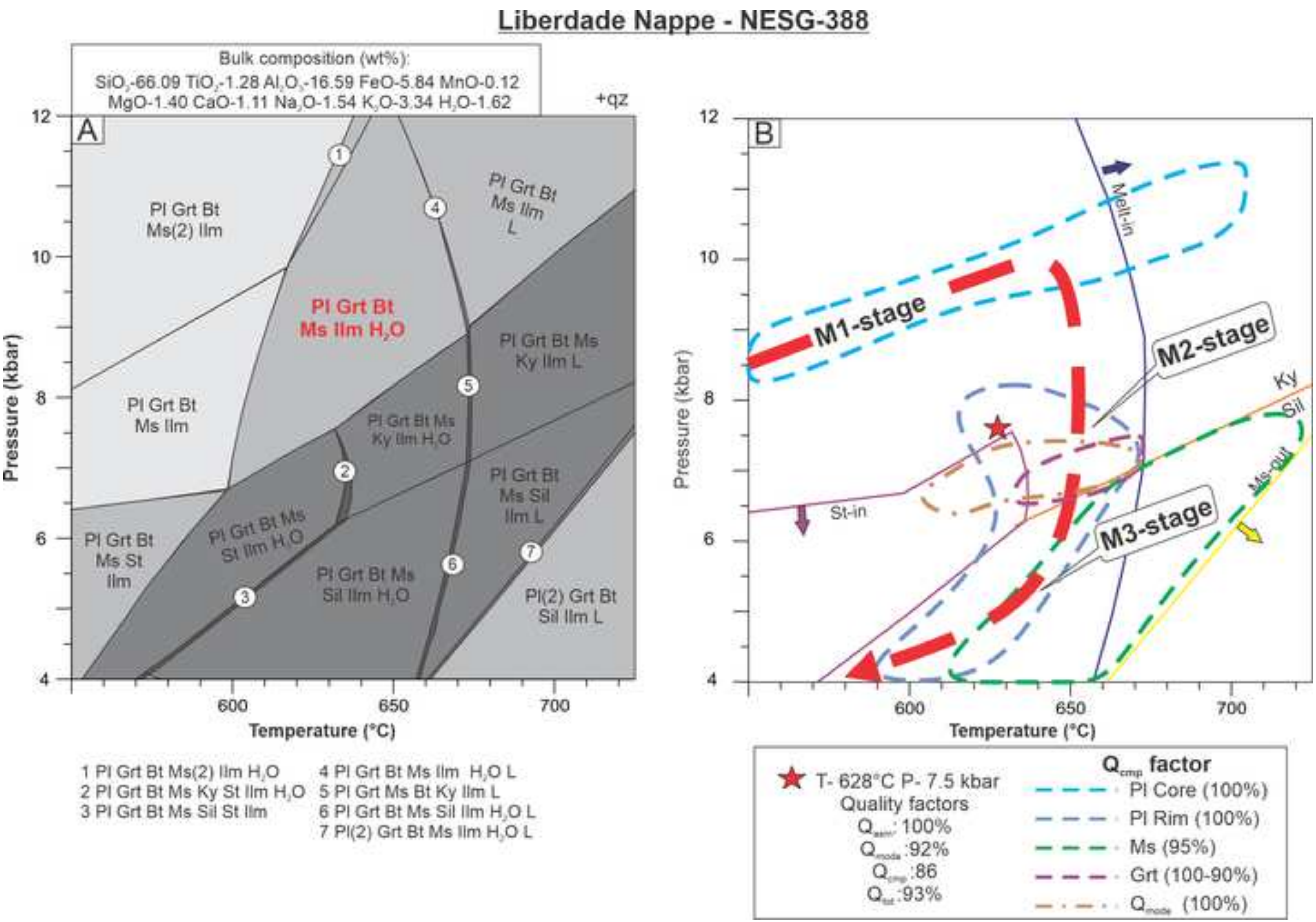
Liberdade Nappe - NESG-388
Bulk composition (wt%):
SiO2-66.09 TiO2-1.28 Al2O3-16.59 FeO-5.84 MnO-0.12
MgO-1.40 CaO-1.11 Na2O-1.54 K2O-3.34 H2O-1.62
+qz
A
Pl Grt Bt Ms(2) Ilm
Pl Grt Bt Ms Ilm
Pl Grt Bt Ms Ilm H2O
Pl Grt Bt Ms Ilm L
Pl Grt Bt Ms Ky Ilm L
Pl Grt Bt Ms Ky Ilm H2O
Pl Grt Bt Ms St Ilm
Pl Grt Bt Ms St Ilm H2O
Pl Grt Bt Ms Sil Ilm H2O
Pl Grt Bt Ms Sil Ilm L
Pl(2) Grt Bt Sil Ilm L
Pressure (kbar)
Temperature (°C)
1 Pl Grt Bt Ms(2) Ilm H2O
2 Pl Grt Bt Ms Ky St Ilm H2O
3 Pl Grt Bt Ms Sil St Ilm
4 Pl Grt Bt Ms Ilm H2O L
5 Pl Grt Ms Bt Ky Ilm L
6 Pl Grt Bt Ms Sil Ilm H2O L
7 Pl(2) Grt Bt Ms Ilm H2O L
B
M1-stage
M2-stage
M3-stage
Melt-in
St-in
Ky
Sil
Ms-out
Pressure (kbar)
Temperature (°C)
T- 628°C P- 7.5 kbar
Quality factors
Qasm: 100%
Qmode: 92%
Qcmp: 86
Qtot: 93%
Qcmp factor
Pl Core (100%)
Pl Rim (100%)
Ms (95%)
Grt (100-90%)
Qmode (100%)

Figure

Click here to access/download;Figure;fig.11.tif

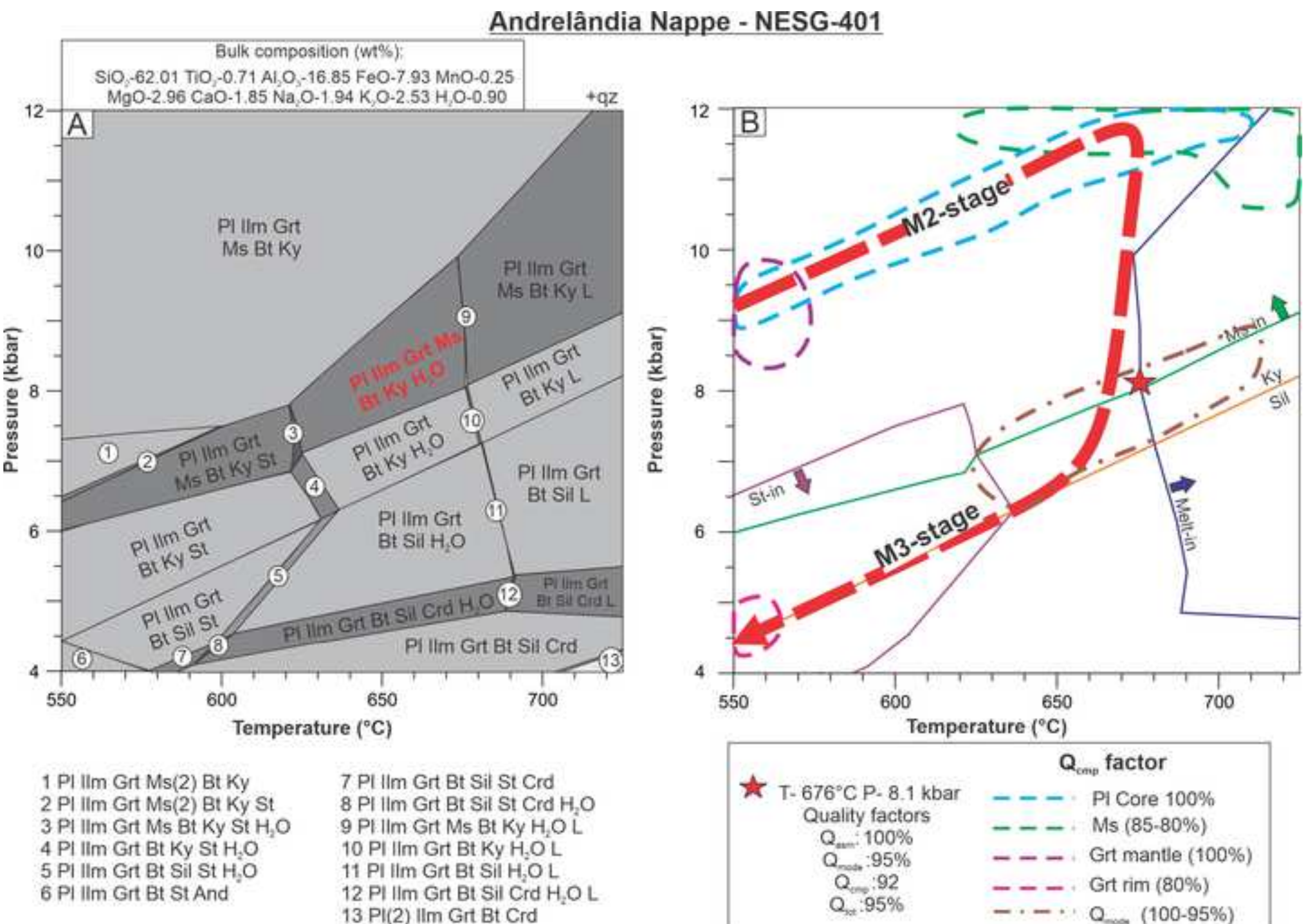

Figure

Click here to access/download;Figure;fig.12.tif

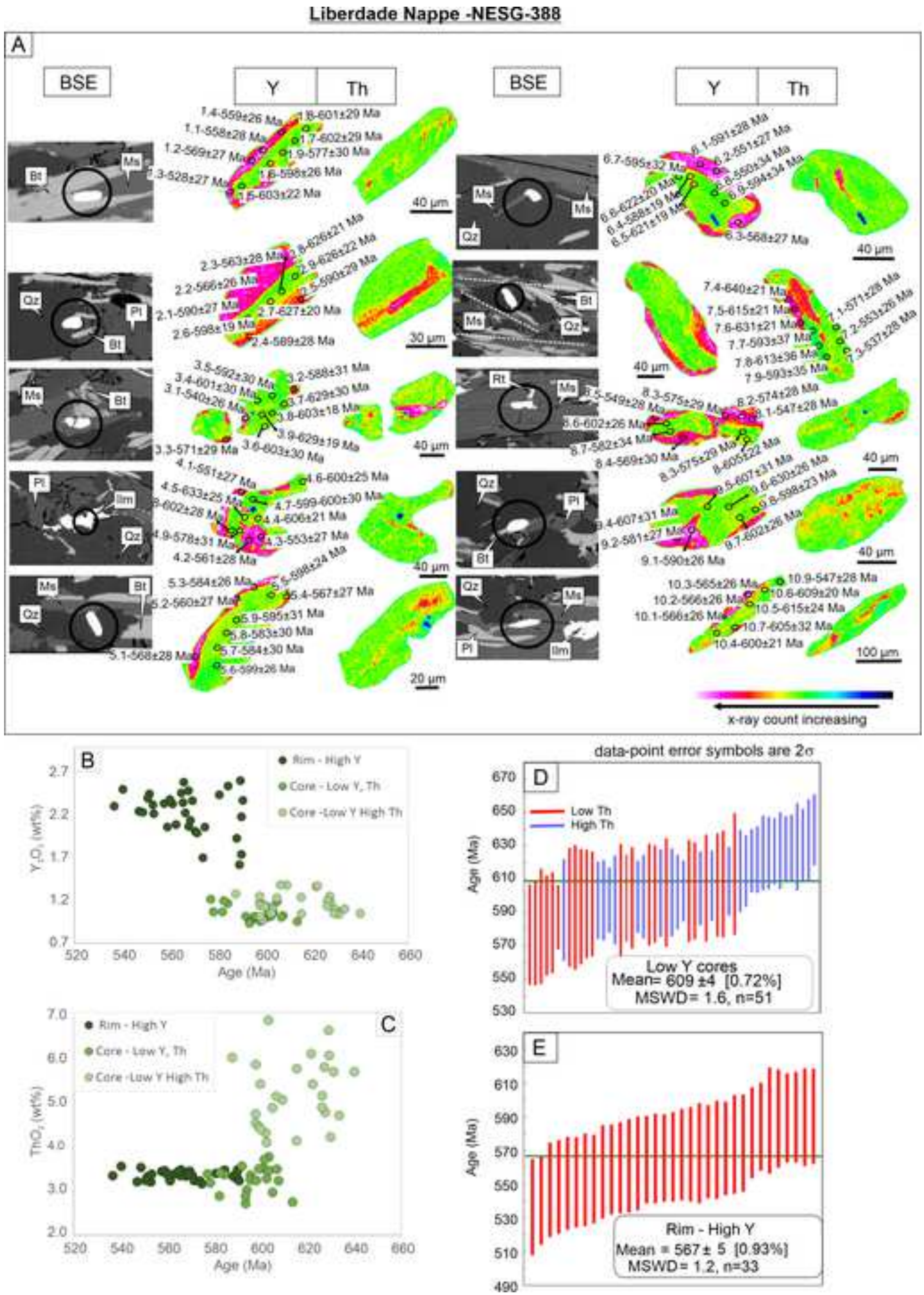

Figure

Click here to access/download;Figure;fig.13.tif

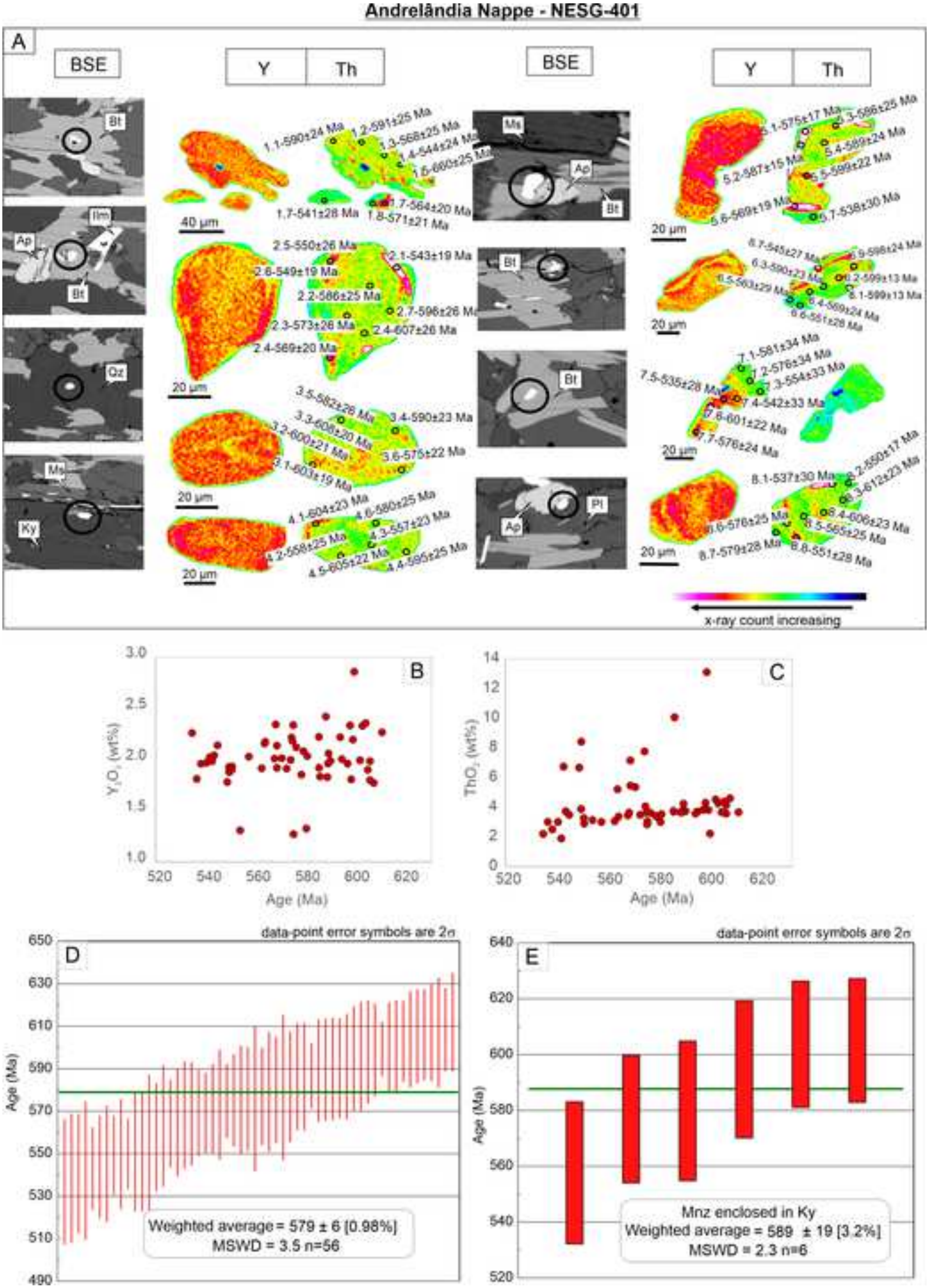

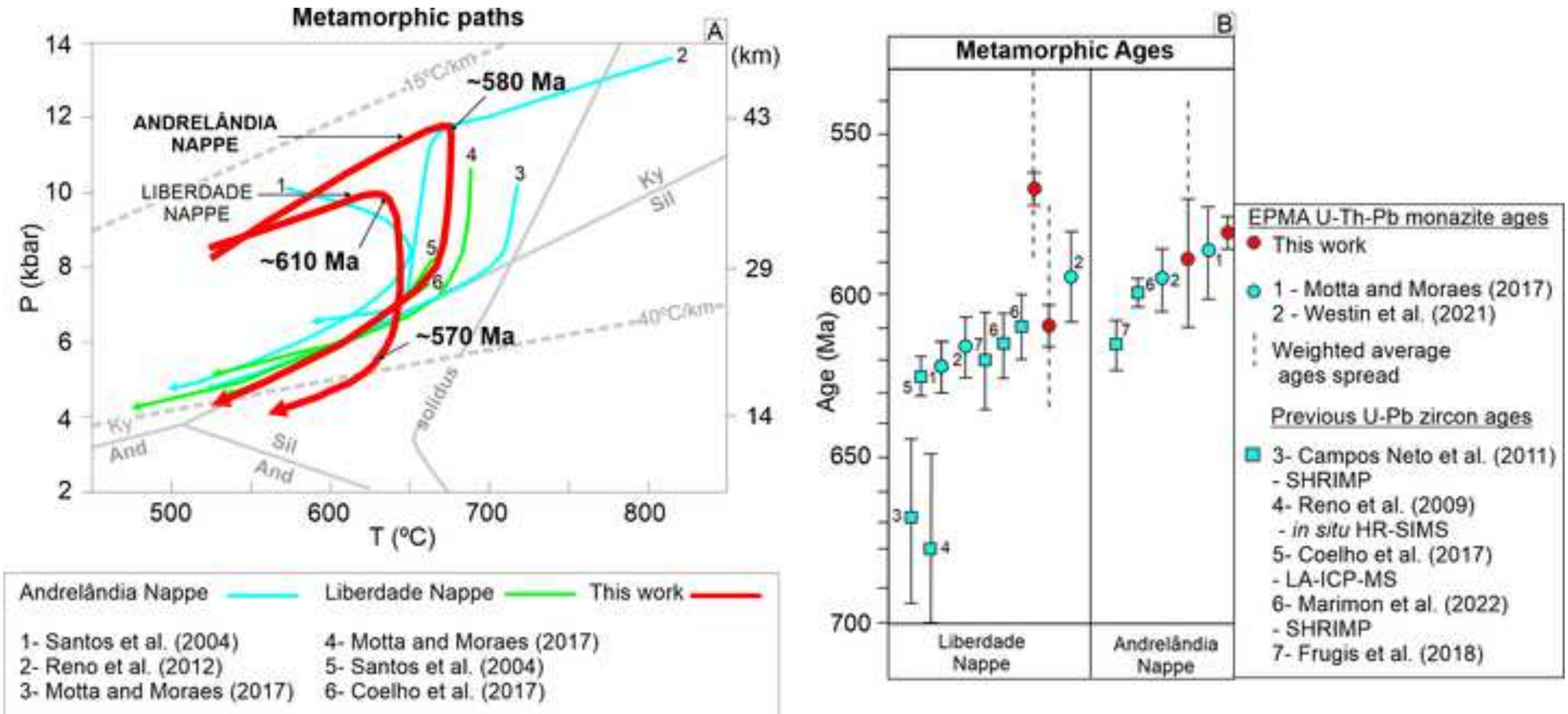
Metamorphic paths
A
P (kbar)
T (ºC)
(km)
~580 Ma
~610 Ma
~570 Ma
ANDRELÂNDIA NAPPE
LIBERDADE NAPPE
15°C/km
40°C/km
Ky
Sil
And
solidus
Andrelândia Nappe
Liberdade Nappe
This work
1- Santos et al. (2004)
2- Reno et al. (2012)
3- Motta and Moraes (2017)
4- Motta and Moraes (2017)
5- Santos et al. (2004)
6- Coelho et al. (2017)
B
Metamorphic Ages
Age (Ma)
Liberdade Nappe
Andrelândia Nappe
EPMA U-Th-Pb monazite ages
This work
1 - Motta and Moraes (2017)
2 - Westin et al. (2021)
Weighted average ages spread
Previous U-Pb zircon ages
3- Campos Neto et al. (2011) - SHRIMP
4- Reno et al. (2009) - in situ HR-SIMS
5- Coelho et al. (2017) - LA-ICP-MS
6- Marimon et al. (2022) - SHRIMP
7- Frugis et al. (2018)

Figure

Click here to access/download;Figure;Fig 15_new.tif

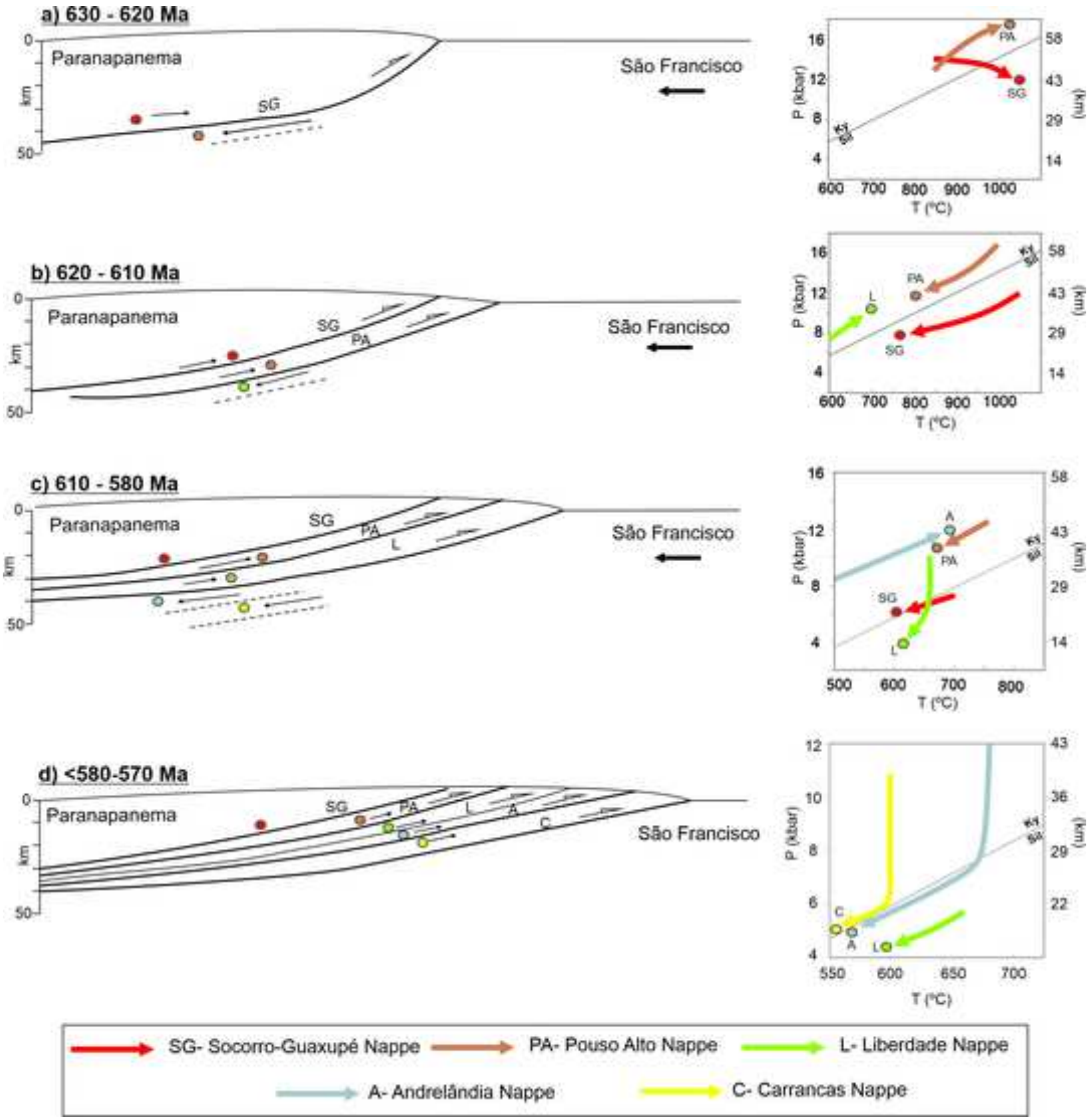

Click here to access/download
Supplementary material/Appendix (Files for online publication only)
Supplementary Table File A.xls

Declaration of interests

☒The authors declare that they have no known competing financial interests or personal relationships that could have appeared to influence the work reported in this paper.

☐The authors declare the following financial interests/personal relationships which may be considered as potential competing interests: